Using Nanomaterials to Manipulate Drug Aggregation in order to Enhance Passive Transmembrane Transport

Cai, Xiulian Jesmine

Awarding institution:
King's College London

Using Nanomaterials to Manipulate Drug Aggregation in order to Enhance Passive Transmembrane Transport

---

Xiulian Jesmine Cai

In fulfilment of the requirement
for the degree of Doctor of Philosophy (PhD)
in Pharmaceutical Science

Department of Pharmacy
King's College London

April 2016

To my family Ji ji*, Steve, Magdalene and Jean.*

Acknowledgements

First and foremost, I would like to express my sincere gratitude to my supervisors for their continuous support with this project. To Dr. Stuart Jones, who gave me the freedom to explore on my own and at the same time the guidance to recover when I faltered, thank you for the valuable support and motivational encouragement. I am also very thankful to Dr. Patrick Mesquida, for his thoughtful advice and encouragement. I could not have asked for a better person to show me the ropes of the AFM. I am also grateful to Arcadia for her insightful and detailed comments when proofreading this thesis.

I would like to thank the technical team of KCL, especially Dave, Helena and Bill, who provided various forms of support during this PhD. Thanks to all my colleagues, who have became my precious friends (Aateka, Hanpeng, Jasminder, Melis, Raquel and everyone else on the 5th floor), for making my time at King's an enjoyable one.

Last but certainly not least, none of this would have been possible without the love and patience of my parents and sister – my constant source of love, support and strength. I would also like to especially thank Mike, for encouraging me throughout this endeavour and always knowing how to make me smile.

Thanks for believing in this project and me.

List of Publications

Journal articles

X.J. Cai, T. Patel, A. Woods, P. Mesquida, S.A. Jones. (2016). Investigating the influence of drug aggregation on the percutaneous penetration rate of tetracaine when applying low doses of the agent topically to the skin. *International Journal of Pharmaceutics*. **502**(1-2): 10-17.

X.J. Cai, A. Woods, P. Mesquida, S.A. Jones. (2016). Assessing the potential for drug-nanoparticle surface interactions to improve drug penetration into the skin. *Molecular Pharmaceutics*. **13**(4): 1375-1384.

X.J. Cai, P. Mesquida, S.A. Jones (2016). Topical tetracaine formulations containing nanomaterials to increase percutaneous skin permeation. *Manuscript submitted for publication.*

R. Inacio, S. Poland, X.J. Cai, S. Cleary, S. Ameer-Beg, J. Keeble, S.A. Jones (2016). The application of local hypobaric pressure – a novel means to enhance marcromolecule entry into the skin. *Journal of Controlled Release.* **226**: 66-76.

Abstracts

X. Cai. and S. A. Jones. Molecular aggregation of the anesthetic tetracaine in topical therapy (P1729). 22nd Congress of the European Academy of Dermatology and Venerology. Istanbul, Turkey (2013).

X.J. Cai, P. Mesquida, S.A. Jones. Modulating tetracaine aggregation using nanoparticles to enhance topical administration (PD-096). 5th Pharmaceutical Sciences World Congress, Melbourne, Australia (2014).

X.J. Cai, P. Mesquida, S.A. Jones. Understanding the consequences of the tetracaine adsorption onto the surface of nanoparticles when characterising the topical drug delivery profile for a novel nanomedicine (FIPSUB-1273). 75th FIP World Congress of Pharmacy and Pharmaceutical Sciences, Dusseldorf, Germany (2015).

R. Inacio, J. Cai, J. Keeble, S.A. Jones. The delivery of macromolecules to the skin by the application of local hypobaric pressure (PD-135). AAPS Biotechnology Conference, San Francisco, USA (2015).

K. Vandera, H. Chen, J. Cai, S. Baba Hamed, M.B. Baba Hamed, S.M.E.A. Abi-ayad, S.A. Jones. Novel inhaled medicines fabricated using natural cellulose nanocarriers (PP12). 1st CRS International Congress Greek Local Chapter in Small Molecules (Original-Generics) and Biotechnological Drugs (Biosimilars), Athens, Greece (2015).

Abstract

Topical nanomaterials can enhance the passive diffusion of therapeutic agents into biological tissues but the mechanism by which they function is not yet fully understood. The aim of this study was to elucidate the interactions between the model drug tetracaine and the surfaces of nanomaterials with the view to understand and optimise the transmembrane transport process. Tetracaine was observed to form aggregates in aqueous solutions in the μM range and this aggregation process changed its percutaneous permeation. Nanoparticles co-administered on the membrane surface upon drug application were shown to manipulate the drug aggregation, thereby enhancing transmembrane transport. Tetracaine adsorbed strongly to the surface of carboxyl-modified polystyrene nanoparticles ($Nano_{PSCOOH}$) and minimally to silica nanoparticles ($Nano_{SiO_2}$). The $Nano_{SiO_2}$ enhanced tetracaine transport by 3.6-fold while the $Nano_{PSCOOH}$ hindered tetracaine transport, leading to the conclusion that a mild perturbation of the tetracaine aggregation by a nanoparticle surface produced the most interesting effects in terms of transmembrane transport. These results were translated to a topical HPMC spray formulation. The co-administration of HPMC tetracaine spray formulation with $Nano_{SiO_2}$ enhanced tetracaine transport by 95-fold, improved accumulative by 307-fold and reduced the lag time by 15.6-fold when compared to the commercially available Ametop. The superiority was attributed to the $Nano_{SiO_2}$ breaking of tetracaine aggregates, known to hinder permeation. In addition, the decrease in formulation macroviscosity was hypothesized to have reduced drug-vehicle interactions and thus facilitate permeation. The strategy of utilising nanomaterials to manipulate drug aggregation described herein represents a potential technology platform worthy of clinical evaluation.

Table of Contents

List of Figures

List of Tables

List of Equations

List of Abbreviations

m_{45min}	Accumulative mass at 45 minutes
AR	Aspect ratio
AFM	Atomic force microscopy
BNF	British National Formulary
$Nano_{PSCOOH}$	Carboxyl-modified polystyrene nanoparticles
C	Concentration
ΔC_s	Concentration difference of solute across the membrane
$\frac{\partial C}{\partial x}$	Concentration gradient
C_B	Concentration of the bound tetracaine
C_v	Concentration of the drug in the vehicle
C_t	Concentration of the unbound tetracaine analysed at the time point
CAC	Critical aggregation concentration
CMC	Critical micellar concentration
D	Diffusion coefficient for the solute in the membrane
γ	Effective activity coefficient of the agent in the skin barrier phase
ER	Enhancement ratio
n_{final}	Final mass of the nozzle
$\lambda_{emission}$	Fluorescence emission wavelength
λ_{max}	Fluorescence emission wavelength at which maximum intensity occurs
FTIR	Fourier transform infrared spectroscopy

HPLC	High performance liquid chromatography
HCl	Hydrochloric acid
HPMC	Hydroxypropyl methylcellulose
C_0	Concentration of the initial tetracaine
$n_{initial}$	Initial mass of the nozzle
t_{lag}	Lag time
LOD	Limit of detection
LOQ	Limit of quantification
$n_{recover}$	Mass of the formulation recovered in the nozzle
D_{max}	Maximum diameter of spray film outline
D_{mean}	Mean diameter of spray film outline
D_{min}	Minimum diameter of spray film outline
NLC	Nanostructured lipid carriers
NIST	National Institute of Standards and Technology
ANOVA	One-way analysis of variance
K	Partition coefficient of the solute between the skin
k_p	Permeability coefficient of a permeant through a membrane
PCS	Photon correlation spectroscopy
PMT	Photonmultiplier tube
PCL	Poly(e-caprolactone)
PLA	Poly-lactic acid
PLGA	Poly(glycolic-co-lactic-acid)
PS	Polystyrene

SCCNP	Scientific Committee on Cosmetics and Non-Food Products
$Nano_{SiO_2}$	Silica nanoparticles
NaCl	Sodium chloride
SDS	Sodium dodecyl sulfate
SLN	Solid lipid nanoparticles
x	Space coordinate measured normal to the section
SD	Standard deviation
J_1	Steady state flux of tetracaine from the tetracaine
J_2	Steady state flux of tetracaine from the tetracaine-nanoparticle mixture
J	Steady state flux of the solute
$\propto$	Thermodynamic activity of the drug in its vehicle
h	Thickness of the membrane

CHAPTER ONE

General Introduction

1.1 Introduction

Drug delivery to the skin for both systemic (transdermal) and local (topical) actions has an important role in modern clinical practice. This is evident from the fact that the transdermal drug delivery market was worth US$ 25 billion in 2013 and it is anticipated to surpass US$ 40 billion by 2018 (Reuters, 2014). The systems used for drug delivery to the skin include transdermal patches, topical gels and topical spray formulations. For numerous drugs, these delivery systems represent an attractive alternative to other routes of administration, especially when the clinical condition is located in or close to the skin (Brown et al., 2006). For example, unlike the oral route, drug delivery to the skin can avoid the drug degradation in the gastrointestinal tract or the first-pass effect of the liver, which can metabolise a significant proportion of drugs prior to them reaching their site of action. Applying a drug to the skin also offers the possibility of sustained, localized and controlled release of drugs. Moreover, drug delivery to the skin is typically non-invasive and usually has high rates of patient compliance.

Despite the success of the topical and transdermal delivery products on the market, it is known that efficient drug delivery across the skin can be problematic to achieve due to the relative impermeability of the *stratum corneum* (Scheuplein & Blank, 1971). The main function of the *stratum corneum* is to regulate substance exchange, preventing exogenous materials from entering while minimising water loss from the body. This regulatory role of the skin restricts the type of molecules that can pass into the barrier. Researchers have translated this restrictive potential into a range of physicochemical

characteristics that drugs that can readily enter the skin by passive diffusion should possess – log P of between 1-3 (Hadgraft & Somers, 1956) and molecular weight of < 500 Da (Bos & Meinardi, 2000). A drug that does not possess these characteristics often requires to be administered to the skin tissue in the presence of a penetration enhancement strategy in order to try and get enough of the active compound to its site of action. Penetration enhancement strategies can be classified into physical and passive methods. Some of these approaches, such as electroporation and iontophoresis, have been found to be expensive. Other approaches, like chemical penetration enhancers and microneedles, disrupt the integrity of the *stratum corneum* and may present a potential issue in terms of tissue infection due to long-term damage of the skin (Williams & Barry, 2012). There is not, at present, a single system that can enhance the penetration of all compounds across the skin. Hence, an approach has been taken to develop numerous systems to account for the different types of molecules that need to be applied to the skin.

One skin penetration enhancement method that has received considerable attention into the skin is the use of nanomaterials (Prow et al., 2011). However, it is interesting to note that despite the vast surfaces areas that nanoparticles generate, drug-nanoparticle surface interactions remain poorly characterised in topical pharmaceutical systems. One area in which the interaction of drugs with nanoparticle surfaces is particularly important is when the drug is prone to molecular aggregation as it is possible that nanoparticles could have a role in regulating this process for the purpose of enhancing drug delivery into the skin. Therefore, there is a need to investigate further if drug-

nanoparticle surface interactions are important in the skin penetration enhancement of drugs applied using nanomaterials. To achieve that, knowledge of the manner in which nanomaterials influence the process of drug absorption is required. The first stage towards this goal is to understand the basic physiology of the skin layers and how nanoparticles interact with the skin barrier.

1.2 Skin barrier and the potential routes of drug absorption

The skin is the largest and heaviest organ of the human body, accounting for 10% of the body mass of an average person and a total area of nearly 2 m^2 (Williams, 2003). The main functions of the skin are to maintain homeostasis, to sense the external environment and to provide a protective barrier against foreign material ingress (Elias, 1983; Lee et al., 2006; Walters, 2002). This protective function is achieved primarily by its highly stratified structure. A comprehensive review of the structure of the skin and its barrier functions can be found in the literature and hence, a summary of its properties will be provided in this thesis (Barry, 1983; Elias, 1981; Scheuplein & Blank, 1971; Williams, 2003).

The skin constitutes 3 main tissue layers – the epidermis, the dermis and the hypodermis (Fig. 1.1); each consisting of different cells performing distinct functions. The epidermis has a multi-lamellar structure representing the different stages of cell differentiation. The *stratum corneum,* the outermost layer of the skin is treated as a separate membrane and the term viable epidermis is used to describe the other 4

underlying layers. In addition, there are 3 types of appendages originating from the dermis that traverse through the different skin layers – the hair follicle, the sebaceous gland and the sweat gland. It is important to understand each of these three layers in detail, as each of them can be a target for a drug after administration topically to the skin.

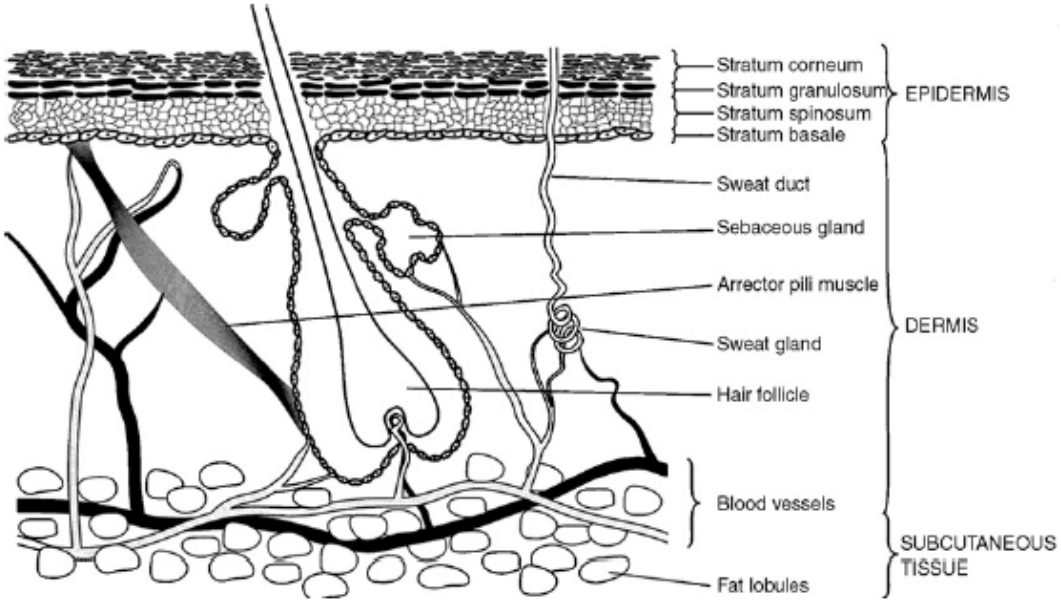

Figure 1.1. Structure of the skin. Obtained from Williams (2003).

1.2.1 *Stratum corneum*

The *stratum corneum* is the final product of the differentiation process, comprising of dead keratinized cells, known as corneocytes, interspersed within a lipid rich matrix. It has a thickness of 10 to 20 μm when dried (Christophers, 1971; Christophers & Kligman, 1964) and 40 μm upon hydration (Blank et al., 1967). The 'brick-and-mortar' model can explain the *stratum corneum* structure, with the 'bricks' composing of

corneocytes connected by corneodesmosomes and the 'mortar' consisting of multiple lipid layers of ceramides, fatty acids, cholesterol and cholesterol esters (Elias, 1983; Michaels et al., 1975). The *stratum corneum* serves as the rate-limiting barrier of drug delivery and is known to exhibit selective permeability, allowing only relatively lipophilic compounds to pass, given its lipophilic nature (Scheuplein & Blank, 1971). This skin layer accounts for more than 80% of the impermeability of the skin (Cevc, 1997) and when absent, has been shown to increase the diffusion of small water-soluble non-electrolytes into the systemic circulation by one thousand times (Barry, 2001).

1.2.2 Epidermis

The epidermis, a stratified squamous epithelium, is 100 to 150 μm thick (Bouwstra et al., 2003). It is thinner on the eyelids and thicker on certain body sites such as the palms and soles due to friction and weight bearing. Unlike the dermis, blood vessels and nerve endings are absent in this skin region and thus, nutrients, waste products and drug molecules must permeate across the epidermis, cross the dermo-epidermal layer, in order to enter systematic circulation (Williams, 2003). Approximately 95% of the epidermis comprises of keratinocytes, which arise from the *stratum basale* and undergo progressive differentiation, known as keratinisation or cornification, while migrating towards the *stratum corneum.* This differentiation process is characterised by the formation of keratin and lamellar bodies (responsible for the secretion of *stratum corneum* lipids) and ultimately, the loss of its nuclei and organelles to form corneocytes (Fig. 1.2). The main function of keratinocyte differentiation is to maintain the *stratum*

corneum through the replenishment of *stratum corneum* lipids and corneocytes (Eckert, 1989). The other 5% of cells present in the epidermis include Langerhans cells, which are involved in immunity, melanocytes, which are responsible for skin pigmentation and Merkel cells, which contribute to sensory response (Dragicevic & Maibach, 2015).

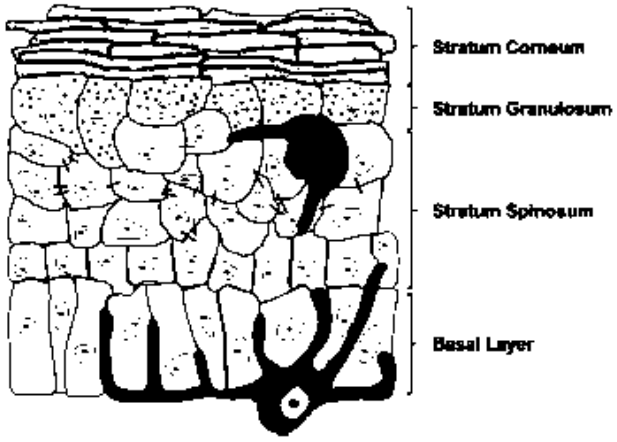

Figure 1.2. Epidermis depicting different levels of differentiation of keratinocytes. Obtained from Dragicevic & Maibach (2015).

1.2.3 Dermis

The dermis is 3 to 5 mm thick and it makes up the bulk of the skin (Barry, 1983). The predominant cells are fibroblasts found in an interwoven network of fibrous proteins (collagen, elastin, reticulin) embedded in the extracellular matrix. The fibroblasts are responsible for synthesizing the extracellular matrix. The collagen fibres provide structural support while the elastin fibres provide flexibility, cushioning the body from stress and strain (Wilkes et al., 1973). The dermis can be further categorised into the upper papillary layer and the lower reticular layer. The papillary layer is thin and has mainly reticular fibres with lesser amounts of collagen and elastin while the reticular

layer is thick and has mainly collagen and elastin networks with smaller amounts of reticular fibres (Kanitakis, 2002).

Cells that are involved in immunity and mobilising defence such as macrophages and dendritic cells are also present in the dermis (Dragicevic & Maibach, 2015). The dermis also incorporates nerve endings, blood vessels and lymphatic vessels. The blood supply is responsible for thermal regulation, delivery of oxygen and nutrients to the skin and removal of toxins and waste products. The lymphatic system serves to regulate interstitial pressure, facilitate immunological responses and waste removal. When delivering drug to the skin, it is this maintenance of concentration gradient between the applied formulation and the vasculature that provides the driving force for drug permeation (Scheuplein & Blank, 1971). Dermal blood flow is responsible for the clearance of relatively small solutes (e.g. lidocaine) while the lymphatic flow provides clearance for larger molecules (e.g. interferon)(Cross & Roberts, 1993). There are appendages found on the human skin that originate in the dermis and will be elaborated in Section 1.2.5.

1.2.4 Hypodermis

The hypodermis is the innermost layer of the skin, typically in order of a few millimetres, consisting of subcutaneous fat tissues. It is absent in some areas of the body such as the eyelids. The main cell type present in the hypodermis is the adipocytes. This layer of adipose tissue functions as a thermal insulator for the body, a mechanical

cushion against physical shock and a reserve depot of readily available high-energy molecules (Kanitakis, 2002).

1.2.5 Appendages

There are three main types of skin appendages that traverse from the dermis to the skin surface: hair follicles, sebaceous glands and sweat glands (eccrine or apocrine)(Fig. 1.3). Hair follicles are found over the entire surface of the skin except for the lips, palms and soles. The sebaceous gland associated with the hair follicle produces sebum, comprising of free fatty acids, cholesterol, cholesterol esters, squalene (Stewart, 1992). The sebum lubricates the skin surface and maintains the skin surface acid mantle of approximately pH 5 (Katz & Poulsen, 1971). Eccrine sweat glands are present on most of the body (at a density of 200-250 /cm^2 of skin)(Szabo, 1962). When stimulated in response to heat and emotional stress, the glands secrete sweat, a dilute salt solution at a pH around 5. On the other hand, apocrine glands are larger and are limited to specific areas of the skin such as the axillae, nipples and ano-genital regions. They open into the hair follicle and secrete lipodal and ‘milk’ proteins, which are responsible for producing the characteristic odour of sweat (Williams, 2003).

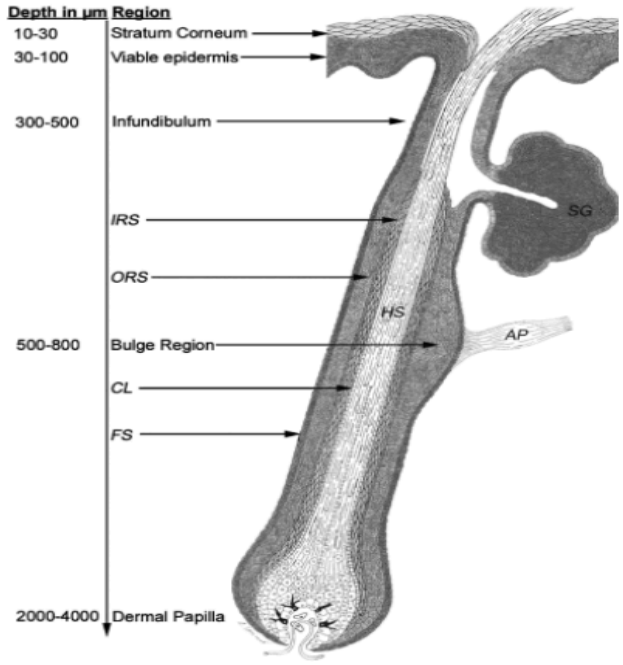

Figure 1.3. Target structures of terminal hair follicles depicting the hair follicle (HF), outer root sheath (ORS), inner root sheath (IRS), companion layer (CL), fibrous sheath (FS), sebaceous gland (SG) and arrector pilli (AP). Obtained from Toll et al. (2004).

Knowledge of the skin barrier and function enables the understanding of the routes of drug administration into the skin. This is important because topical drug delivery must be understood in terms of the drug properties, the type of formulation, the transport route and the site of action in the skin. Only if the principles of drug delivery to this unique barrier are understood can a mechanism of penetration enhancement, such as the use of nanocarrier, be investigated. Therefore, the subsequent section will elucidate the current knowledge regarding the routes of drug entry into the skin in order to understand in greater detail the challenges posed when attempting to deliver a topically administered drug into the tissue.

1.2.6 Routes of drug permeation across the skin

When a therapeutic drug is applied as a formulation to intact skin, the drug goes through processes before permeating through the skin. Firstly, the drug incorporated in a vehicle has to partition out of the vehicle, onto the surface of the skin. Only drug molecules at the vehicle-skin interface can further partition into the outermost layer of the *stratum corneum* and diffuse through the skin. The latter is considered the main barrier to drug delivery through the skin. Compounds can traverse the skin by passive diffusion using three main pathways (Fig. 1.4): 1) the transcellular pathway, between the corneocytes; 2) the intercellular pathway, crossing through the corneocytes and the interspersed lipids; and 3) the transappendageal pathway (shunt route transport, i.e. hair follicles and sweat glands)(Scheuplein, 1965).

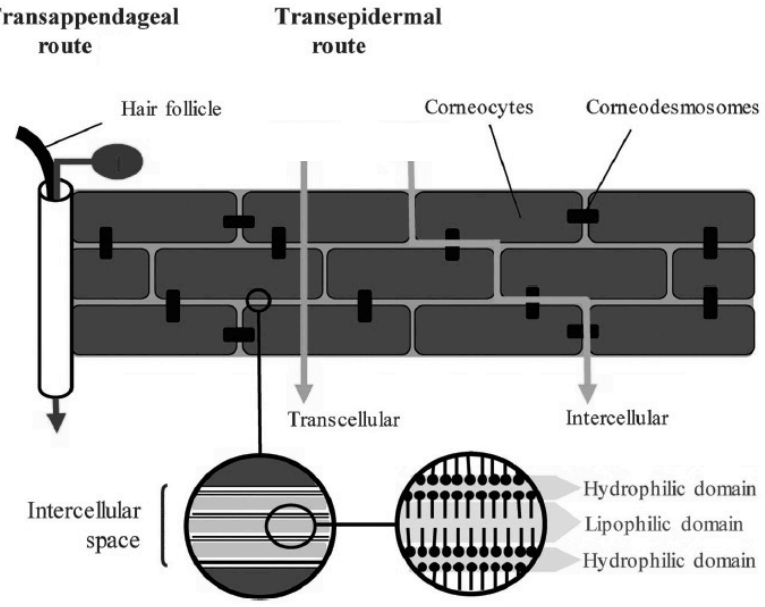

Figure 1.4. Routes of drug permeation. Obtained from Hadgraft & Lane (2011).

In the transcellular pathway, molecules partition into and diffuse across both corneocytes and intercellular lipid lamellae. Although this pathway provides a shorter route and larger surface area to cross the *stratum corneum*, the repeated diffusion across hydrophilic and lipophilic domains makes the transcellular pathway highly unfavourable. As such, the intercellular pathway is the preferred pathway (Albery & Hadgraft, 1979; Hadgraft & Guy, 1989). In the intercellular pathway, molecules can navigate across the tortuous path within the intercellular lipids surrounding the corneocytes (Menon & Ghadially, 1997; Michaels et al., 1975). After the molecules penetrate the *stratum corneum*, they arrive at the *stratum corneum*/viable epidermis interface where they must partition and diffuse into the hydrophilic viable epidermal tissue before reaching the epidermis/dermis junction. At this junction, the molecule has to repeat the partition and diffusion process into a more hydrophilic dermis to progress any further.

The transappendageal pathway provides a penetration route that circumvents transport across the *stratum corneum* barrier. It makes use of hydrophilic natural openings that can be up to a few microns in size (Pegoraro et al., 2012). However, as the skin appendages occupy only 0.1% of the skin surface (Scheuple, 1967), it is widely considered that this route of entry into the skin is not the principle mechanism whereby most topically applied drugs penetrate into the tissue. The transepidermal (transcellular and intercellular) pathway is usually regarded the principal means of entry for therapeutic agents (Williams, 2003). However, it would be over simplistic to assume that the transappendageal pathway does not play a role in drug permeation because it is

feasible that the 3 routes of permeation mentioned herein can occur concomitantly and the relative contribution is determined by several factors including the nature of the permeant, the components of the formulation, the type of administration system and of the mechanism of action of enhancement strategies that are applied to the delivery system.

1.2.7 Influence of compound physicochemical properties on drug transport

The drug permeation route is dependent on the size and polarity of the drug. Polar or hydrophilic compounds are more likely to traverse through the transcellular pathway (Barbero & Frasch, 2006), while lipophilic compounds are more likely to be transported *via* the intercellular pathway (Abraham et al., 1995). Lipophilic drugs may be retained in the lipophilic *stratum corneum* and partitioning into the more hydrophilic viable epidermis may be deterred, thus making the *stratum corneum* the rate-limiting step for the drugs. On the other hand, the transappendageal pathway plays a more important role for hydrophilic molecules such as caffeine (Otberg et al., 2008), which would encounter more resistance from the *stratum corneum* (Barry, 1987). The transappendageal pathway also contributes to the delivery of vesicular structures through the skin. It is debatable if vesicles can penetrate the *stratum corneum* intact, but these structures are known to penetrate into the pilosebaceous units (Lauer et al., 1996).

Knowledge regarding the routes of delivery through the skin can help understand the movement of drug molecules applied to the surface of the tissue as a topical formulation

into the underlying barrier. However, it is important to appreciate that the means by which topical products are formulated can alter the route taken by drugs as the relative importance of each pathway can change depending on the manner the administration method applied the drugs to the skin. For example, the transappendageal pathway is central in iontophoretic drug delivery, which uses electrical charge to drive molecules into the skin. Drugs are more likely to penetrate into the appendages because they provide less resistance than the *stratum corneum*. Therefore, information regarding the formulation properties of a topical product must be integrated with the route of delivery into the skin and the site of action of the drug. To help understand how formulations act to deliver molecules into the skin, the mathematical models that describe this process are usually employed.

1.3 Mathematical models

Drug permeation through the skin often requires the drug to partition and diffuse through the vehicle, *stratum corneum* and epidermis, as is the case for a wide range of drugs. Their site of action is within the viable cells of the skin. This process is dependent on a number of factors related to the physical, chemical and biological properties of the molecules and the skin tissue. To try and simplify the multitude of parameters that can influence skin drug delivery, researchers have attempted to develop a series of mathematical models that simplify the process, usually by considering only the most important elements in the permeation process.

1.3.1 Fick's 1st law

The definition of the *stratum corneum* as the main barrier has allowed several relatively simple mathematical relationships to describe the drug permeation process because the skin is simplified to represent a single homogenous membrane. As the transport through this barrier is passive, i.e., it is energy independent, diffusion through the skin it is underpinned by Fick's 1st Law (Moser et al., 2001):

$$J = -D \frac{\partial C}{\partial x} \qquad \text{(Equation 1.1)}$$

where J is the steady state flux of the solute, D is the average diffusion coefficient for the solute in the membrane, $\frac{\partial C}{\partial x}$ is the concentration gradient, C is the concentration and x is the space coordinate measured normal to the section. The most common form of Fick's law is in its integrated form (Scheuplein & Blank, 1971):

$$J = \frac{KD\Delta C_s}{h} \qquad \text{(Equation 1.2)}$$

where K is the partition coefficient of the solute between the skin and vehicle, ΔC_s is the concentration difference of solute across the membrane and h is the thickness of the membrane.

The permeability coefficient (k_p) of a permeant through a membrane can be expressed as:

$$k_p = \frac{KD}{h} \qquad \text{(Equation 1.3)}$$

which can be substituted into the previous equation (Eq. 1.3) to give:

$$J = k_p \Delta C_s \qquad \text{(Equation 1.4)}$$

An appreciation of these equations enables the process of drug permeation to be described. The parameters that influence them have to be identified and consequently, the means by which penetration enhancement strategies act to accelerate molecule entry into the skin can be investigated using these models. There is however, like in all areas of science, debate in the published literature regarding the most important parameters in the equations and this can be exemplified by the Higuchi's equation.

1.3.2 Thermodynamic activity and the Higuchi's equation

In 1960, Higuchi adapted Fick's 1st Law in order to highlight the importance of drug thermodynamic activity (Higuchi, 1960), which was,

$$J = \frac{\propto D}{\gamma h} \qquad \text{(Equation 1.5)}$$

where $\propto$ is the thermodynamic activity of the drug in its vehicle and γ is the effective activity coefficient of the agent in the skin barrier phase. This laid down a seminal principle for a number of modern theories to follow in subsequent years. This approach stated that an ideal saturated system, where the drug solute is dissolved in a solution that is in equilibrium with the solid state exhibiting a thermodynamic activity of unity ($\propto = 1$), should result in the same penetration rate irrespective of the vehicle composition or drug concentration. There are three important assumptions made in Higuchi's idealised scenario – 1) the system is homogenous. This applies to the drug, vehicle and membrane and assumes there are no interactions between the constituents (drug, vehicle, polymer etc.) and the membrane; 2) the thermodynamic activity of the drug in the vehicle is homogenous throughout the system; 3) the membrane determines the rate of drug permeation. In practice, very few topically applied pharmaceutical systems meet all of these criteria, but with consideration of drug-vehicle-membrane interactions, it is possible to use this relationship in a comparative manner to analyse transport data (Walters, 2002).

1.4 Enhancement strategies

Increased understanding of the skin barrier and the drug permeation models have led to an emergence of different approaches to overcome the *stratum corneum* barrier and enhance drug delivery across the skin. The strategies that have been developed can be classified according to their mode of action, i.e. physical and passive approaches (Fig. 1.5).

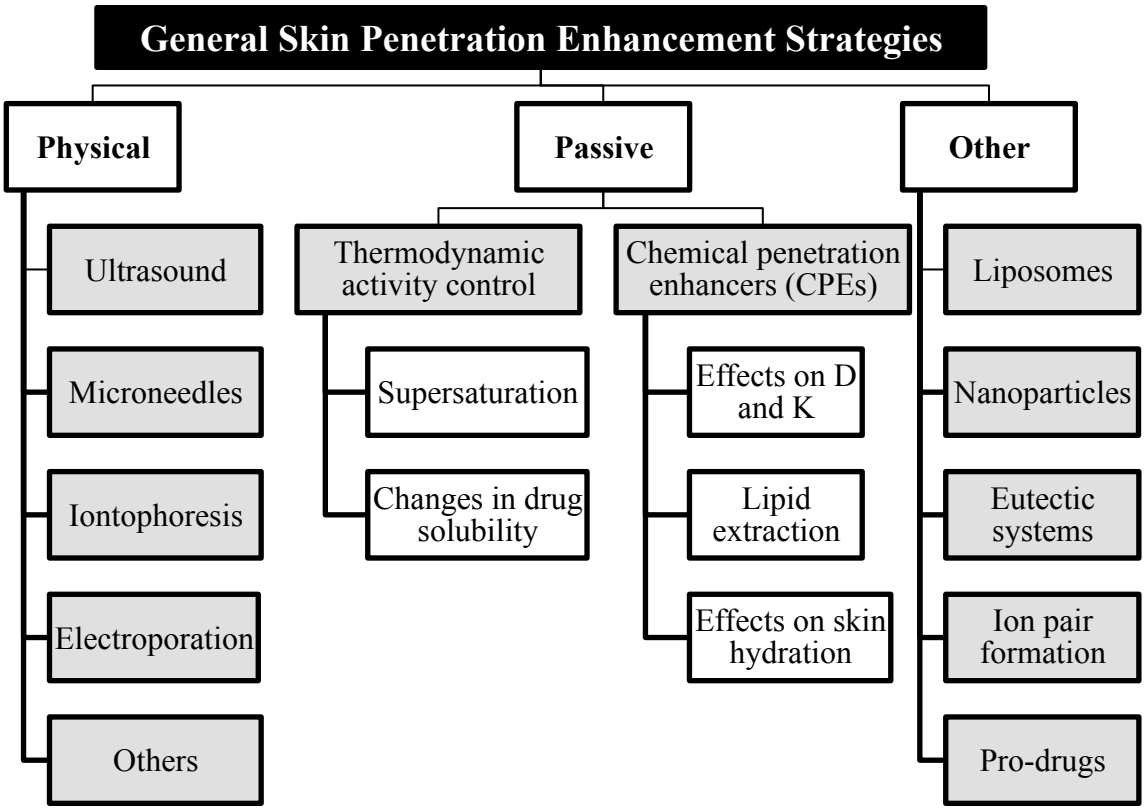

Figure 1.5. General skin penetration enhancement strategies obtained from Hadgraft & Lane (2011).

Drug transport can be increased by physical means through: 1) increasing skin permeability *via* the provision of a transport driving force or in some circumstances, disruption of the *stratum corneum* lipid bilayers (e.g. ultrasound, iontophoresis, electroporation); 2) bypassing the *stratum corneum* barrier (e.g. microneedles, jet injection); and 3) removing the *stratum corneum* (e.g. thermal ablation). However, these approaches can be expensive, difficult to self-administer and present the potential for significant side effects due to the damage induced to the *stratum corneum* (Williams & Barry, 2012).

Passive enhancement strategies seek to manipulate the permeation characteristics of the drug by optimising the partition coefficient (K) and the diffusion coefficient (D) of the permeating molecule *via* the co-administration of formulation excipients that act as chemical penetration enhancers. The changes brought about by the formulation excipients can be induced through the manipulation of the skin properties or by the changes in the physical interactions in the formulation. Both these penetration enhancement methods can have potential drawbacks. For example, if chemical penetration enhancers elicit their activity by fluidizing the *stratum corneum* lipid, this leads to a temporal decrease in its barrier function and can change its hydration, which can induce skin sensitization, irritation and toxicity (Prausnitz & Langer, 2008).

An ideal drug enhancement strategy would increase drug permeation without perturbing the skin, be economical, safe to use and easy to apply. One penetration enhancement strategy that has the potential to fulfil these criteria is the use of nanomaterials.

1.5 Nanomaterials

According to the British Standards Institution (2007), the term ‘nanoscale’ encompasses structures with a size range of 1-100 nm. In drug delivery, the size of nanomaterials ranges from a few nm to 1000 nm (Fig 1.6)(Donnelly & Singh, 2015). Between 2010 and 2013, the emerging nanotechnology market has increased 40-45% per year from $339 billion in 2010 to more than $1 trillion in 2013 (National Science Foundation, 2014). In 1986, L’Oreal (online) introduced the first nanometric skin product to the

world, the Niosome, which proved to be an efficient transporter of active ingredients such as retinol or vitamin E and more companies have followed suit. Nanomaterials can be categorised into vesicular carriers and rigid nanoparticles. Vesicular carriers stem from conventional liposomes and have been developed to include niosomes, ethosomes and transfersomes to name a few. Rigid nanoparticles can be further classified based on their materials into lipid, polymeric, metal and ceramics. To understand how these nanomaterials enhance the topical delivery of agents into the skin, one must understand how the different nanomaterials are classified, produced and by which important properties they can be characterised.

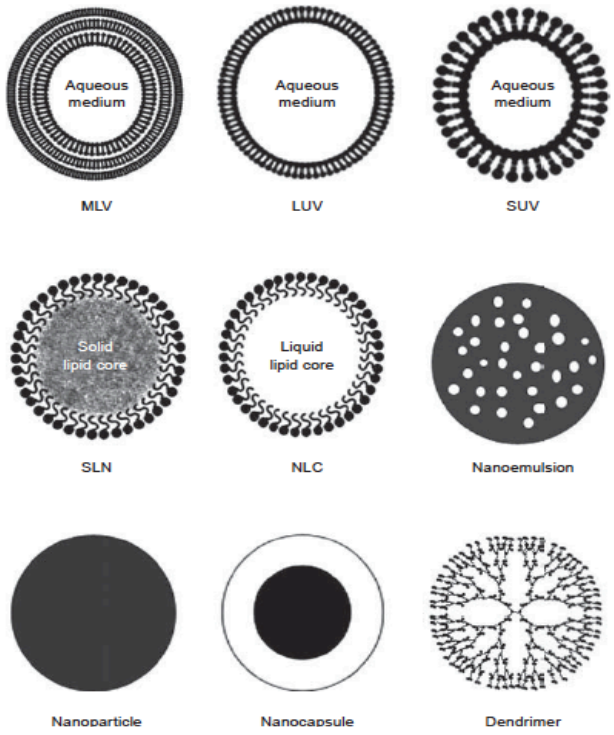

Figure 1.6. Different types of nanomaterials depicting multilamellar vesicle (MLV), large unilamellar vesicle (LUV), small unilamellar vesicle (SUV), solid lipid nanoparticle (SLN), nanostructured lipid carrier (NLC), nanoemulsion, nanoparticle, nanocapsule and dendrimer. Obtained from Walters (2002).

1.5.1 Types of nanomaterials

1.5.1.1 Vesicular carriers

Liposomes are vesicular carriers consisting of phospholipids and cholesterol. These vesicle structures are typically 10-1000 nm in size (Walters, 2002). By varying the composition of the lipid and method of preparation, the physicochemical properties of liposomes (size, charge and deformability) can be changed to suit the needs of application. Liposomes can be formed of one or more concentric bilayers forming spherical colloids with an enclosed inner aqueous core (Mezei & Gulasekharam, 1980). Both hydrophilic and hydrophobic drugs can be incorporated into the liposome, with the former located in the aqueous space inside the colloid, in contact with the polar head region (hydrophilic moiety) of the liposome, and the later solubilised in the lipophilic bilayers of the liposome. Conventional liposomes can be further developed into new types. An exhaustive list has recently been compiled by Wagner and Vorauer-Uhl (2011).

1.5.1.2 Lipid nanoparticles

Lipid nanoparticles may be categorised into solid lipid nanoparticles (SLN) and nanostructured lipid carriers (NLC) and can be distinguished based on their solid matrix organization. SLN comprise of a single lipid that solidifies at room temperature and have crystalline matrices. The drug is either entrapped in the core or dispersed in the solid lipid matrix. The crystalline matrix of the SLN gets perturbed when large amounts

of drug are added and thus, drug loading within the matrix is limited. The drug molecules in such cases may adsorb onto the surface or separate from the particles (Fireman et al., 2011). However, NLCs are made of both solid lipids and liquid lipids that blend into a distorted crystalline lattice structure when solidified. The drug is incorporated into its core and the average particle size of these nanomaterials is 50-1000 nm (Schäfer-Korting et al., 2007). NLCs were considered as an improvement of the SLNs, as they exhibited a higher loading capacity of drugs, required lesser water to encapsulate the drug and were less likely to expel its contents during storage (Mehnert & Mader, 2001).

1.5.1.3 Polymeric nanoparticles

The polymeric nanomaterials investigated for skin enhancement strategies include polystyrene (PS), poly-lactic acid (PLA), poly(glycolic-co-lactic-acid)(PLGA), poly(e-caprolactone)(PCL) and dendrimers (Guterres et al., 2007; Valenta & Auner, 2004). Non-biodegradable polymers, such as PS, have been shown to encapsulate the active ingredient, penetrate into the superficial layers of the *stratum corneum* and release its contents into deeper skin layers (Alvarez-Roman et al., 2004a).

Biodegradable polymers, i.e. PLA, PLGA and PCL, exhibit excellent biocompatibility and degrade naturally, avoiding the potential cytotoxicity that their non-biodegradable counterparts present (Kumari et al., 2010). Based on their composition, these materials can be further categorised into nanocapsules or nanospheres. Nanocapsules contain oil

and have a vesicular structure, while nanospheres have a matrix organisation of polymers (Guterres, Alves et al., 2007). The drug can be entrapped within or adsorbed on the surface of both types of nanoparticles.

1.5.1.4 Metal oxide nanoparticles

Metal oxide nanomaterials can be used to administer drugs to the skin. This has a basis in the fact that metal oxides (i.e. titanium oxide and zinc oxide) are commonly used to protect the skin against UV damage due to their ability to scatter light. They are usually coated with aluminium oxide, silica dioxide or silicon oils to increase dispersion stability, resulting in a size of about several mm for titanium oxide and 30 to 200 nm for zinc oxide (Baroli, 2010b). Sunscreen formulations should remain on the skin surfaces to scatter light and not penetrate into the deeper layers. Gontier et al. (2008) used transmission electron microscopy and scanning transmission ion microscopy to investigate the penetration abilities of titanium oxides ranging from 20 to 100 nm using different skin samples such as porcine skin and healthy human skin. The authors concluded that titanium oxides nanoparticles are confined within the first 3 to 5 corneocyte layers of the *stratum corneum*. In an earlier study by Pflucker et al. (2001) using electron microscopy and light microscopy visualisation, titanium dioxide with different surface characteristics ranging from 20-100 nm were found deposited on the outermost surface of the *stratum corneum* and were absent in deeper layers of the *stratum corneum* and beyond. A similar observation was reported using titanium oxide of the same size range (20-100 nm) using different surface coatings (Schulz et al.,

2002). Transmission electron microscopy and particle-induced-X-ray emission analysis of 20 nm titanium oxide indicated that 90% of the titanium oxide particles were recovered in the *stratum corneum* and the rest were localized in the furrows and opened infundibulum of the skin, suggesting some importance of the transfollicular route (Mavon et al., 2007). The most important investigation to date was the series of *in vivo* and *in vitro* studies performed by the EU Scientific Committee on Cosmetics and Non-Food Products (SCCNFP) in 2000 on titanium oxide within 10 to 1000 nm. All the studies concluded that titanium oxide nanoparticles are confined on the skin surface or on the outer layer of the *stratum corneum* and do not penetrate into the living skin. Zinc oxide nanoparticles, the other nanoparticle often used in sunscreens, are also impeded by the *stratum corneum*. Roberts et al. (2008) demonstrated 30 nm zinc oxide particles did not penetrate into the human skin through *in vitro* and *in vivo* techniques using multiphoton tomography. This is in accordance with the results obtained by Cross et al. (2007) using transmission electron microscopy to observe the *in vitro* penetration of zinc oxide of approximately 30 nm. All the above reports suggest that metal nanoparticles are unlikely to penetrate the *stratum corneum*.

1.5.2 Nanomaterial-facilitated drug penetration across the skin

The wide number of studies that have reported that nanomaterials enhance the permeation of drugs across the skin has drawn attention to their mode of action (Table 1.1). For example, podophyllotoxin-loaded SLNs with an average diameter of 35 to 210 nm demonstrated a ~4-fold increase in drug permeation as compared to their

hydroalcohol counterparts with no nanoparticles (Chen et al., 2006). A 3.45-fold increase in drug flux permeation from triptolide loaded SLNs as compared to aqueous solutions was also observed (Mei et al., 2003). Adapalene-loaded PLGA particles with the topical aqueous gel required 10-fold less concentration were also shown to achieve the same pharmacological activity as that without nanoparticles (Rolland et al., 1993).

There are several crucial questions that arise in understanding the enhancement mechanism. Firstly, does the nanomaterial stay on the surface and release its contents into the skin or does it penetrate into the skin and release its contents? If so, does the nanomaterial penetrate intact? In order to answer these questions, a review on nanomaterial penetration through the skin is important (Table 1.2).

Some investigations have shown that nanoparticles are able to penetrate through the skin. For example, Cevc and Blume (1992) suggested the intact permeation of elastic deformable liposomes (transfersomes) into the dermis layer. Baroli et al. (2007) demonstrated that rigid magnetic nanoparticles smaller than 10 nm can penetrate into the *stratum corneum*. Ryman-Rasmussen et al. (2006) also showed that quantum dots with a particle size of 4.6 to 12 nm penetrated into the epidermis and dermis layers of intact porcine skin. However, these studies focus on very small nanomaterials. The majority of nanomaterials used to facilitate molecular penetration into the skin involves objects with a size of greater than 20 nm and there is a wealth of data that suggest that these materials do not penetrate beyond the superficial layers of the *stratum corneum* into the deeper living tissue (viable epidermis and dermis)(Table 1.2).

Nanomaterials	Barrier	Control vehicle	Residence in skin (ER)	Penetrate to receptor (ER)	Proposed mechanism	References
SLNs (35-210 nm)	*In vitro* permeation, full-thickness porcine skin	Hydroalcohol vehicle	3.84	No	Drug carrier	(Chen et al., 2006)
SLNs and NLCs (150-250 nm)	*In vitro* permeation, full-thickness porcine ear skin	Oil-in-water cream	4 (SLN); 3 (NLC)	-	Drug carrier	(Borgia et al., 2005)
SLN (150-200 nm)	*In vitro* permeation, full-thickness porcine skin	Oinment	3 - 4	Decreased	Drug carrier	(Jensen et al., 2011)
PLGA (320 nm)	*In vitro* permeation, full-thickness porcine ear skin	Non particle form	Yes with massage	-	Hair follicle reservoir	(Lademann et al., 2006)
PS (20, 200 nm)	*In vitro* permeation and tape stripping, full-thickness porcine ear skin	Water vehicle	Yes	-	Hair follicle reservoir	(Alvarez-Roman et al., 2004a)
PCL (40 and 130 nm)	*In vitro* permeation, Hairy guinea pig skin	30% ethanol	1.5	1.7	Hair follicle reservoir	(Shim et al., 2004)
TiO2 (20-50 nm)	*In vitro* permeation, full-thickness porcine skin	10% DMSO solution	Slight increase	4	Barrier interaction	(Peira et al., 2014)
SLN (200-400 nm)	*In vitro* permeation and tape stripping, full-thickness human skin	Hydrogel	3	Reduced	Barrier interaction	(Puglia et al., 2008)
PMMA and PBC (N.A.)	*In vitro* permeation, hairless mouse skin	Water vehicle	-	2	Barrier interaction	(Cappel & Kreuter, 1991)
SLN (280 nm)	*In vivo* tape stripping, human skin	Oil-in-water cream	2	-	Barrier interaction	(Dingler et al., 1999)
SLN (120-180 nm)	*In vitro* permeation, full-thickness rat skin	Water vehicle	-	3.45	Changing drug properties	(Mei, Chen et al., 2003)
PCL (202 and 277 nm)	*In vitro* permeation, human skin epidermis and *in vivo* tape stripping, full thickness human skin	Hydrophilic gel	Yes	-	Changing drug properties	(Alves et al., 2007)
SLN (185 and 330 nm)	*In vitro* permeation and tape stripping, full-thickness porcine skin		3.4 (SC) and 1.3 (Viable epidermis)	-	Changing drug properties	(Fangueiro et al., 2012)

Table 1.1. Permeation enhancement summary of nanomaterial, where ER represents the enhancement ratio due to the the addition of nanomaterials.

Particle type	Diameter (nm)	Skin type	Permeation	References
Iron oxide	10	Human	Yes	(Baroli, Ennas et al., 2007)
Quantum dots	4.6-12	Porcine	Yes	(Ryman-Rasmussen et al., 2006)
TiO_2	20-50	Human	No	(Pflucker, Wendel et al., 2001)
TiO_2	20-100	Human	No	(Schulz, Hohenberg et al., 2002)
TiO_2	30	Porcine	No	(Gamer et al., 2006)
TiO_2	20	Human	No	(Stracke et al., 2006)
TiO_2	20	Human	No	(Mavon, Miquel et al., 2007)
TiO_2	20-100	Porcine, human	No	(Gontier, Ynsa et al., 2008)
ZnO	80	Porcine	No	(Gamer, Leibold et al., 2006)
ZnO	30	Human	No	(Cross, Innes et al., 2007)
ZnO	20-30	Human	No	(Zvyagin et al., 2008)
ZnO	30	Human	No	(Roberts, Roberts et al., 2008)
PS	20, 200	Porcine	No	(Alvarez-Roman et al., 2004a)
PS	750-6000	Human	No	(Toll, Jacobi et al., 2004)
PLGA	300	Human	No	(Stracke, Weiss et al., 2006)
PLGA	300	Human	No	(Luengo et al., 2006)
PLGA	320	Porcine	No	(Lademann et al., 2007)
PS, PMMA	<100	Porcine	No	(Wu et al., 2009)
PLA	200-400	Human	No	(Rancan et al., 2009)

Table 1.2. Summary of rigid nanomaterial penetration through the skin.

The transappendageal pathway may also play a role in nanomaterial interaction with the skin (Fig 1.7)(Blume-Peytavi et al., 2010; Knorr et al., 2009; Meidan, 2010; Schaefer & Lademann, 2001). However, the skin barrier extends to include the follicles, albeit it allows a recess in its continuum, and they should theoretically prevent nanomaterials

from penetrating into the living skin (Langbein et al., 2002; Rancan et al., 2012; Toll, Jacobi et al., 2004). Nevertheless, hair follicles, sweat glands and pores can act to encourage nanomaterial accumulation and subsequently drug deposition. Nanomaterials are known to aggregate in the hair follicle openings or skin furrows without penetrating into living skin (Lademann et al., 1999; Mavon, Miquel et al., 2007). They can be stored until cleared by hair growth or sebum production. As clearance in regions of the skin are much slower compared to the skin surface due to avoidance from natural desquamation, contact and washing on the skin surface, the pores, hair follicles and sweat glands provide an excellent depot for the drugs (Lademann et al., 2005; Lademann et al., 2007; Schaefer & Lademann, 2001). The penetration of nanomaterials in the hair follicle is also size dependent, with smaller nanomaterials penetrating deeper into the hair follicle (Alvarez-Roman et al., 2004a; Toll, Jacobi et al., 2004; Vogt et al., 2006). It is thought that the hair follicle orifices need to be open and this can be achieved during sebum production and/or active hair growth (Lademann et al., 2001; Otberg et al., 2004).

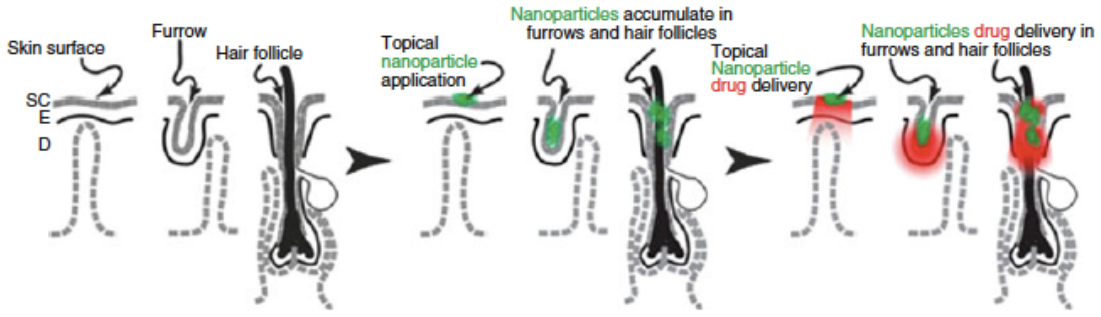

Figure 1.7. Deposition of drug from nanomaterials *via* the transappendageal pathway. Obtained from Dragicevic & Maibach (2015).

There is limited data on skin penetration of nanoparticles through diseased or damaged skin. Hypothetically, nanoparticles could penetrate through diseased skin lesions more efficiently due to the damaged *stratum corneum*, inflammation and increased keratinocyte turnover. However, the current available data seemed to suggest otherwise. The Australian Government Therapeutic Goods Administration (2006) highlighted a toxicokinetic *in vivo* assessment of human diseased skin, which did not detect an increase in systemic zinc levels following application of zinc oxide nanoparticles. Similarly, using a multi-photon imaging technique, Prow et al. (2011) did not observe the penetration of 35 nm zinc oxide through skin lesions. The same concern can be applied to flexed skin where mechanical stress on the skin can make the skin more permeable for nanoparticles. Tinkle et al. (2003) showed that human skin treated with 1 μm beads and then flexed for 60 min resulted in dermal penetration of the beads. However, the data from the flexing experiment was not reproducible when applied to 35 nm zinc oxide (Prow et al., 2011). Lademann et al., has also shown no penetration of nanoparticles in the stratum corneum after massaging. Overall, the current evidence suggests that nanoparticles do not penetrate through the skin, healthy or modified.

Given the increased attention to the use of nanomaterials, concerns have also been raised about the possible risks that they may bring. There are mixed reviews on the toxicity of nanomaterials. While some data reports that nanomaterials are safe to use, others show that the cellular uptake of nanomaterials may eventually perturb cellular pathyways and induce toxicity (Nohynek et al., 2007, 2008, Newman et al., 2009, Borm et al., 2006., Baroli et al., 2010b, Oberdörster et al., 2005). The latter would raise more

concerns if nanoparticles penetrated into viable skin and the weight of current evidence show otherwise, that nanoparticles do not penetrate beyond the *stratum corneum* and does not pose a health risk.

1.6 Interpreting nanomaterials drug-facilitated transport using traditional skin penetration models

Although the drug enhancement effect of nanomaterials in skin drug delivery is widely accepted, the mechanism of permeation enhancement remains unknown (Table 1.2). It is possible that small flexible nanomaterials such as ethosomes and transfersomes could enhance penetration into the skin by direct entry into the barrier (Honeywell-Nguyen et al., 2004). However, it is unlikely that such a mechanism of action applies to rigid solid nanomaterials with a size greater than 20 nm, i.e., the nanomaterials most regularly employed in drug delivery studies, because they are too large to pass into the skin, as discussed in Section 1.5.2. As such, drugs must be released at or near the skin surface before they can further permeate the skin. In these cases, enhancement of drug transport can be achieved by acting as a drug carrier, modifying the membrane barrier or changing the physical drug interactions in the formulation, each of these potential mechanisms of action will be subsequently explained in further detail below (Fig. 1.8).

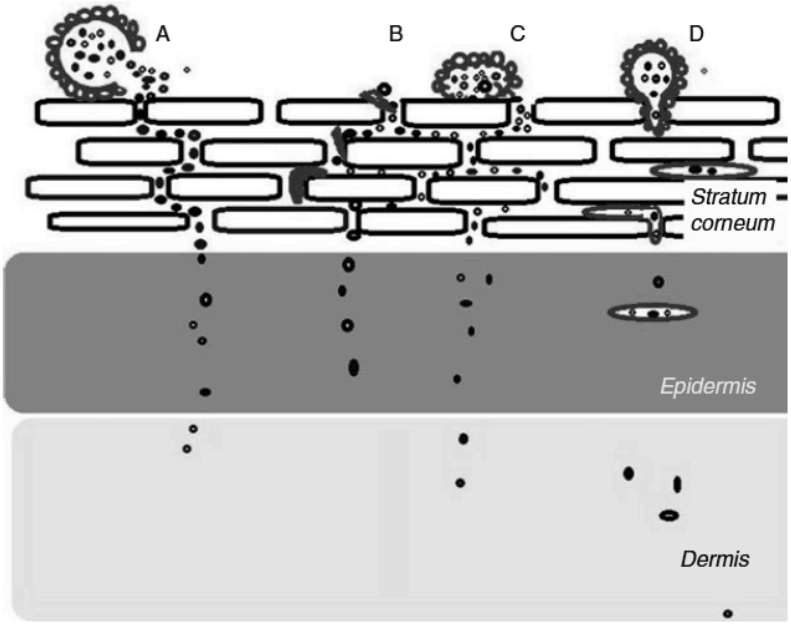

Figure 1.8. Possible mechanisms of nanomaterials. Nanomaterials may A) act as a drug carrier and deposit the contents at the skin surface; B) act as a penetration enhancer and modify the skin surface such that drugs easily permeate through; C) form an occlusive layer or fuses with the skin membrane to enhance drug permeation; or D) penetrate through the drug as intact vesicles to deposit the drug in deeper layers of the skin. Obtained from El Maghraby et al. (2006).

1.6.1 Action as a drug carrier

Traditionally, larger particles such as microparticles are used as carriers – to load, store and release the drug. Nanoparticles can have the same function. When used as a carrier, nanomaterials can be used to mask colour and odour (Kuelkamp-Guerreiro et al., 2013; Souto et al., 2005), control release of drugs across the membrane (Jenning et al., 2000; Puglia et al., 2008) and provide chemical protection through immobilisation of the active until release by the particle (Dingler et al., 1999; Trombino et al., 2009). They have been proposed to have the potential to target certain cells and can be designed to avoid immunogenic pathogens of the body (Fireman, Toledano et al., 2011). The drug

can either be incorporated into or deposited on the surface of the nanomaterial when it acts as a carrier.

There are three ways, depending on their ultimate fate, in which nanomaterials may deposit their drug into the skin. If, as previously suggested, the nanoparticles remain on the skin surface and are unable to cross the impermeable *stratum corneum* barrier the encapsulated drug will be released on the superficial layers of the *stratum corneum*. Subsequent drug transport into the deeper layers of the tissue occurs after the nanoparticle contents have been released. This mechanism has been shown using confocal laser microscopy (Alvarez-Roman et al., 2004a; Alvarez-Roman, Naik et al., 2004b).

Alternatively, nanoparticles carriers can accumulate in the shunts available in the bottom of the *stratum corneum* and deposit the drug contents in this region of the skin. This encourages drug transport specifically *via* the transappendageal pathway, which provides less resistance compared to the transepidermal pathway (Blume-Peytavi, Massoudy et al., 2010; Knorr, Lademann et al., 2009; Lademann, Otberg et al., 2001; Schaefer & Lademann, 2001). The transappendageal pathway provides an excellent site for accumulation due to its slower clearance and the provision of a shorter diffusion distance to the living tissues.

If nanoparticles can penetrate the skin (see earlier example of transfersomes), they can partition into the layers of the skin and then release the drugs directly into the tissue

(Honeywell-Nguyen & Bouwstra, 2003; Honeywell-Nguyen et al., 2002; Honeywell-Nguyen et al., 2004). In general, rigid nanomaterials are not expected to enter the *stratum corneum* as intact entities but whether highly deformable nanomaterials able to penetrate into the living tissue or even through the *stratum corneum* intact remains debatable.

Despite the potential that nanoparticles have to offer, the use of nanomaterials as a drug carrier to administer drugs in a clinical setting is still rare. This may be because if nanoparticles are used as a carrier, they are more expensive to manufacture and they introduce a second rate-limiting release step into the topical drug delivery process (Baroli, 2010a). These nanocarriers also poses challenges in the fact that they can have a low loading capacity (Schäfer-Korting, Mehnert et al., 2007), can prematurely releases drugs (Zhao et al., 2010) and may result in poor drug release if the affinity between drug and the carrier is high. All the disadvantages are diminished if an approach is taken to use nano-sized material to control drug aggregation through their surface interactions when delivering a drug to the skin.

1.6.2 Nanoparticle modification of the skin barrier

One of the suggested modes of action of nanomaterials is the modification of the skin barrier function. This can be achieved by acting as a penetration enhancer, which can take the form of adsorption and/or fusion with the *stratum corneum*. Nanomaterial constituents, such as ethanol, non-ionic surfactants and lipid esters, may act as

permeation enhancers. These nanomaterial constituents may penetrate into the skin and disorganise the *stratum corneum* lipid matrix to the extent that drugs may permeate more easily through the skin. For example, Hofland et al. (1994) investigated the permeation of estradiol from liposomes through the human *stratum corneum*. In order to investigate the penetration enhancing effects of the liposomes, *stratum corneum* were treated with empty surfactant carriers prior to application of the estradiol. An increase in flux was observed, hinting that penetration-enhancing effect of surfactant molecules was important in drug enhancement process. Using freeze fracture electron microscopy, the authors continued to study the interactions between liposomal formulations and the human *stratum corneum* (Hofland et al., 1995). The fusion of phospholipid constituents of the liposomes and *stratum corneum* lipids induced ultra-structural changes in the deeper layers of the *stratum corneum* and this modification of the *stratum corneum* was believed to have aided drug permeation through the skin. In another study, El Maghraby et al. (1999) demonstrated a 4-fold drug permeation enhancement from skin pre-treated with liposomes and a 8-fold enhancement from drug encapsulated liposome, emphasising the penetration enhancing effect of nanomaterials through a process of membrane barrier disruption. Fusion with the *stratum corneum* is another mode of action within the remit of modifying the skin barrier that can increase drug partitioning into the *stratum corneum* to facilitate an improvement in drug permeation (Kirjavainen et al., 1999).

Another mechanism that nanomaterials may modify the skin barrier is by adsorption to the skin to form an occlusive layer (Wissing et al., 2001; Wissing & Muller, 2002;

Wissing & Muller, 2003). When nanomaterials adhere to the superficial surface of the skin, they can form an adhesive film, which creates occlusion. Smaller nanoparticles are better at occluding the skin surface due to their larger surface area (Wissing & Muller, 2003). The occlusive layer hydrates the skin, resulting in a change in *stratum corneum* structure that facilitates drug permeation through the skin (Wissing, Lippacher et al., 2001; Wissing & Muller, 2002; Wissing & Muller, 2003). Wissing and Muller (2003) observed that nanoparticles smaller than 400 nm demonstrated a 4-fold increase in occlusivity compared to microparticles. However, this mechanism will only be applicable to very hydrophobic drugs, which use the transcellular pathway e.g. corticosteroids, other hydrophilic agents can be retarded by hydration of the *stratum corneum* e.g. caffeine.

1.6.3 Changing physical drug interactions in the formulation

Nanomaterials may also enhance drug permeation through the skin by changing the physical interactions of the drug in the applied formulation. One consequence of modifying the formulation's physical interactions with the drug can be an increase in drug thermodynamic activity. An increase in thermodynamic activity of a drug in a formulation can result in an increase in drug permeability through the skin. The *in vitro* porcine skin permeation experiments of α-tocopherol and α-tocopherol acetate delivered by lipid nanoparticles showed a 3.4-fold increase in drug permeation into the *stratum corneum* and 1.3-fold increase in the viable epidermis was attributed to changes in drug thermodynamic activity (Fangueiro et al., 2012). In another study, triptolide actives

were found to permeate 3.45 times higher through rat skin using solid lipid nanoparticles in comparison to their aqueous counterparts as a consequence of changes in the drug thermodynamic activity (Mei, Chen et al., 2003). Polymeric nanoparticles were also found to increase nimesulide permeation through human skin through the same mechanism (Alves et al., 2007).

Clearly, changing the physical interactions of a drug in a formulation presents a potential strategy to enhance drug permeation. At present, there seems to be an emphasis in the published literature on changing the thermodynamic activity of the drug. However, there is more than one way that the control of physical interactions can influence drug properties in an effort to enhance skin permeation. One of the less explored mechanisms is the concept of modifying drug aggregation.

1.7 Nanomaterial-facilitated control of drug aggregation

There are many ways to optimise skin drug delivery, but the idea of controlling molecular aggregation of therapeutic molecules is a concept that has not gained significant attention to date. This would suggest that drug-drug interactions are not considered to be an important concept in skin delivery, however drug-drug interactions are known to occur in formulations applied to the skin (Walters, 2002). A number of drugs are amphiphilic and demonstrate the tendency to self-associate at high concentrations (Berge et al., 1977).

1.7.1 Drug aggregation

Amphiphilic compounds are composed of 2 distinct portions: an ionic or non-ionic polar head portion and a hydrophobic portion. When placed in an aqueous solution, these compounds can form organised structures, such as micelles, monolayers, bilayers, cubic and hexagonal phases, or disorganised structures. The type of structures formed depends on their molecular structure. In the pharmaceutical field, simple classical surfactants are the most extensively researched for their aggregation properties and their biological activity. They are able to interact with membranes, promote lysis, denature proteins or disrupt lipids and solubilize within the membrane (Helenius & Simons, 1975). Surfactants tend to self-associate to form micelles, which are spherical aggregates with the hydrophobic portion sequestered from the polar surrounding. In 1935, Goodeve envisioned a stepwise addition of monomer molecules to existing micelles (Wyn-Jones & Gormally, 1983). This aggregation process can be presented in the form of several equilibria and equilibration constants or a phase separation process, ultimately cumulating to a critical concentration, often known as critical micellar concentration (CMC) or the critical aggregation concentration (CAC) depending on the structures formed. Beyond this concentration, further addition of monomers form aggregates. Aggregation is a dynamic process, with aggregates forming within a microsecond lifetime (Patist et al., 1999). Micelles are usually characterised by their CMC, aggregation number, particle size, and hydrophilic-hydrophobic balance (Schreier et al., 2000). In some cases, pre-micellar aggregation is investigated (Ernandes et al., 1977; Schreier et al., 1978).

Amphiphilic drugs present a unique group of aggregates that share certain similarities with surfactants and dyes (Wyn-Jones & Gormally, 1983). For example, cationic ammonium germicides have structures resembling surfactants and they form spherical micelles. On the other hand, phenothiazine tranquilisers have rigid aromatic ring systems and form aggregates resembling to the base-to-base stacking of cationic dyes. Despite some resemblances, amphiphilic drugs are not identical to surfactant structures because they tend to be smaller and more compact molecules. This results in the drug aggregation process generally being continuous, unlike the step-wise micellar association. Examples of amphiphilic drugs include local anaesthetics, phenothiazine, benzodiazepine tranquilizers, antibiotics, tricyclic antidepressants, antihistamines, anticholinergics, anti-cancer drugs and non-steroidal anti-inflammatory drugs. Their biological and pharmaceutical implications have been comprehensively reviewed by Schreier et al. (2000). The molecular aggregation characteristics are dependent on the structure of the drug molecules. For example, drugs such as the tricyclic antidepressants and phenothiazine have been shown to form micelles and phenanthrene narcotic analgesics are known to associate in a non-micellar manner (Wyn-Jones & Gormally, 1983). Similar to surfactants, amphiphilic drugs are known to aggregate and disrupt membranes.

Molecular aggregation is concentration-, temperature-, ionic strength-, and pH-dependent. As early as 1913, aggregates formed by an increased concentration of sodium stearate have been found to exhibit a different conductivity to those of sodium acetate (McBain, 1913). Later in 1930, Bury and Davies introduced the term ‘critical

concentration for micelles' and noted the decrease of this CMC with an increase in temperature. Drug aggregation is also affected by the ionic strength of the surroundings. For example, an increase in aggregation number and a decrease in CMC were observed on 5 different drugs (antihistamines, diphenhydramine hydrochloride, bromodiphenhydramine hydrochloride, chlorcyclizine hydrochloride and diphenylpyraline hydrochloride) when the electrolyte concentration was increased (Attwood & Udeala, 1975). Attwood and Natarjan (1981) also observed a higher critical micelle concentration at a low pH (0.5-5.5) in 5 different piperazine drugs (trifluoperazine, opirpramol, thiopropazate, flupenthixol and clopenthixol).

Aggregation is commonly characterised by determining the CAC or the CMC in the case where a micelle is formed. The National Institute of Standards and Technology (NIST) have identified 71 methods to determine CMCs, which were measured by detecting an abrupt change in physical property such as surface tension, electrical conductivity, light scattering, refractive index, osmotic pressure or density (Mukerjee, 1971). Due to their small size and dynamic nature, direct examination to look at the structures of monomers and aggregates is difficult and indirect measurement methods are employed to try to understand their structure and the functional consequences of aggregation.

1.7.2 Influence of aggregation on skin drug delivery

The drug aggregation process, whether by unorganised self-association or by incorporation into an organised assembly, such as micelles and emulsions, can affect the physicochemical properties of the drug. There has been evidence found to suggest that aggregation can result in a pK_a shift and a change in the rates and/or mechanism of molecular reactions (Schreier, Malheiros et al., 2000). In addition, the impact of drug aggregation on membranes has been described. However, in most pharmaceutical systems, the consequences of drug aggregation on functional properties, i.e. skin transport, are not considered. Expanding the knowledge of drug-drug aggregation is particularly important when the therapeutic agents must cross a biological barrier to reach their intended site of action. For example, when applied to the skin, aggregation has the potential to significantly influence percutaneous penetration particularly through changes in the self-diffusion coefficient of the molecules in the application vehicle and the tissue interactions upon passage through the skin.

1.7.3 Strategies to de-aggregate drugs

There have been a number of published studies that describe methods to control molecular aggregation, but they can be principally categorised into electrolyte, surfactants and polymers. Counter-ions associated can form ion-pairs with charged drugs and this can have an influence on the association of molecules in the solution state. For example, the hydrochloride salt of tripelnnamine appears to form micelles

association, but the maleate salt of mepyramine, brompheniramine and chlorpheniramine associates to form unorganised structures (Attwood & Udeala, 1975). Surfactants have also been used to break up the aggregation of small molecular weight agents such as phthalocyanines and larger therapeutic agents such as insulin. As surfactants are amphiphilic, they have the characteristics that can readily disrupt the self-association process by direct interaction with the molecules (Darwent et al., 1982; Rossetti et al., 2011; Shao et al., 1993; Spikes & Bommer, 1986).

The addition of polymers can modify the molecular aggregation of drugs. Pygall et al. (2011) noted that different interactions between hydroxypropyl methylcellulose (HPMC) and two structurally related drugs, diclofenac sodium and meclofenamic acid sodium, occurred upon addition to the applied surfactant of a hydrophobic membrane. Contrary to diclofenac sodium, meclofenamate formed self-assembled aggregates on addition of HPMC leading to a change in the viscosity, reduction in the vehicle gel point and a decrease in the self-diffusion coefficient of the drug.

1.7.4 Using nanomaterials: Benefits of using solid surfaces

Nanoparticles can be used as an alternative to surfactants in that they have surface activity and adsorb at the interfacial surface. There has been evidence to show that drug penetration increased when nanoparticles were used instead of surfactants to stabilise emulsions (Frelichowska, Bolzinger, Pelletier, et al., 2009; Frelichowska, Bolzinger, Valour, et al., 2009). Frelichowska et al. (2009) demonstrated that Pickering emulsions

(silica particle-stabilised w/o emulsions) exhibited 3-fold higher caffeine flux than conventional emulsions (surfactant-stabilised w/o emulsions) even though both vehicles had the same physicochemical properties in terms of droplet size and viscosity.

It is proposed that nanoparticles can break up the aggregation of the drug, thus improving drug mobility. It is noteworthy that in this project nanoparticles are introduced to control the physical interactions of the drug in the topical formulation in order to facilitate drug permeation, rather than being used as a drug carrier that encapsulates drugs to transport them across the membrane (Fireman, Toledano et al., 2011; Prow, Grice et al., 2011).

1.8 Aim and scope

The aim of this PhD was to investigate the interactions between the surfaces of nanomaterials and co-formulated drugs with a view of designing a novel penetration enhancement strategy for drug delivery into the skin. The project hypothesis was that the introduction of the nanoparticle at the point of administration to the surface of the skin would generate a dynamic system that could break up drug-drug aggregation in a manner that could facilitate the temporal increase in drug monomers that could permeate across the skin. The project aim was addressed in 4 work phases:

Phase I: Investigation of molecular aggregation characteristics.

Phase II: Investigation of the effects of nanomaterials on tetracaine permeation

Phase II: Investigation of solid-liquid interfacial interactions.

Phase IV: Generation of *in situ* self-assembly of nanoparticles upon application to the skin

It was anticipated that drug aggregation could influence drug transport and a deeper understanding of how to control drug aggregation could be used to improve transport through the skin. Tetracaine was selected as a model drug. It exists with a positive charge at physiological pH. Its chemical structure has a hydrophilic region (amine portion) and a hydrophobic region (aromatic portion)(Fig. 1.9) and this predisposes it to self-associate in aqueous solution. At concentrations of more than 1 mM, previous literature suggests tetracaine forms an aggregate (Farhadieh et al., 1967; Florence & Attwood, 2011; Johnson & Ludlum, 1969). There have been several studies that document its CMC, for example, Kitagawa et al. (2004) proposed tetracaine hydrochloride had a CMC of 38 mM at 25 °C in an aqueous solution, pH from 4.5 to 5.7. There appears to be a difference of opinions in the literature as to whether tetracaine forms organised micelles (Kitagawa, Oda et al., 2004; Matsuki et al., 1996; Shaikh et al., 2011) or random molecular aggregates (Attwood & Fletcher, 1986; Farhadieh, Hall et al., 1967). In addition, there is less known about at what concentration aggregation commences if indeed a rapid micellisation process is not followed. Guerin et al. (1980) and Umemura et al. (1981) suggested that tetracaine were thought to exist as free monomers below a concentration of 18 mM using Fourier transform infrared spectroscopy (FTIR), but this is close to the limit of detection for this technique.

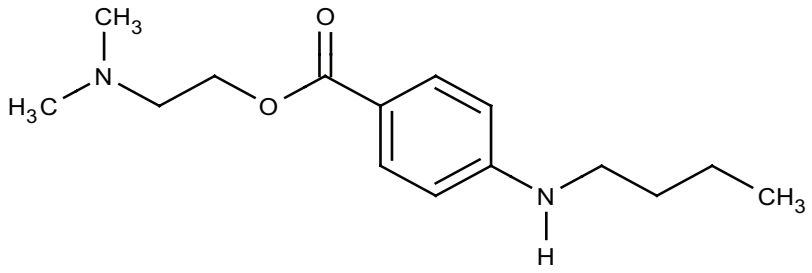

Figure 1.9. The chemical structure of tetracaine. Tetracaine is an amphiphilic molecule with a hydrophilic region (amine portion) and a hydrophobic region (aromatic portion).

Tetracaine is used clinically as a local anaesthetic for topical application, but it has an unusually high penetration lag time. Reducing lag time could improve the drugs performance in patients as it is often used before venepuncture or venous cannulation (Joint Formulary Committee, online). According to the British National Formulary (BNF), the recommended formulation concentration of tetracaine is 0.15 M (Joint Formulary Committee, online). At high dosages, tetracaine can lead to hypersensitivity reactions and cause harm to the central nervous and cardiovascular systems (Joint Formulary Committee, online).

The log P of tetracaine is 2.79, which falls within the ideal range of log P 1 to 3 for skin penetration. Tetracaine is a weak base that is soluble in organic solvents and slightly soluble in water. At 32 °C, the temperature of skin surface, protonation of secondary amine and tertiary amine occurs at pHs 3.24 and 8.24. Using these pK_a values, at pH 4, it was predicted that 100% of the tertiary amine would be ionised and 23% of the secondary amine would be ionized; at pH 8 it was predicted that 72% of the tertiary amine would be ionised and 28% of tetracaine would be unionised. Therefore, it was

necessary to investigate whether the drugs aggregation in different pH vehicles had an effect on tetracaine permeation through synthetic silicone membranes and porcine epidermis (Chapter 2). Once that was established, the effects of nanomaterials on tetracaine permeation were quantified (Chapter 3) and then the nanomaterial-drug interactions were measured (Chapter 4). After examining the effects of nanomaterials on permeation, the nanomaterial with the highest enhancement was selected for the development of a HPMC gel (Chapter 5).

CHAPTER TWO

Influence of Tetracaine Aggregation on its Passive Transmembrane Permeation

2.1 Introduction

The excipients that are used to produce topical pharmaceutical products applied to the skin are often termed ‘inert’. This definition refers to the fact that the excipients have no pharmacological action in themselves, but most excipients are far from ‘inert’ when considering the manner in which they modulate the behaviour of a drug when it is formulated as a medicine. For example, drug-vehicle interactions in topical products have been shown to have a significant influence on their ability to deliver actives into the skin (Benaouda, Brown, Ganguly, et al., 2012; Zhang et al., 2012). In topical products, a degree of physical interactions between the active and the vehicle must occur to facilitate solubilisation of the drug, but if the physical interactions are too strong, drug release from the product after application can be hindered (Benaouda, Brown, Martin, et al., 2012).

Drug-drug interactions are in equilibrium with drug-vehicle interactions in pharmaceutical products and therefore, drug-drug interactions also have the potential to modify the performance of a medicine. Several therapeutic agents formulated in topical products that are applied to the skin are known to exhibit strong drug-drug interactions, which can lead to aggregation in the solution state (Attwood, 1995; Schreier, Malheiros et al., 2000; Wyn-Jones & Gormally, 1983). Molecular aggregation is known to modify the physicochemical properties of the drug such as lipophilicity, molecular size, degree of ionisation, hydrogen bonding and these physicochemical properties can influence drug permeation (Bos & Meinardi, 2000; Potts & Guy, 1992; 1995; Shore et al., 1957).

Therefore, it would seem logical that molecular aggregation would influence the performance of topically applied products. However, the information in the literature regarding the potential of drug-drug interactions to modify drug penetration into the skin remains very limited.

Molecular aggregation, using simple surfactants as models, is known to influence solute transport across the membrane, but even with these relatively simple surfactant structures, it is unclear if only the monomer penetrates through the membrane (Charman et al., 1991; James-Smith et al., 2011; Mikkelson et al., 1980) or both the monomer and the aggregate penetrate the membrane (Moore, Puvvada, et al., 2003; Moore, Shiloach, et al., 2003). In addition, given the small size and dynamic nature of surfactant interactions, understanding the equilibrium between the monomer structures and aggregates is difficult and hence it is usually only measured by indirect analytical methods (Mukerjee, 1971). These problems are amplified when applied to drugs because they demonstrate more heterogeneous aggregation patterns compared to surfactants.

The aim of this chapter was to characterise the molecular aggregation of a model drug that is used for topical administration to the skin, tetracaine, so as to better understand the influence of the molecular aggregation process on transmembrane transport. It was anticipated that this would provide information to determine if nanomaterials could control tetracaine aggregation and this would help in the overall PhD goal of developing a nanomaterial formulation that enhances drug permeation. Aggregation is ionisation-

dependent (Attwood & Natarajan, 1981) and hence, tetracaine aggregation at pH 4 and 8 was determined in order to investigate the influence of tetracaine ionisation on aggregate formation, and subsequently on tetracaine permeation. Parameters known to affect aggregation such as temperature, pH and solvent environment were tightly controlled in all the experiments and the concentration of the model drug was changed in order to try and form different types of aggregates. The tetracaine aggregates were characterised by photon correlation spectroscopy, fluorescence spectroscopy and FTIR The drug transport was studied using a porcine epidermis and a model membrane to understand the manner in which aggregation influence transport through barriers with and without the potential for follicular transport.

2.2 Materials

Material	Grade	Company
Tetracaine	Free base, ≥ 98%	Sigma Aldrich, UK
Hydrochloric acid (HCl)	Fuming 37%	Sigma Aldrich, UK
Deuterium oxide	99.9 atom % D	Sigma Aldrich, UK
Phosphate buffered saline	Tablets, pH 7.4, 0.172 M	Oxoid Ltd, UK
De-ionised water	Electrical conductivity 0.5-1 μS	Produced in house
Sodium phosphate dibasic	Anhydrous, ≥ 99%	Sigma Aldrich, UK
Acetic acid	ACS reagent, ≥ 99.7%	Sigma Aldrich, UK
Acetonitrile	High performance liquid chromatography (HPLC) grade	Fisher Scientific, UK
Methanol	HPLC grade	Fisher Scientific, UK
Water	HPLC grade	Fisher Scientific, UK
Silicone membrane	Thickness of 0.12 and 0.25 mm	GBUK Healthcare, UK

Table 2.1. Materials used in Chapter 2.

2.3 Methods

2.3.1 Test sample preparation

Tetracaine solutions were prepared and adjusted to pH 4.0 or 8.0 using HCl and equilibrated at 32°C unless stated otherwise. Solutions were stirred for at least 24 h and the pH rechecked prior to analysis to ensure they were at equilibrium.

2.3.2 Photon correlation spectroscopy

The derived count rates were analysed by photon correlation spectroscopy (Malvern Nanoseries Zetasizer ZEN3600, Malvern Instruments Ltd, UK). Detection of the light scattering signal was achieved at a 173° backscattering angle with samples equilibrated at 32°C using water as a dispersant (refractive index 1.33, viscosity 0.8872 cP). Each measurement comprised of 10-14 runs. Triplicates of each sample were assessed.

2.3.3 Fluorescence spectroscopy

Fluorescence emission spectra were recorded using a fluorescence spectrometer fitted with a Xenon pulse lamp (Varian Cary Eclipse Fluorescence Spectrometer, Agilent Technologies, UK). A Quartz fluorescence cell with a 3 mm path length (Helima Fluorescence Cell, Helima UK Ltd., UK) was used unless specified. Excitation and emission slits were fixed at 5 nm. In all measurements, the excitation wavelength was

set at 310 nm. The samples were scanned from 320 to 450 nm at a wavelength scan rate of 120 nm/min with a photomultiplier tube (PMT) detector gain of 600 V. The data were smoothed with a Savitzky Golay function filter size 25 using the Cary Eclipse software. The experiments were performed at a temperature of 32°C.

2.3.4 Critical aggregation concentration (CAC) analysis

The CAC was defined as the concentration of molecules at which deviations from linearity of the concentration vs. fluorescence intensity graph occurred. Two methods were used to identify the CACs and their values were compared (Khan & Shah, 2008). In the first method, a second derivative function was applied to the data using OriginPro (OriginPro version 8.6, Origin Lab Corporation, US). The data was fitted non-linearly before a Gaussian distribution function was applied to highlight the critical points, i.e. the regions where local minimum or maximum occurred. In the second method, the intersection of 2 linear slopes was determined.

2.3.5 FTIR analysis

Deuterated water (D_2O, Sigma Aldrich, UK) was employed in the infrared analysis of the tetracaine solutions as it dampened the solvent signal in the 1700 to 1300 cm^{-1} and 3000 to 2850 cm^{-1} ranges. The samples were loaded into a demountable universal transmission cell system (Omni-Cell, Specac Ltd, UK) fitted with calcium fluoride

(CaF_2) windows and a 25 μm Mylar spacer (Specac Ltd., UK). The pHs of the tetracaine solutions were maintained using deuterium chloride (DCl). All spectra were produced using 32 scans collected at a spectral resolution of 4 cm^{-1}. The data was recorded using a Spectrum One spectrometer (Perkin-Elmer Ltd., UK) and analysed with Spectrum software (version 10, Perkin-Elmer Ltd., UK).

2.3.6 Tetracaine transport studies

Two barriers were employed for the transport studies, a silicone membrane (0.12 and 0.25 mm, GBUK Healthcare, UK, no pre-treatment required) and a porcine epidermis. Fresh white adult porcine ears were obtained from a local abattoir (Evans and Sons, UK). Damaged ears were discarded. After cleaning with deionized water and wiping the residue with clean wipes, visible hairs were trimmed carefully. The preparation of epidermal porcine skin was carried out by heat separation (Kligman & Christophel, 1963). Porcine skin was immersed and gently stirred in deionised water at 60°C for 1 min. After removal from the deionized water, the skin was put on a corkboard with the dermal side down and the epidermis was carefully separated from the dermis with tweezers. The separated epidermis was washed with deionized water and floated on filter paper (Whatman no. 1, UK) to act as a support. The samples were wrapped in aluminium foil and stored at -20°C for a maximum of up to 1 month (Harrison et al., 1984). The samples were thawed before use.

The transport studies were carried out using upright individually calibrated Franz

diffusion cells with an average surface area of 2.1 ± 0.1 cm^2 and receptor compartment volume of 9.2 ± 0.5 mL. The barrier was cut, mounted and sealed with parafilm between two chambers of the glass diffusion cell with a 13 mm magnetic flea in the receiver chamber. The cells were inverted and filled with previously filtered and sonicated receiver fluid. pH 4.0 and 8.0 water adjusted with HCl were used as a receiver fluid for the silicone membrane transport studies to investigate the transport of tetracaine through a hydrophobic barrier. Phosphate buffered saline (pH 7.4) was employed as a receiver fluid for the porcine epidermis transport studies to mimic the skin environment. Sink conditions were maintained throughout the transport studies (drug concentration in the receiver fluid does not exceed 10% of its saturated solubility). The saturated solubility of tetracaine was (1.05 ± 0.04) M in pH 4 water and (6.29 ± 0.07) mM in pH 8 water and (7.16 ± 0.05) mM in phosphate buffered saline. The transport studies were performed on a submergible magnetic stirrer plate in a pre-heated water bath set at 37°C to provide a membrane surface temperature of 32°C. After cell equilibration for 1 h, the cells were checked for leaks by inversion and visual inspection for back diffusion. Infinite doses of tetracaine solutions (1 mL) were applied uniformly to the surface of each membrane and the donor compartment was covered with a parafilm to minimise donor phase evaporation. In this chapter, 10 μM and saturated concentration of tetracaine were applied on the porcine epidermis while different concentrations of tetracaine at pH 4 (Table 2.3) and pH 8 (Table 2.4) were applied on the silicone membrane to understand the permeability through a non-porous hydrophobic membrane. At predetermined time intervals, 1 mL aliquots were removed from the receiver phase and replaced with fresh receiver fluid to keep the liquid volume

in the receiver compartment constant. The collected samples were analysed by HPLC. A total of 5 replicates of each experiment were performed.

Cumulative amounts of drug (ng) penetrating the unit surface of the membrane area (cm^2) were corrected for sample removal and plotted against time (h). The steady-state flux (J) was calculated from the slope of the linear portion of the curve ($R^2 \geq 0.98$), using at least 4 points with values above the assay limit of quantification (LOQ). The permeability coefficient of tetracaine was calculated using equation 2.1 (Williams, 2003):

$$k_p = \frac{J}{C_v} \qquad \text{(Equation 2.1)}$$

where J represents the flux, k_p is the permeability coefficient of the permeant across the membrane and C_v is the concentration of the drug in the vehicle.

2.3.7 Tetracaine quantification

The quantification of tetracaine was performed using a reverse-phase HPLC system consisting of a pump with autosampler (Hewett-Packard series 1050, Agilent Technologies UK Ltd., UK) connected to a fluorescence detector (Shimadzu detector RF-551, Shimadzu corp., Japan). The system was controlled *via* a computer with Chromeleon software (Dionex Corp., USA), which was also used to record and interpret the analytical data. The mobile phase comprised acetonitrile-methanol-acetate buffer (0.1 M)(25:25:50 (v/v), pH 5.1) set at a flow rate of 1.0 $mL.min^{-1}$. Tetracaine was

separated using a Luna 3 µm C18(2)(150 X 4.6 mm) stationary phase (Phenomenex, UK) at room temperature with a 100 µL injection volume and the fluorescence detection at an excitation wavelength of 310 nm and an emission wavelength of 372 nm. The retention time for tetracaine was 4.2 min. The calibration curves were constructed on the basis of the peak area measurements using standard solutions of known tetracaine concentrations dissolved in an identical fluid as the receiver phase for the transport studies. The assay was shown to be "fit for purpose" in terms of sensitivity (LOD – 4.08 ng/mL, LOQ – 74 ng/mL, n=25), precision (6% CV), and linearity ($R^2 \geq 0.99$).

2.3.8 Statistical analysis

All values were expressed as their mean ± standard deviation (SD). The statistical analysis of data was performed using the statistical package for social sciences, SPSS version 21, (IBM Corp., USA) with a significance level of 0.05. The normality (Sapiro-Wilk) and homogeneity of variances (Levene's test) of the data were assessed prior to statistical analysis. Transport data were analysed statistically using one-way analysis of variance (ANOVA) tests for normally distributed data and a non-parametric Kruskal-Wallis tests for non-Gaussian distributed data. Post hoc comparisons of the means of individual groups were performed when appropriate using Dunnet's test for normal distributed data and Games Howell test for non-Gaussian distributed data. For all pair-wise comparison of means, Student's independent t-test or Mann-Whitney test was applied. Data were presented using OriginPro software (OriginPro version 8.6, OriginLab Corporation, US).

2.4 Results

2.4.1 Fluorescence spectroscopy method development

Fluorescence spectroscopy was used to confirm the concentration at which tetracaine aggregated in the μM concentration range (see Section 2.4.2 for the results). However, as fluorescence is a very sensitive technique that can be influenced by a number of experimental parameters, the method was initially tested and developed for its intended purpose prior to use. The solvent (pH 4 water) showed the Raman peak of water at 346 nm (Fig 2.1), which was in the correct location according to theoretical calculations using an excitation wavelength of 310 nm (Lawaetz & Stedmon, 2009). The tetracaine in pH 4 water solutions emitted a fluorescence signal at 372 nm (Fig. 2.1).

In this study, the temperature and pH of the system were maintained. Moreover, the system was chemically stable over 6 days and the effect of ion pairing was not significant (Fig. 2.1). Although an increase in fluorescence intensity was observed as the temperature increased, an analysis of the data illustrated similar aggregation characteristics in terms of CACs.

(A)

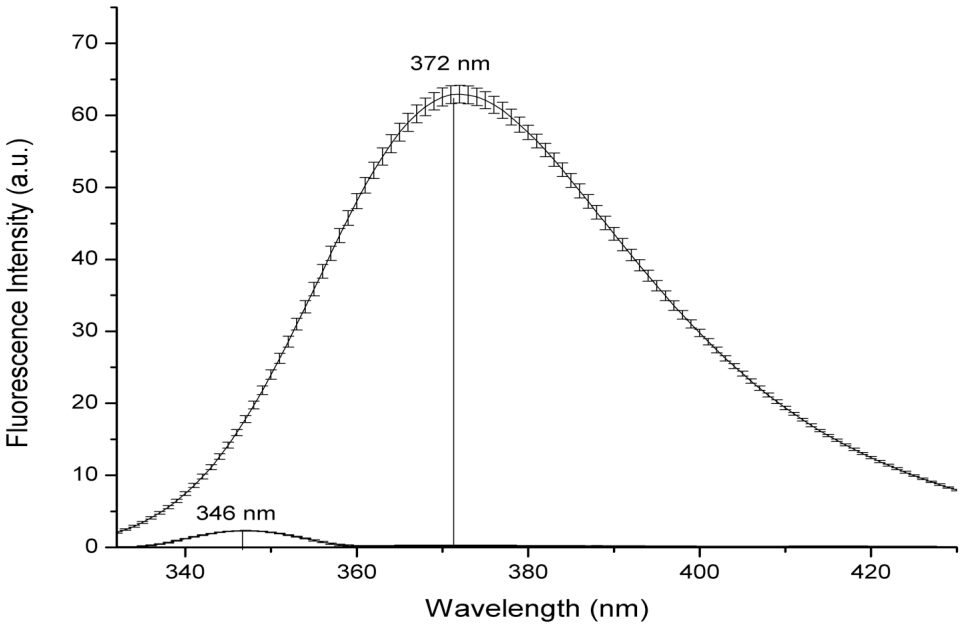

(B)

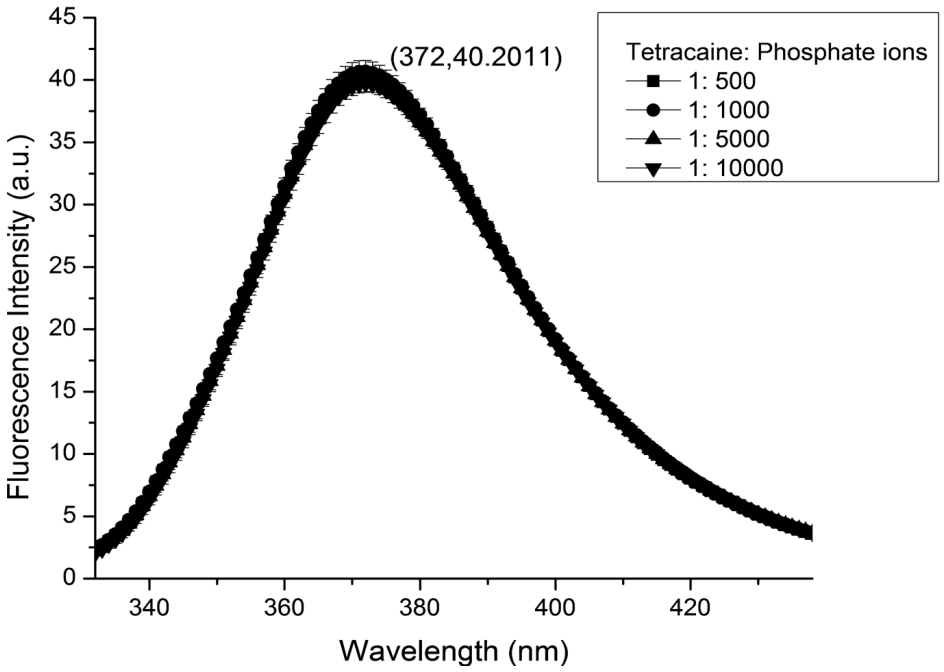

Figure 2.1. A) The fluorescence spectrum of tetracaine (λ_{max} = 372 nm) and pH 4 water (λ_{max} = 346 nm). B) The fluorescence spectrum of tetracaine in the presence of different molar ratios of tetracaine: phosphate ions, where tetracaine concentration was 10 μM.

(C)

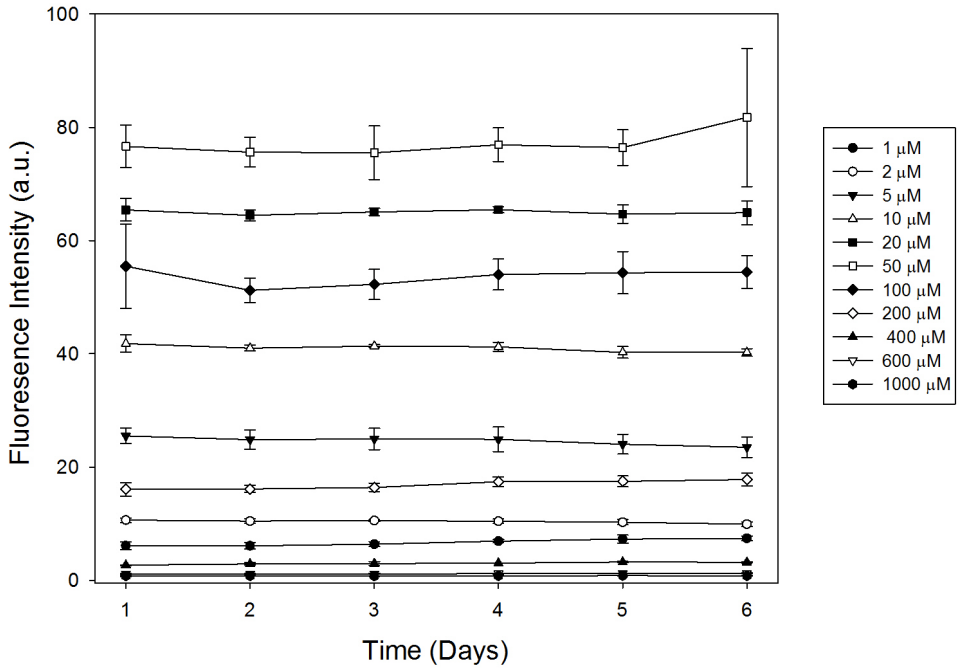

(D)

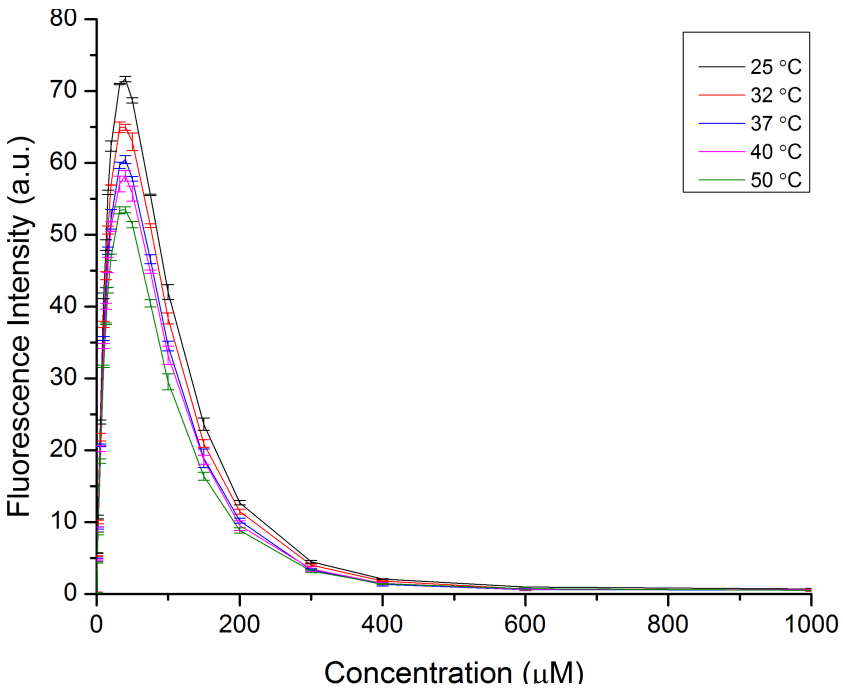

Figure 2.1. C) The fluorescence intensity readings at 372 nm (the fluorescence spectrum peak wavelength), depicting the chemical stability of tetracaine at those concentrations over 6 days. D) The fluorescence intensity reading at 372 nm at 5 different temperatures.

An example of how aggregation data was interpreted from the fluorescence spectrum of tetracaine is demonstrated graphically with a 10 mm path length cuvette (Fig. 2.2.). At the low tetracaine concentrations, only the small Raman band of water peak was observed at the beginning of the spectrum (Fig. 2.2). At the medium tetracaine concentrations, the fluorescence emission peak increased as the concentration increased. Beyond 40 μM of tetracaine, the fluorescence intensity began to decrease. The plot of the fluorescence signal at the λ_{max} (372 nm), shown in the last graph of Fig. 2.2, contained several critical points and it was these that were used to characterise the aggregation process of tetracaine.

(A)

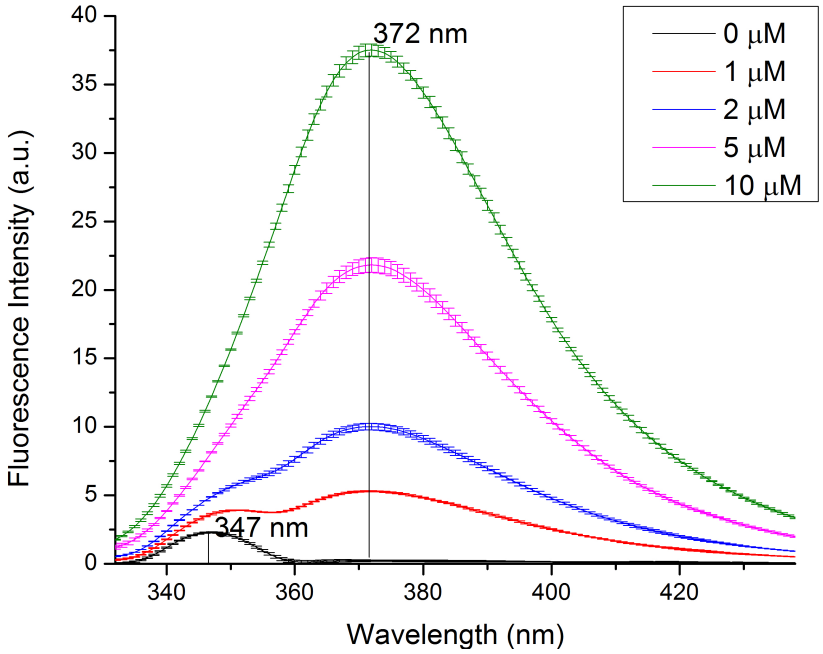

(B)

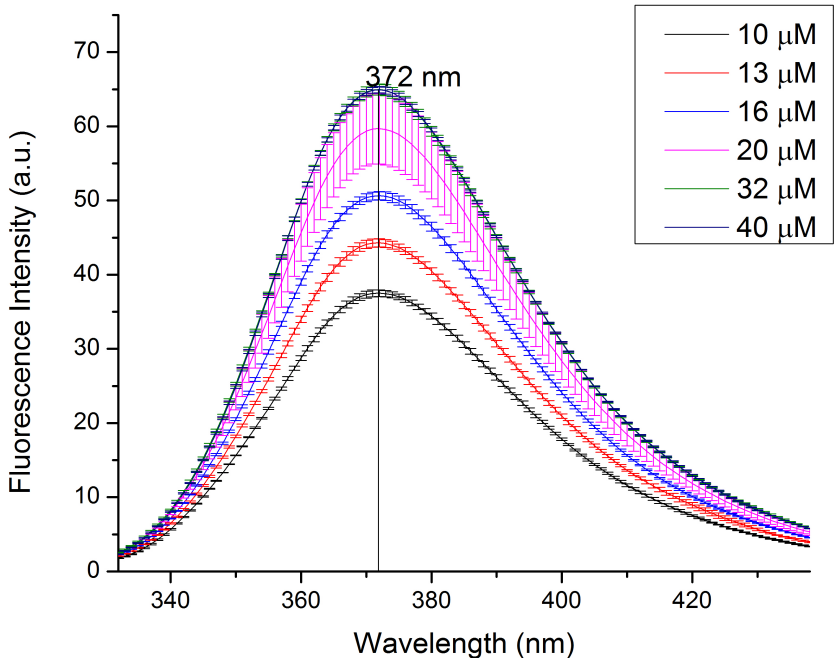

Figure 2.2. The fluorescence spectrum of the A) low (0-10 μM) and medium (10-40 μM) concentration ranges of tetracaine, where fluorescence intensity increases as concentration increases.

(C)

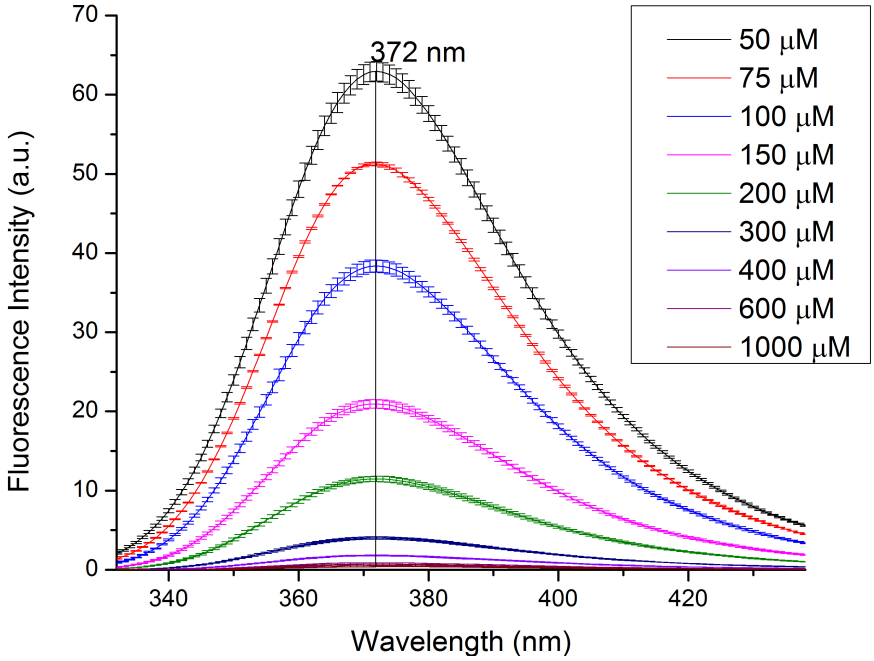

(D)

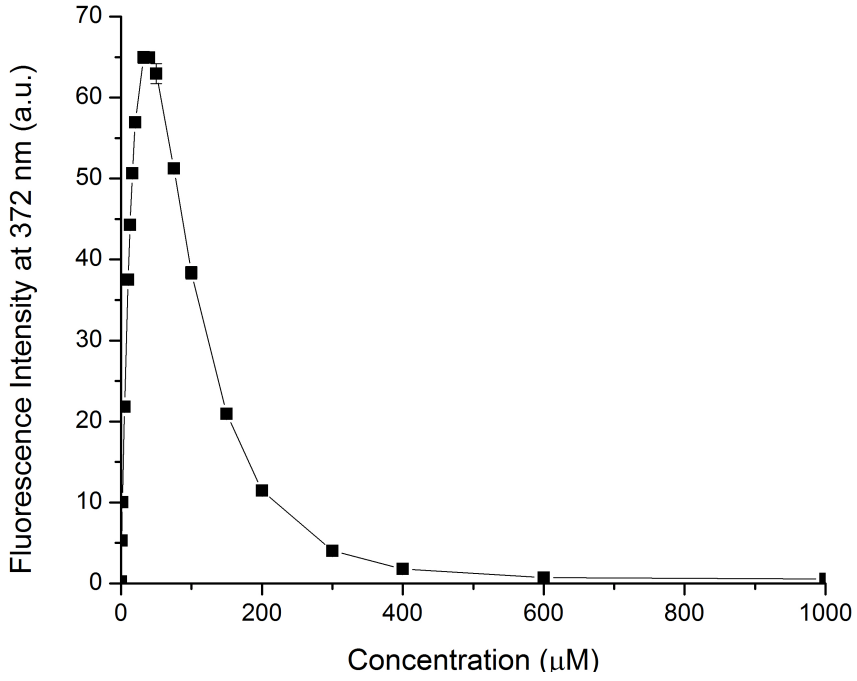

Figure 2.2. C) The fluorescence spectrum of the high (40-1000 μM) concentration ranges of tetracaine, where fluorescence intensity decreases as concentration increases. D) The re-plot of the fluorescence reading at the maximum wavelength 372 nm at various concentrations of tetracaine.

Using a 10 mm path length cuvette, high sample optical density attenuation due to absorption of the incident light or the emitted light can lead to a decrease in fluorescence intensity and a possible change in spectral distribution (Albani, 2008; Lakowicz, 2009). In light of the possibility of having a deviation in linearity due to the concentration of tetracaine and not the molecular aggregation, a path length of 3 mm was used to provide an off-centre illumination in order to minimise concentration-related quenching effects (Fig. 2.3). The fluorescence data obtained from the 3 mm path length cuvette implied that concentration-dependent quenching did not occur at low tetracaine concentrations (only at 200 μM did the quenching become similar to the 10 mm path length cuvette). Hence, for subsequent experiments, the 3 mm path length cuvette was used and critical points below the region of 200 μM were obtained. These measures were thought to be suitable to reduce the interference of the readings by concentration-dependent quenching.

(A)

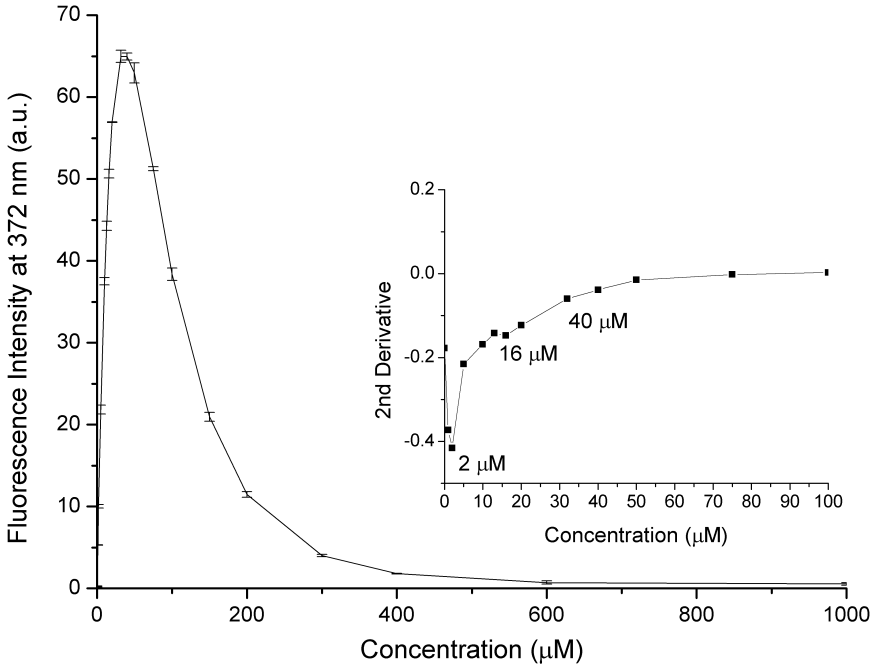

(B)

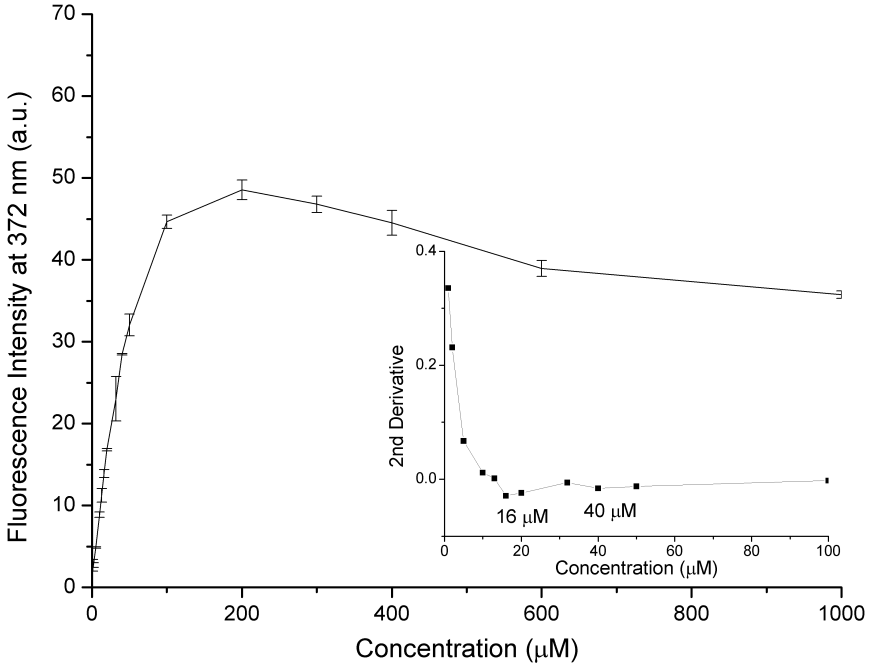

Figure 2.3. Graphs depicting the changes in the fluorescence intensity at $\lambda_{emission}$ = 372 nm using A) a 10 mm path length cuvette and B) a 3 mm path length cuvette. The insert shows an expansion of the data when a second derivative function is applied.

2.4.2 Tetracaine aggregation

Tetracaine aggregation in the mM region was determined by photon correlation spectroscopy (Table 2.2). Two methods were used to interpret the data. By applying a second differential function to the un-attenuated derived count rate values with respect to tetracaine concentrations, multiple CACs were detected due to the association nature of tetracaine and the sensitivity of the second derivative function of the OriginPro programme. It appeared that the first CAC detected significantly decreased ($p<0.05$) from 40 to 0.3 mM when the pH increased from 4 to 8. Determining the CAC's using the intersection method generated, a similar trend of decreasing CAC when the vehicle pH was increased (Fig. 2.4). The CAC significantly decreased ($p<0.05$) from 95.10 to 2.91 mM when the pH increased from pH 4 to 8.

Tetracaine aggregation in the μM region was monitored by fluorescence spectroscopy (Table 2.2). When the second derivative method was applied to the data, the first CACs detected significantly decreased ($p<0.05$) from 16 to 10 μM as pH increased from 4 to 8. In the case where CACs were calculated using the intersection of 2 linear slopes (Fig. 2.4), the CACs also significantly decreased ($p<0.05$) from 11.06 μM in pH 4 to 7.38 μM in pH 8. In addition, the wavelength at which maximum fluorescence intensity was observed experienced a significant blue shift ($p<0.05$) from 373 nm in pH 4 to 361 nm in pH 8 (Table 2.2).

pH	Critical aggregation concentrations (CACs) using photon correlation spectroscopy (mM)		Critical aggregation concentrations (CACs) using fluorescence spectroscopy (μM)		λ_{max} (nm)
	Second derivative test	Intersection of 2 linear slopes	Second derivative test	Intersection of 2 linear slopes	
4	40, 200	95.10	16, 50	13.56	373
6	20, 100	53.25	16, 40	8.89	372
8	0.3, 2	2.91	10, 32, 100, 200	7.38	361

Table 2.2. Characteristics of tetracaine aggregation in different pHs using fluorescence spectroscopy and photon correlation spectroscopy, where λ_{max} represents the wavelength at which maximum fluorescence intensity occurs.

(A)

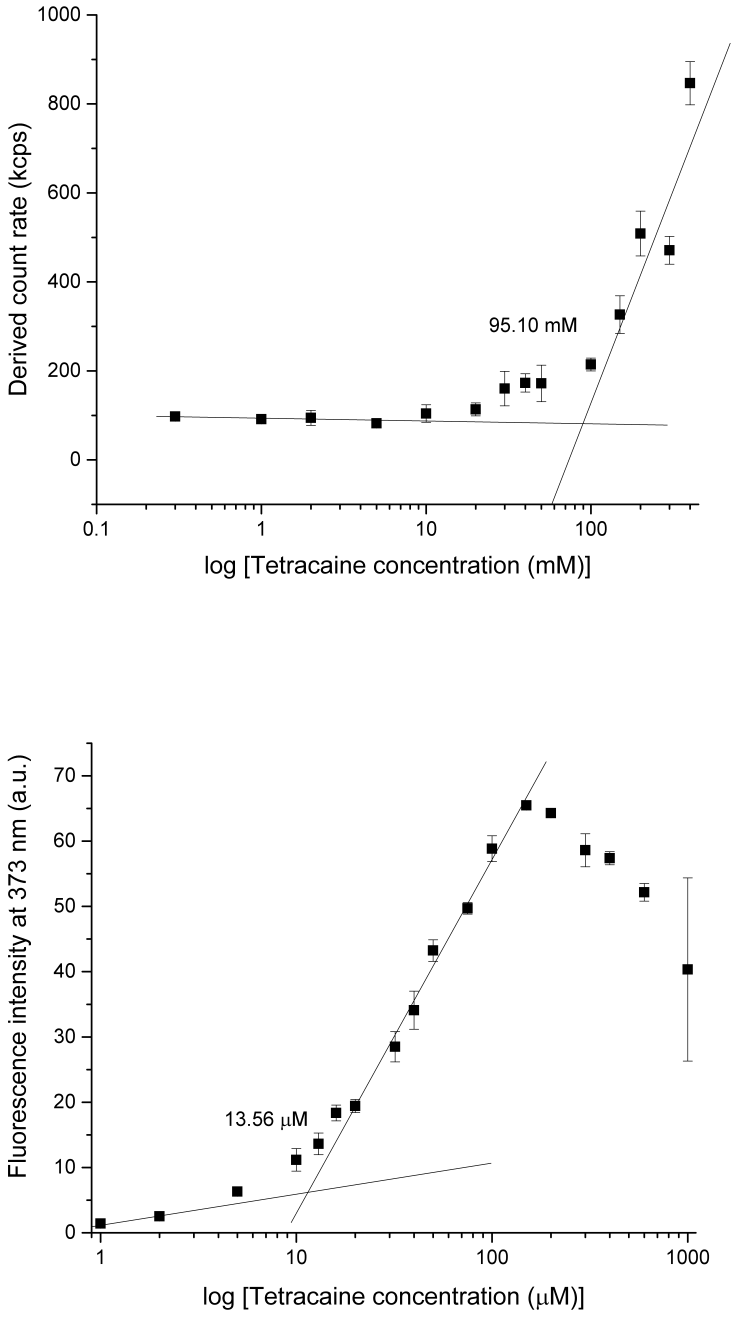

Figure 2.4. Graphs depicting critical aggregation concentrations (CACs) using photon correlation spectroscopy (top) and fluorescence spectroscopy (bottom) in A) pH 4.

(B)

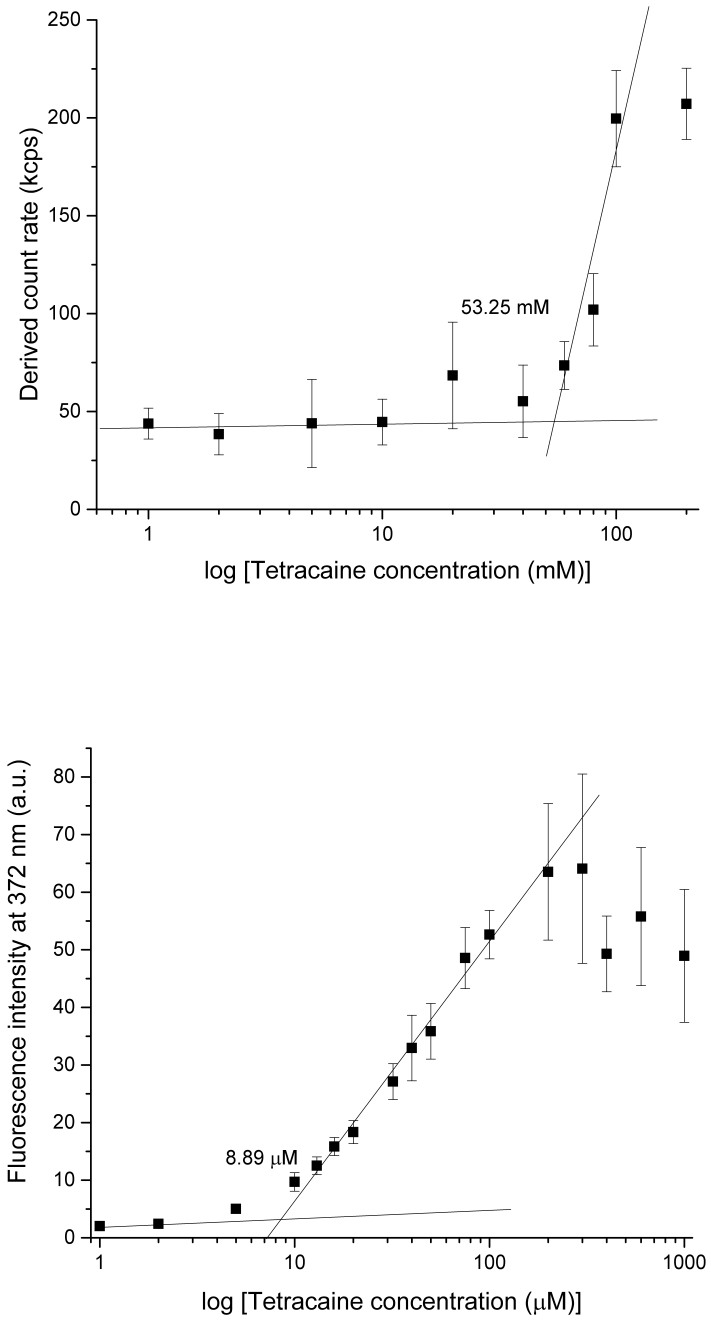

Figure 2.4. Graphs depicting critical aggregation concentrations (CACs) using photon correlation spectroscopy (top) and fluorescence spectroscopy (bottom) in B) pH 6.

(C)

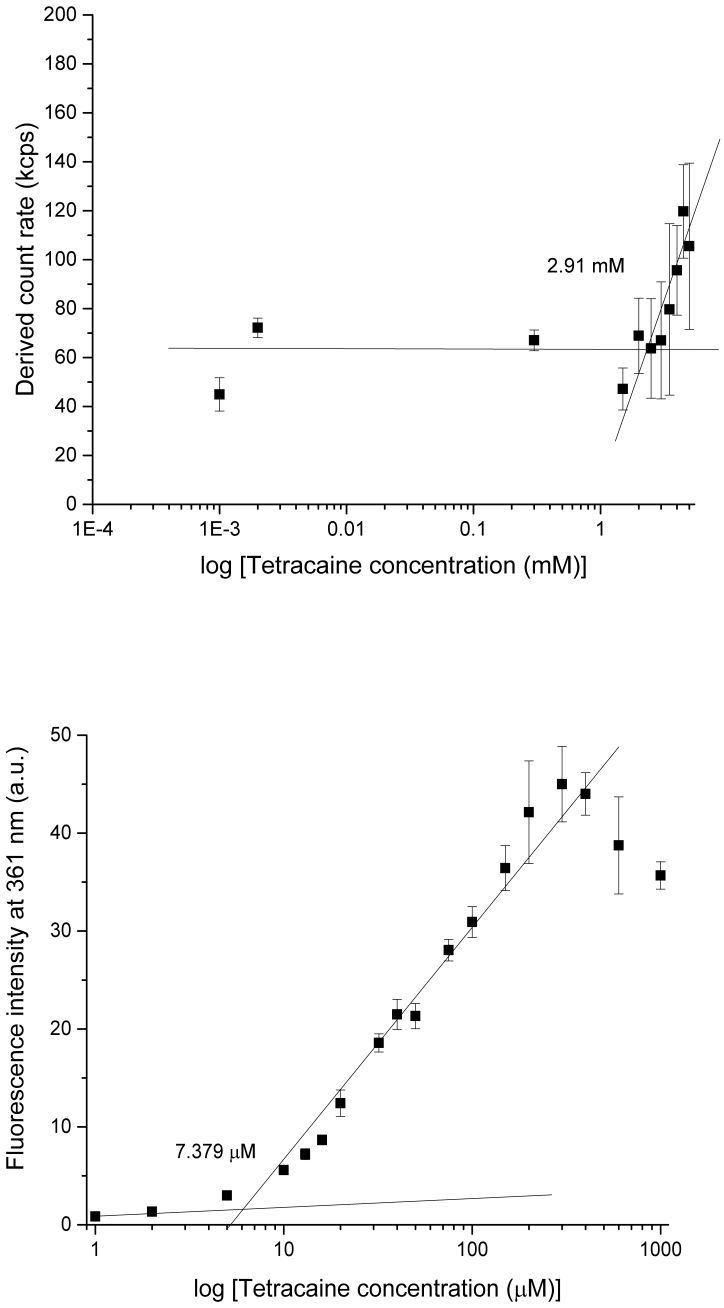

Figure 2.4. Graphs depicting critical aggregation concentrations (CACs) using photon correlation spectroscopy (top) and fluorescence spectroscopy (bottom) in C) pH 8.

To probe nature of the bonds formed between the aggregates in different tetracaine ionisation states, FTIR was employed. Based on the different CACs in different pHs (Table 2.2), 100 mM of tetracaine in pH 4 and 10 mM of tetracaine in pH 8 were used to ensure that aggregates predominantly existed in the solutions that were analysed. The FTIR spectrum recorded for the tetracaine solutions were presented as collected by the absorbance method, without deconvolution or solvent subtraction due to significant visible shifts in the regions of interest without further spectral manipulation (Fig. 2.5). The absorbance spectrum was normalised by the absorbance value at the CH_3 region (2939 cm^{-1}) to correct different laser intensities due to the varied concentrations used. As the pH increased from 4 to 8, a reduction in intensity of carbonyl group peaks (1690 and 1606 cm^{-1}) and secondary amide groups (1526 cm^{-1}) was observed. An increase in intensity at the region associated with carboxylate groups were formed (1469 cm^{-1}) was also observed.

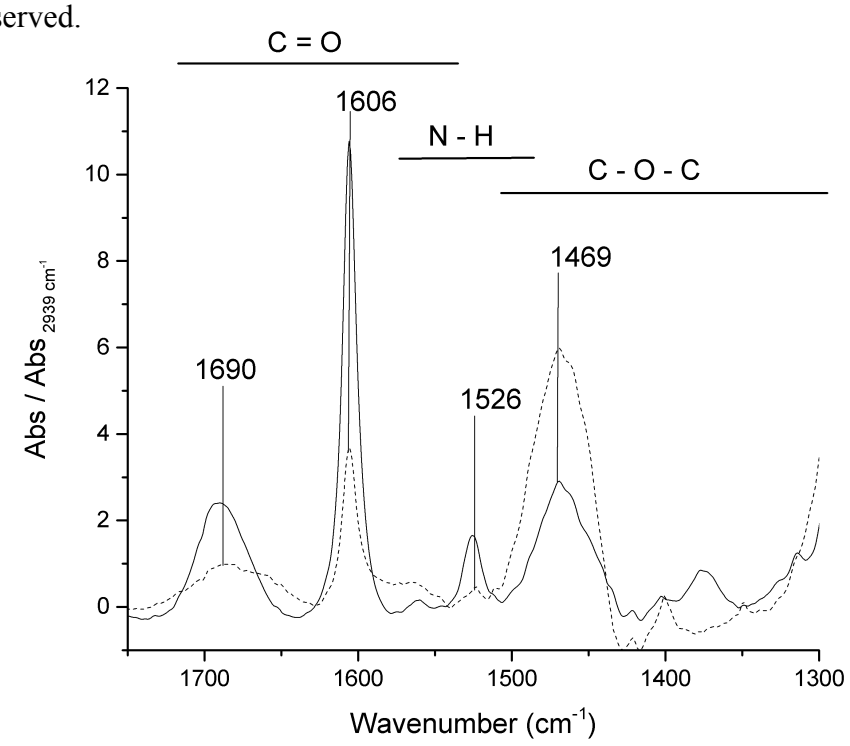

Figure 2.5. FTIR data of tetracaine in pH 4 (filled line) and 8 (dotted line).

2.4.3 Tetracaine transport

Two membranes were used to investigate the influence of tetracaine aggregation on its transport properties. The transport was studied in the silicone membrane first using a sequence of different tetracaine concentrations. Since each critical point recorded in the fluorescence spectra was referred to a change in the solution state equilibrium, it was suggested that at each critical concentration, a different arrangement of the molecules was present in the solution. In accordance with this interpretation at a tetracaine concentration of 16 and 50 μM, 2 different forms of aggregates of tetracaine were thought to be formed respectively at pH 4. Thus, the varying concentrations of tetracaine in the μM region were selected to try and test the tetracaine transmembrane transport in the presence of different aggregate forms (Table 2.2). Only the most interesting tetracaine donor concentrations were subsequently tested using the porcine membrane.

In the pH 4 vehicle, the permeability coefficient through the porcine epidermis significantly decreased ($p<0.05$) from (13.7 ± 4.3) to (0.06 ± 0.6) x 10^{-3} cm/h when the tetracaine concentration increased from 10 μM to the saturated concentration of 1.05 M. When the same test systems were applied to a silicone membrane, a significant decrease ($p<0.05$) from (0.7 ± 0.2) x 10^{-3} cm/h at 10 μM to (0.034 ± 0.005) x 10^{-3} cm/h at saturated tetracaine concentration was also observed. However, for the intermediate tetracaine concentrations where the types of aggregates formed were thought to change (Table 2.2), no effect on the permeability coefficient through the silicone membrane

occurred ($p>0.05$)(Table 2.3, Fig. 2.6 and 2.7 for permeation profiles of tetracaine through porcine epidermis and silicone membrane respectively).

Concentration (μM)	Porcine epidermis		0.12 mm silicone membrane	
	Flux ($ng/cm^2/h$)	k_p (10^{-3} cm/h)	Flux ($ng/cm^2/h$)	k_p (10^{-3} cm/h)
10	36.2 ± 11.3	13.7 ± 4.3	2.0 ± 0.6	0.7 ± 0.2
20	-	-	3.4 ± 0.7	0.7 ± 0.1
40	-	-	9.4 ± 0.7	0.8 ± 0.1
100	-	-	13.6 ± 3.3	0.5 ± 0.1
1000	-	-	177.9 ± 44.6	0.7 ± 0.2
1.05×10^6	$(1.6 \pm 0.6) \times 10^4$	$0.06 \pm 0.02^*$	$(9.4 \pm 1.4) \times 10^3$	$0.034 \pm 0.005^*$

Table 2.3. Steady state flux and permeability coefficients, k_p, of different concentrations of tetracaine in pH 4 across porcine epidermis and silicone membrane. Data represent mean ± standard deviation of 3 independent tetracaine samples. * Significant differences were observed based on Games Howell test.

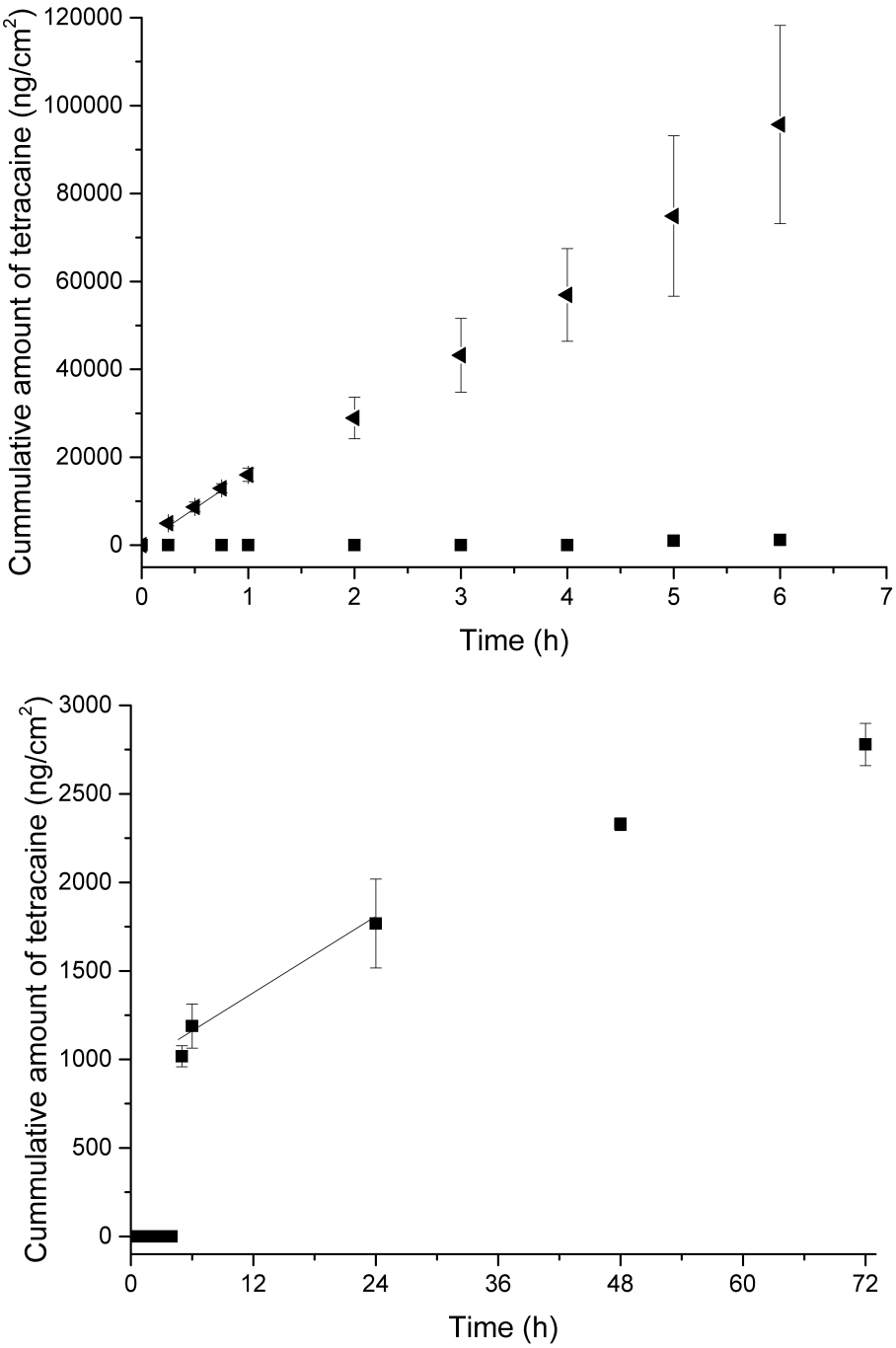

Figure 2.6. Permeation profiles of 10 μM and 1.05 M (◄) of tetracaine in pH 4 through porcine epidermis. Each point represents mean ± standard deviation (n=5). The straight lines represent the steady-state portion of the permeation profiles.

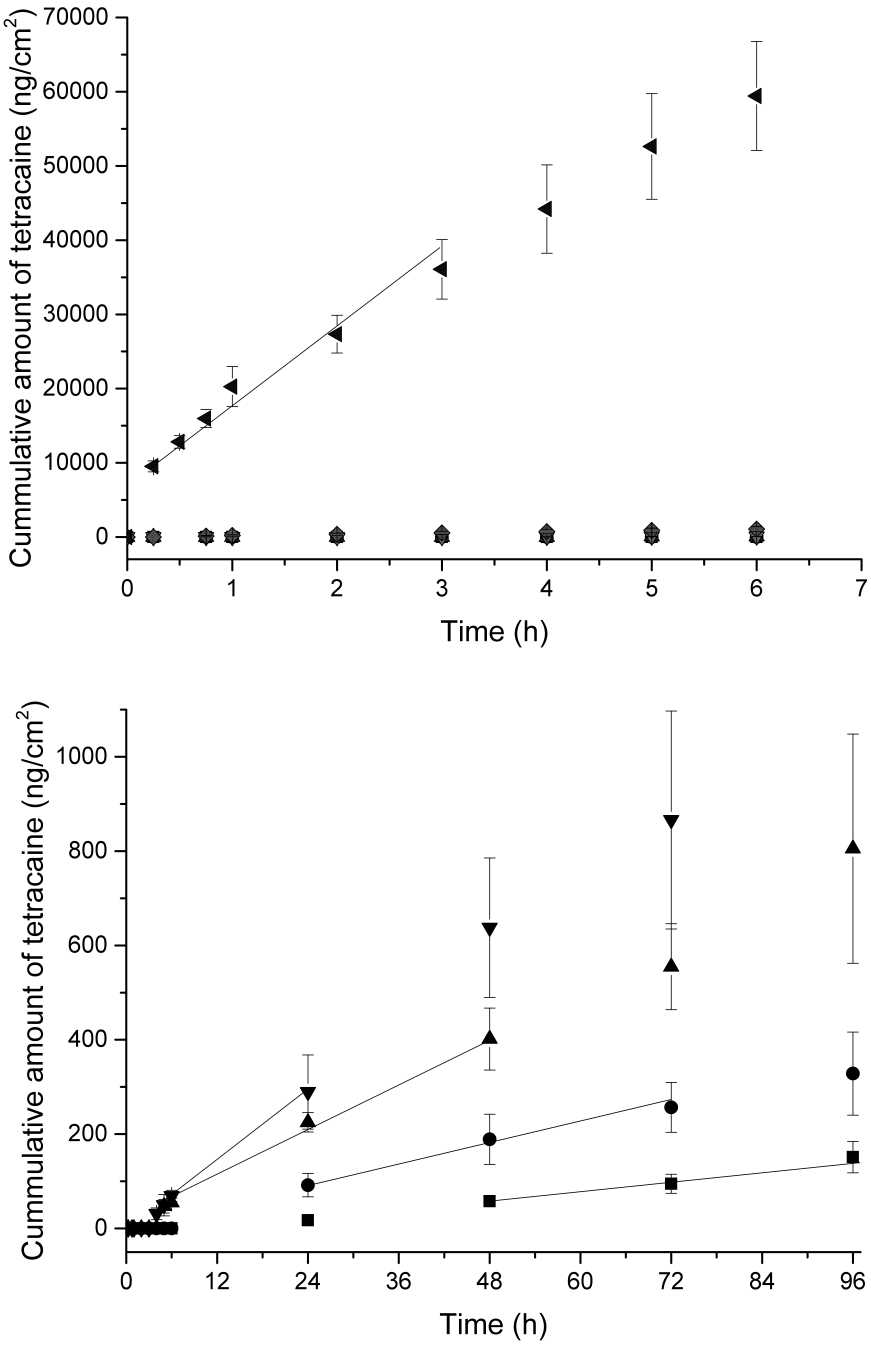

Figure 2.7. Permeation profiles of 10 μM (■), 20 μM (●), 40 μM (▲), 100 μM (▼), 1000 μM (♦) and 1.05 M (◄) of tetracaine in pH 4 through silicone membrane. Each point represents mean ± standard deviation (n=5). The straight lines represent the steady-state portion of the permeation profiles.

A different trend was observed when a different ionisation state of tetracaine was introduced in pH 8 (Table 2.4, Fig. 2.8 and 2.9 for permeation profiles of tetracaine through porcine epidermis and silicone membrane respectively). The permeability coefficient through the porcine epidermis significantly increased ($p<0.05$) from (29.9 ± 9.9) to (75.1 ± 41.7) x 10^{-3} cm/h as the tetracaine concentration increased from 10 μM to the saturated concentration (6.29 mM). Using a silicone membrane, the permeability coefficient also significantly increased ($p<0.05$) from (23.5 ± 6.2) to (201.5 ± 38.2) x 10^{-3} cm/h. The increase in permeability coefficient was observed in the μM region; when the 40 μM tetracaine donor solution was applied, a higher permeability coefficient of (48.1 ± 5.4) x 10^{-3} cm/h was obtained as compared to those from 10 μM.

	Porcine epidermis		0.25 mm silicone membrane	
Concentration (μM)	Flux (ng/cm^2/h)	k_p (10^{-3} cm/h)	Flux (ng/cm^2/h)	k_p (10^{-3} cm/h)
10	79.1 ± 26.1	29.9 ± 9.9	62.2 ± 16.5	23.5 ± 6.2
40	-	-	508.5 ± 56.9	48.1 ± 5.4*
6.29 X 10^3	(1.2 ± 0.7) x 10^5	75.1 ± 41.7*	(3.4 ± 0.6) x 10^5	201.5 ± 38.2*

Table 2.4. Steady state flux and permeability constants, k_p, of different concentrations of tetracaine in pH 8 across porcine epidermis and silicone membrane. Data represent mean ± standard deviation of 3 independent tetracaine samples. * Significant differences were observed based on Games Howell test.

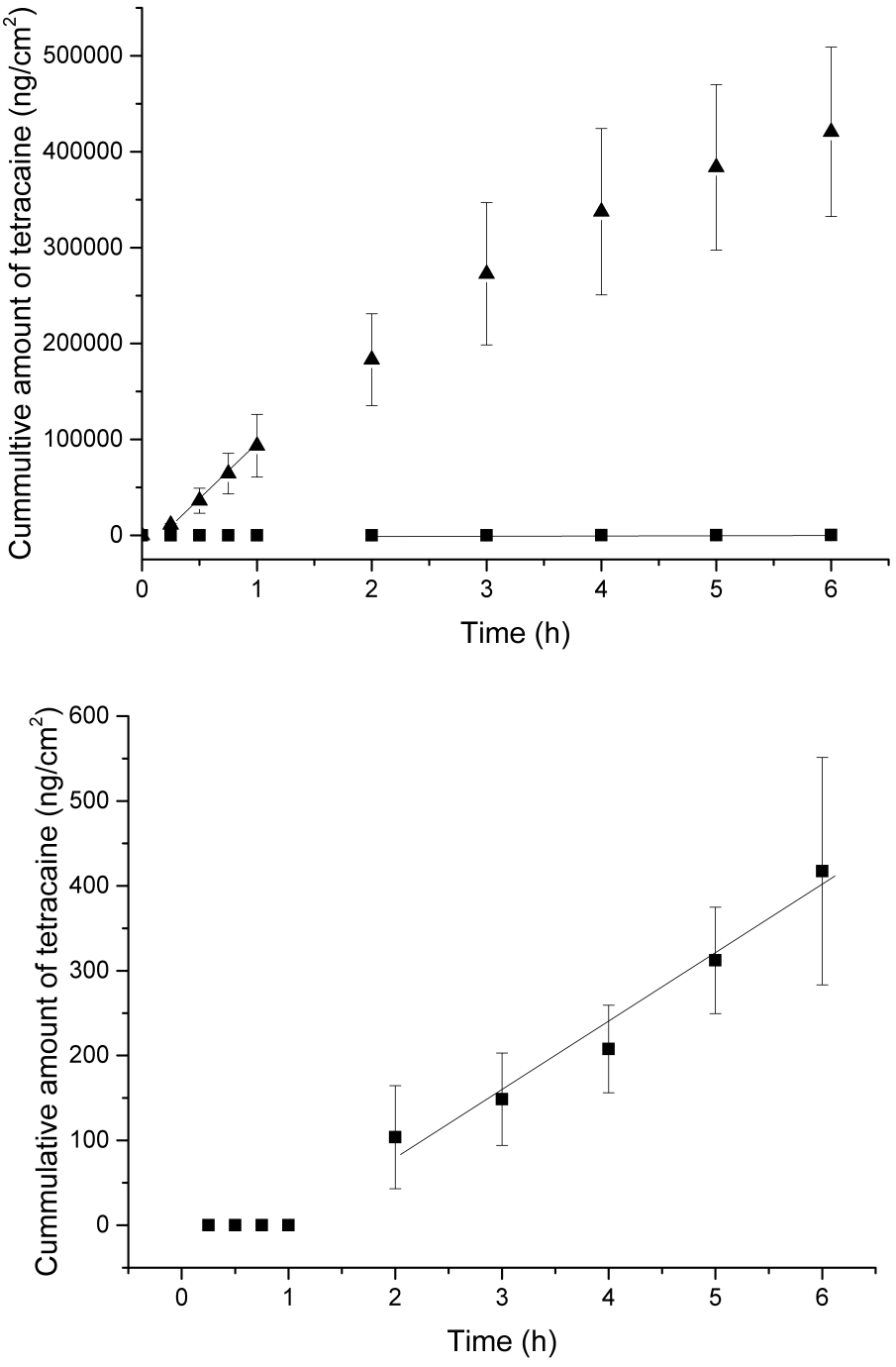

Figure 2.8. Permeation profiles of 10 μM (■) and 6.28 mM (▲) of tetracaine in pH 4 through porcine epidermis. Each point represents mean ± standard deviation (n=5). The straight lines represent the steady-state portion of the permeation profiles.

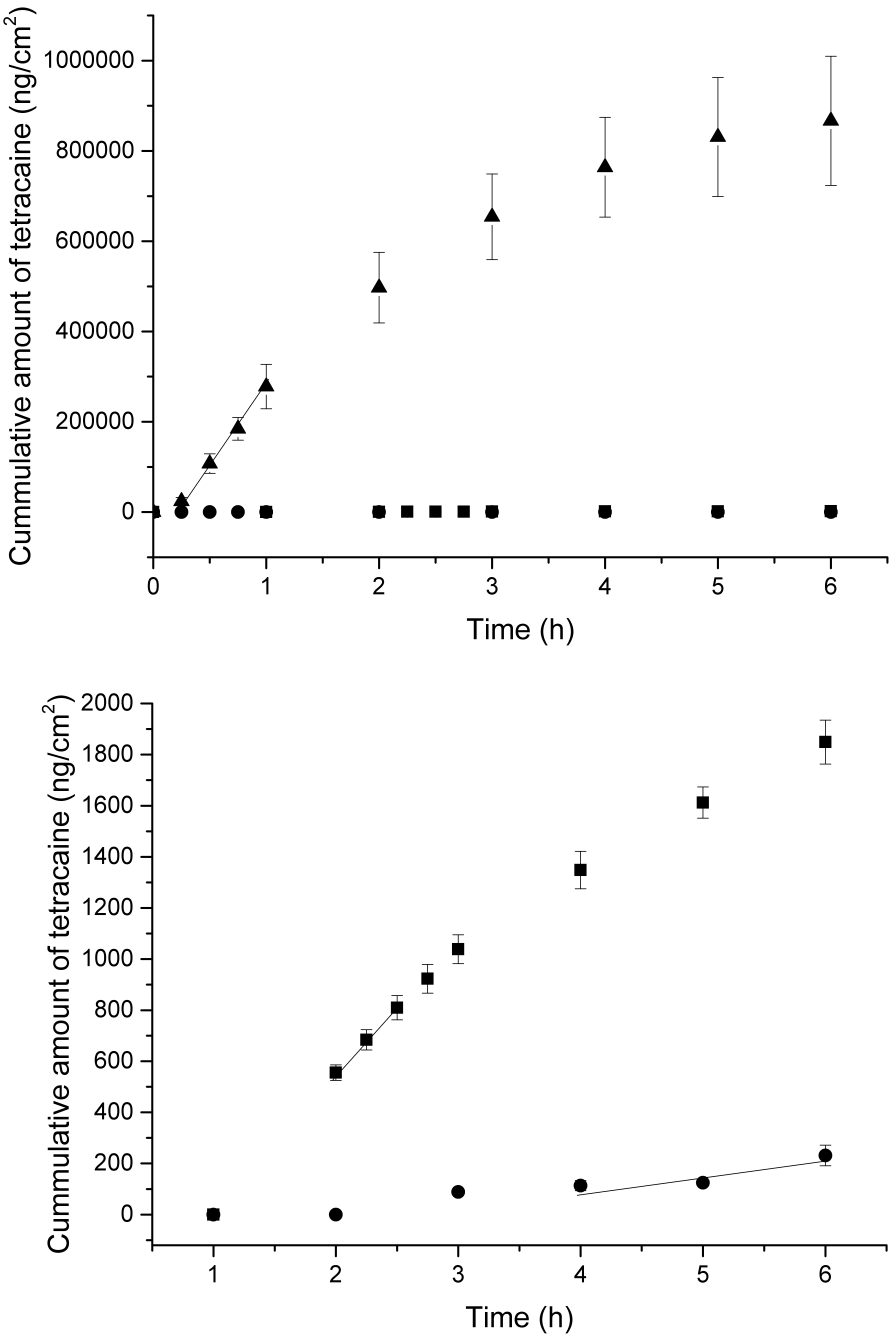

Figure 2.9. Permeation profiles of 10 μM (■), 40 μM (●) and 6.28 mM (▲) of tetracaine in pH 4 through silicone membrane. Each point represents mean ± standard deviation (n=5). The straight lines represent the steady-state portion of the permeation profiles.

2.5 Discussion

2.5.1 Tetracaine solution state interactions

Tetracaine, also known as amethocaine, is an amphiphilic molecule, which is positively charged at physiological pH. The chemical structure has a hydrophilic region (amine portion) and a hydrophobic region (aromatic portion) and this predisposes it to self-associate in aqueous solution. At concentrations of more than 1 mM, previous literature suggests tetracaine forms an aggregate (Farhadieh, Hall et al., 1967; Florence & Attwood, 2011; Johnson & Ludlum, 1969). There appears to be a difference of opinions in the literature as to whether tetracaine forms organised micelles (Kitagawa, Oda et al., 2004; Matsuki, Ichikawa et al., 1996; Shaikh, Dagade et al., 2011) or random molecular aggregates (Attwood & Fletcher, 1986; Farhadieh, Hall et al., 1967). In addition, there is less known about at what concentration aggregation commences.

There have been several studies that document tetracaine's CAC. For example, Kitagawa et al. (2004) proposed tetracaine hydrochloride had a CAC of 38 mM at 25°C in an aqueous solution, pH ranged from 4.5 to 5.7, using an electrode method. A higher CAC value of 128 mM was reported based on surface tension, density and Kraft point measurements, at a pH of approximately 5.0 (Matsuki et al., 1994; Matsuki, Ichikawa et al., 1996; Miller et al., 1993). In all these previous work, relatively high drug concentrations were investigated and this was probably a consequence of experimental limitations (i.e. caused by the solvents and analytical equipment employed to detect the

aggregates)(Farhadieh, Hall et al., 1967; Guerin, Dumas et al., 1980; Kitagawa, Oda et al., 2004; Shaikh, Dagade et al., 2011; Umemura & Mantsch, 1981). It is noteworthy that a high CAC value may be attributed to a high limit of detection of any given analytical machine. Therefore, in these cases, the CAC only represents a point where the aggregation equilibrium changes and a new type of structuring occurs, rather than the initial point of aggregation.

Using photon correlation spectroscopy, the CAC results at pH 4 (40 and 200 mM) were close to those obtained previously (Kitagawa, Oda et al., 2004; Matsuki, Hashimoto et al., 1994; Matsuki, Ichikawa et al., 1996; Miller, Goodwin et al., 1993). Tetracaine CAC at pH 8 has not been investigated before. As the light scattering technique could have suffered from the same detected sensitivity problems as the previously reported methods of analysis, tetracaine aggregation was determined using fluorescence spectroscopy in addition to this technique.

Fluorescence spectroscopy detects tetracaine aggregation as a consequence of the interactions between the monomers result in the shielding of the electrons in the aromatic ring to generate signal quenching. The deviation from linearity in concentration titration experiments can signify a change in tetracaine aggregation in the solution if all the other conditions that may influence this process (i.e. temperature, pH, ionization strength) are kept constant. In this study, the temperature and pH of the system were maintained. Moreover, the system was chemically stable over 6 days and the effect of ion pairing was not significant. The deviation from linearity in

concentration titration experiments signified a change in tetracaine aggregation in the solution as low as 16 μM in pH 4 and 10 μM in pH 8. Such low values for aggregation have not been previously reported.

The photon correlation spectroscopy measurements helped to support the fluorescence measurements, even though the samples used were at two very different concentration ranges, because similar patterns of data were obtained from the two techniques. Both the photon correlation spectroscopy and fluorescence spectroscopy results show that as the pH increased, the CAC decreased. This phenomenon has also been shown with drug molecules. Attwood and Natarajan (1981) observed a higher critical micelle concentration at a low pH (0.5-5.5) in 5 piperazine containing drugs (trifluoperazine, opirpramol, thiopropazate, flupenthixol and clopenthixol). The structure of trifluoperazine is close to tetracaine (pK_a 3.41 and 8.24); Trifluoperazine has an aromatic hydrocarbon and two nitrogen atoms which protonates at pK_a 3.8 and 8.4. According to Attwood and Natarjan (1981), the increase in CMC as pH decreases is attributed to the increase in electrical charge of the molecule as the nitrogen atoms get protonated.

Both fluorescence and FTIR studies seem to suggest that tetracaine ionization affects the type of aggregates being formed. In pH 8, the formation of tetracaine aggregates is accompanied by a change in the drug's hydrophobic environment and this gave rise to the blue shift in λ_{max} (Table 1). A similar trend has been observed by Mertz et al. (1990), who showed a fluorescence blue shift when tetracaine aggregates were

subjected to molecules known to form hydrogen bonds. The infrared spectra analysis of this work showed that the carbonyl bands intensity of tetracaine in pH 8 decrease upon aggregation. An investigation by Guerin et al. observed a similar decrease in carbonyl band intensity (1980). Tetracaine is thought to associate by stacking of the aromatic rings, involving mostly $N-H\cdots N$ tertiary association with some $N-H\cdots C=O$ ester and $N-H\cdots N-H$ bonds and it is this process that results in the carbonyl band changes.

In topical medicinal products, currently tetracaine is formulated at 0.15 M. Hence the drug probably exists as aggregates in aqueous vehicles that are presented to the skin. It is therefore probable that the transport of a tetracaine product is significantly influenced by the aggregation state of the drug. If this holds true, drug aggregation may be the cause of the high lag time and low penetrating amount of tetracaine (Inacio et al., In-press).

2.5.2 Tetracaine transmembrane permeation

The process of passive transmembrane penetration is most commonly interpreted using Fick's second law of diffusion, which is based upon the assumption that the system is homogeneous i.e. there are no 'specific interactions' between the components of the system (drug, vehicle and membrane)(Godin & Touitou, 2007; Kalia & Guy, 2001; Mitragotri et al., 2011). In an ideal scenario, i.e., one which obeys Fick's law, the permeability coefficient should be constant for a drug when changing the initial loading

concentration of the permeating compound. Hence, any changes in permeability coefficient represent deviations from ideal, which can result from drug-membrane, drug-vehicle or drug-drug interactions.

Molecular aggregation is driven by the equilibration between non-aggregates and aggregates in the solution state. Given its pK_a, in pH 4, aggregates are most likely to be formed of charged tetracaine molecules. There are two hypotheses that can be generated to explain the decrease in the permeability coefficient of the drug when aggregates were formed. The first is based on the fact that only non-aggregated molecules drive tetracaine transport. Therefore, as the concentration of tetracaine in the solution increases, more aggregation occurs. Hence, there is less availability of free molecules, which reduces the permeability of tetracaine. Another possible hypothesis is that tetracaine transport is driven by both aggregates and non-aggregates. In this scenario, it is most likely that the charged tetracaine aggregates permeate through the skin *via* the shunt route (Edwards & Langer, 1994). The shunt route can become saturated as it is only present in certain regions of the skin and the aggregates may become bigger as the drug concentration increases. This can limit the amount of tetracaine molecules that can go through the appendages; hence resulting in a decrease of relative permeability of tetracaine. A silicone membrane is often employed in transport studies to provide a theoretical understanding of the simple permeation process rather than the complex multiple processes occurring in the heterogeneous skin, as it has no pores or availability of shunt routes. As such, the similar trend from the transport of pH 4 tetracaine through

the silicone membrane as tetracaine aggregates were formed suggests that the former of the two hypotheses is more plausible.

As the molecule in pH 8 forms a significant proportion of uncharged microspecies (28%), it is predicted that aggregates formed at this pH would be less polar than at pH 4 (no uncharged microspecies). The less polar aggregates formed at pH 8 are more likely to travel through the skin *via* the intercellular pathway (Abraham, Chadha et al., 1995; Pugh et al., 1996). Just like at pH 4, the similar trend in the permeation coefficient data through the porcine membrane and silicone membrane suggests that aggregates do allow a significant amount of drug to travel through the shunt route and thus, this supports the fact that the non-follicular route is favoured at pH 8. There are two possible hypotheses to explain the increase in the permeability coefficient of tetracaine when aggregates were formed given that the intercellular pathway is preferred at this pH. The first hypothesis is an extension of the monomer penetration model (Charman, Lai et al., 1991), which states that only non-aggregated molecules pass through the epidermis. Aggregates will dissociate and re-associate continually in solution and therefore, the number of free aggregates that are available to participate in the skin diffusion process is to some extent dependent upon on the aggregate kinetics. This is because as more monomers penetrate through the membrane, the decrease in monomer concentration in the donor solution will force the dynamic equilibrium between the monomers and aggregates in the donor solution to re-balance. If this occurs quickly, then the drug permeation will be higher compared to if the equilibration is slow. As tetracaine concentration increases, the concentration of aggregates should increase, leading to an

increase in the thermodynamic drive to dissociate when monomers are lost through adsorption through the skin. While this hypothesis seems appealing, it fails in one critical aspect. The time to transport tetracaine across the *stratum corneum* is much slower than the time for aggregate to dissociate (around 10^{-4} to 10 s)(Patist, Jha et al., 1999). As such, the rate-determining step of tetracaine diffusion through the skin should be controlled by the rate of tetracaine transport through the *stratum corneum*, not the rate of aggregate dissolution. The second hypothesis is that tetracaine transport is driven by both aggregates and non-aggregates through the intercellular pathway (Moore, Puvvada et al., 2003). An increase in tetracaine concentration provides a supply of both monomers and aggregates, thus resulting in an increase in permeability of tetracaine.

2.6 Conclusion

In order to satisfy the aim of the thesis, a model drug that aggregates is required. In addition, the role of aggregation on the transport of the model drug across a membrane needs to be understood in order to discover if nanoparticle surface interactions can modify this transport process. In this chapter, tetracaine was shown to be a model drug that aggregates. It was shown to form aggregates in aqueous solutions in the μM range. In the different ionisation states, the type of aggregates formed differed in terms of CAC and types of bonds formed. Tetracaine aggregation changed its drug permeation process. At pH 4, aggregates decreased tetracaine permeability coefficient but at pH 8, aggregates had the opposite effect. Thus, it seems plausible that nanoparticles could modify aggregation in the design of a strategy to enhance tetracaine permeation through the skin – a concept that will be investigated with the application of nanomaterials in Chapter 3.

CHAPTER THREE

Harnessing the Unique Surface Properties of Nanomaterials to Improve Drug Penetration Into the Skin

3.1 Introduction

In the previous chapter, drug aggregation was shown to be able to influence the ability of a molecule to move through a membrane passively. Drug aggregates can arise from drug-drug interactions or drug-excipient interactions. In either case, the molecules that form aggregates exhibit different physicochemical properties in solution compared to non-aggregated molecules and this is one of the main reasons why the permeation properties through a membrane are modified. Knowledge of this phenomenon provides a basis to suggest that controlling the aggregation process can be used as a strategy to enhance drug percutaneous penetration. The control of drug aggregation could be achieved by the addition of substances that interact with a drug and thus, compete with the molecule's ability to self-associate. However, such a strategy has not been used to deliberately improve the topical penetration of topical agents into the skin to date.

Studies that investigated the interactions in pharmaceutical formulations have shown that the addition of electrolytes (Attwood & Udeala, 1975), surfactants and polymers (Pygall, Griffiths et al., 2011) can disrupt drug molecular aggregation by interacting with the molecule that is self-associating. For example, simple surfactants have been used to break up the aggregation of small molecular weight agents such as phthalocyanines and larger therapeutic agents such as insulin (Darwent, McCubbin et al., 1982; Rossetti, Lopes et al., 2011; Shao, Li et al., 1993; Spikes & Bommer, 1986). Surface-active solid nanomaterials could be used to facilitate drug-drug aggregation and thus, may modify the subsequent drug penetration through a membrane. However, the

link between drug aggregation, nanomaterial surface effects and transmembrane transport needs further study.

A myriad of nanomaterials have been used in pharmaceutical and cosmetic formulations – lipids, polymers, metals, minerals etc. (Muller et al., 2002; Prow, Grice et al., 2011) (reviewed in Section 1.5). The body of literature that has been generated during the development of these systems has suggested that nanomaterials can be used to mask colour and odour (Kuelkamp-Guerreiro, Berlitz et al., 2013; Souto, Muller et al., 2005), control release of drugs across the membrane (Jenning et al., 2000; Puglia et al., 2008) and provide chemical protection by loading inside a particle (Dingler et al., 1999; Trombino, Cassano et al., 2009). One of the most exciting attributes of nanoparticles is that they have also shown to enhance drug transport across the skin (Alves et al., 2007; Borgia et al., 2005; Chen et al., 2006).

The introduction of nanomaterials into a topical product applied to the skin does not always guarantee drug percutaneous enhancement. This is especially the case if the materials are used as drug carriers, i.e., the drug is loaded within the nanoparticle. These nanocarriers can add a second rate-limiting step to the drug penetration process (Baroli, 2010a) and they pose additional challenges when they have low loading capacity (Schäfer-Korting, Mehnert et al., 2007), premature drug release (Zhao, Brown et al., 2010) and poor drug release (Muller & Kreuter, 1999). These issues can to some extent be circumvented if rather than being employed as a drug carrier nanomaterials, are employed to control drug aggregation through their surface interactions.

As such, the aim of this chapter was to study the influence of nanomaterials on transmembrane transport when co-administered to the skin. It was hypothesized that nanomaterials could be used to perturb drug aggregation in the way that promotes drug permeation and it was hoped that such a penetration enhancing strategy could be applied to the topical delivery of amphiphilic drugs. Negatively charged carboxyl-modified polystyrene nanoparticles and silica nanoparticles were used to represent two different nanomaterial surfaces and their properties were characterised using light scattering and atomic force microscopy (AFM). The addition of simple counter-ions to the drug in solution was used to investigate if the drug would respond to binding to the nanoparticle surface in a similar manner. In addition, the effect of the nanoparticles equilibrating with the drug in solution was investigated. Two barriers, the porcine epidermis and a silicone membrane, were used in the studies in order to understand the delivery of the drug through a barrier with and without the follicular transport route. The follicular transport route has previously been shown to be important when nanomaterials are presented to the barrier topically (Knorr, Lademann et al., 2009).

3.2 Materials

Material	Specifications	Company
Tetracaine	Free base, ≥ 98%	Sigma Aldrich, UK
$Nano_{PSCOOH}$	Carboxyl-modified polystyrene nanoparticles with a diameter of 60 nm (PC02N)	2B Scientific, UK
$Nano_{SiO_2}$	Silica nanoparticles with a diameter of 200 nm (Psi-0.2)	Kisker Biotech GmbH and Co., Germany
Hydrochloric acid (HCl)	Fuming, 37%	Sigma Aldrich, UK
Phosphate buffered saline	Tablets, pH 7.4, 0.172 M	Oxoid Ltd, UK
De-ionised water	Electrical conductivity 0.5-1 μS	Produced in house
Poly-L-lysine solution	0.1% w/v	Sigma Aldrich, UK
Ethanol	200 Proof, ACS Reagent	Sigma Aldrich, UK
Mica surfaces	-	Agar Scientific, Elektron Technology UK Limited
Cantilevers	Uncoated Si_3N_4 cantilevers with integrated pyramidal tips (Model: NSC15/noAl)	MikroMasch, Germany
Sodium phosphate dibasic	Anhydrous, ≥ 99.5%	Sigma Aldrich, UK
Centrifugal filters	Amicon Ultra 0.5 mL, Nominal molecular weight limit of 100 kDa	Millipore Limited, UK
Sodium acetate	Anhydrous, ≥ 99%	Sigma Aldrich, UK
Acetic acid	ACS reagent, ≥ 99.7%	Sigma Aldrich, UK

Acetonitrile	High performance liquid chromatography (HPLC) grade	Fisher Scientific, UK
Methanol	HPLC grade	Fisher Scientific, UK
Water	HPLC grade	Fisher Scientific, UK
Silicone membrane	Thickness of 0.12 mm	GBUK Healthcare, UK

Table 3.1. Materials used in Chapter 3.

3.3 Methods

3.3.1 Test sample preparation

Tetracaine solutions were prepared and adjusted to pH 4.0 and 8.0 using HCl and equilibrated at 32°C unless stated otherwise. Solutions were stirred for at least 24 h and their pH was rechecked prior to analysis to ensure they were at equilibrium. The vehicle containing the nanoparticles was corrected to the necessary pH using HCl prior to mixing with tetracaine solutions.

3.3.2 Atomic force microscopy (AFM) imaging

The AFM images were obtained using a Nanoscope V Dimension Icon atomic force microscope (Bruker, US). Uncoated Si_3N_4 cantilevers with integrated pyramidal tips with a reported high resonance frequency of 325 kHz and high spring constant of 46 N/m was used for the tapping mode AFM imaging in air. The $Nano_{PSCOOH}$ and $Nano_{SiO_2}$ images were taken after deposition on freshly cleaved mica surfaces. To facilitate nanoparticle deposition, an aqueous 0.1% (w/v) poly-L-lysine solution was applied to mica prior to the addition of the nanoparticles, After acquisition, the images were flattened and analysed using section analysis with Gwyddion version 2.36, a free SPM data visualization and analysis programme.

3.3.3 Photon correlation spectroscopy

The nanoparticle size was analysed by photon correlation spectroscopy (PCS)(Malvern Nanoseries Zetasizer ZEN3600, Malvern Instruments Ltd, UK). Detection of the light scattering signal was achieved at a 173° backscattering angle with samples equilibrated at 32°C using water as a dispersant (refractive index 1.33, viscosity 0.8872 cP). Each measurement comprised of 10-14 runs. The zeta potential of the nanoparticles was recorded using the same Malvern Nanoseries Zetasizer instrument using zeta potential capillary cells. Prior to the zeta potential measurements, the samples were prepared in 10 mM sodium chloride (NaCl) to normalise the sample osmolality. The measured electrophoretic mobility was converted into zeta potential using Smoluchowski's formula. Each measurement comprised of 50 to 100 runs. Triplicates of each sample were assessed. In an attempt to estimate the pK_a at the nanoparticle surfaces and determine the isoelectric point a zeta potential titration was performed by measuring the zeta potential of the particles at pH units between pH 1 to 11. The pH of the solution was adjusted using HCl. A logarithm curve was fitted onto the zeta potential titration cure using the OriginPro software (OriginPro version 8.6, OriginLab Corporation, US) to calculate the isoelectric point and the pK_a.

3.3.4 Tetracaine transport studies

Infinite dose permeation experiments were conducted as described previously in Section 2.3.6. However, in this chapter a 0.5 mL aliquot of the nanoparticle suspension was

added to 0.5 mL of 20 μM of the tetracaine solution at the 0 h time point after correcting the suspension medium pH to 4 or 8. The final tetracaine concentration in the nanoparticle-tetracaine mixtures was 10 μM. HPLC grade water was added in place of the additives in the control system. The direct mixing of the drug and nanoparticles on the surface of the skin was the preferred application method throughout the study as it minimised any potential interference from chemical or physical instability as a consequence of forming the mixture. A concentration of 0.001 g/mL of $\mathrm{Nano_{PSCOOH}}$ and 6.289 g/mL of $\mathrm{Nano_{SiO_2}}$, which provided an equivalent surface area to volume ratio of 9.43×10^{-10}:1 μm^2/mL, were added to 10 μM tetracaine solutions to investigate the effects of nanomaterials on tetracaine transport.

As a control experiment, the influence of electrolytes on tetracaine transport was determined by subjecting tetracaine to an environment of phosphate ions. At pH 4, the electrolyte used in this study, anhydrous sodium dihydrogen phosphate (which has 3 pK_a at 1.85, 6.89 and 12.70) dissociates to form predominantly the monovalent dihyrogen phosphate ions ($H_2PO_4^-$). To investigate the effects of pre-equilibration of tetracaine-nanoparticles mixtures, the tetracaine solutions were mixed with the nanoparticles for 30 days before application. The vehicle of the nanoparticles, used in the transport studies to test if there was any penetration effect of the solution alone, was obtained by using a centrifugal filter with nominal molecular weight limit of 100 kDa at 1500 g for 10 min (Biofuge pico, Heraeus Instruments, Germany).

The determination of the steady state flux (J) was achieved as per the method described

previously in Section 2.3.6 and the enhancement ratios (ER) due to the various additives were determined using the following equation:

$$ER = \frac{J_2}{J_1} \quad \text{(Equation 3.1)}$$

where J_1 and J_2 are the steady state transmembrane transport rate of tetracaine from the tetracaine and tetracaine-nanoparticle mixture respectively.

3.3.5 Tetracaine quantification

Refer to Section 2.3.7.

3.3.6 Statistical analysis

Refer to Section 2.3.8.

3.4 Results

3.4.1 Particle characterisation

The carboxyl-modified polystyrene nanoparticles ($Nano_{PSCOOH}$) and silica nanoparticles ($Nano_{SiO_2}$) showed properties in accordance with the manufacturers specification (Table 3.2).

Tip-substrate	$Nano_{PSCOOH}$	$Nano_{SiO_2}$
Diameter according to the manufacturer's data (nm)	60.0	200
Mean diameter PCS (nm)	56.9 ± 0.7	246.6 ± 2.6
Mean diameter AFM (nm)	36.8 ± 7.3	197 ± 6.6
Surface area: volume ratio (μm)	$9.43x10^{-10}$:1	$9.43x10^{-10}$:1
Surface functional groups	-COOH, $-SO_4$	-OH
pK_a	≥ 4	4.03
Isoelectric point	N.A.	2.00
Zeta potential at pH 4 (mV)	- 40.3 ± 1.2	- 22.7 ± 1.4

Table 3.2. Summary of nanoparticle properties.

In this study, the size and zeta potential of the nanoparticles when subjected to 10 μM tetracaine concentration remained largely unchanged (Table 3.3).

	Diameter using PCS (nm)		Zeta potential (mV)	
	$Nano_{PSCOOH}$	$Nano_{SiO_2}$	$Nano_{PSCOOH}$	$Nano_{SiO_2}$
pH 4 water	56.9 ± 0.7	242.6 ± 2.6	-40.3 ± 1.2	-22.7 ± 1.4
10 μM of tetracaine	57.0 ± 0.6	239.6 ± 0.9	-39.0 ± 0.9	-24.0 ± 0.7

Table. 3.3. Diameters of carboxyl-modified polystyrene nanoparticles, $Nano_{PSCOOH}$, and silica nanoparticles $Nano_{SiO_2}$.

The mean diameter of the $Nano_{PSCOOH}$ obtained from the cross-sectional analysis of AFM (36.8 ± 7.3 nm)(Fig. 3.1) was significantly smaller (independent t-test, $p<0.05$) than those obtained using photon correlation spectroscopy (56.9 ± 0.7 nm)(Table 3.2). The manufacture of the $Nano_{PSCOOH}$ was such that they would most probably have both carboxyl and sulphated groups present on their surface. The pK_a values for the particles were not available and they could not be measured by simple zeta potential methods applied (Fig. 3.3), but the particle functional groups were expected to be fully ionised between pH 5-9 based on the reference pK_a values for carboxyl and sulphate groups (Manufacturer's data).

The mean diameter of the $Nano_{SiO_2}$ obtained from the cross-sectional analysis of AFM (Fig. 3.2) was significantly smaller (independent t-test, $p<0.05$) to those obtained using photon correlation spectroscopy (242.6 ± 2.6 nm)(Table 3.2). Silica nanoparticles in an aqueous environment are known to have hydroxyl surface groups (Zhuravlev, 2000). The zeta potential data for the $Nano_{SiO_2}$ suggested they had a pK_a of 4.03 and an isoelectric point of 2.00 (Fig. 3.3). In an aqueous solution set at pH 4, the surface charge of the $Nano_{SiO_2}$ was significantly less negative (independent t-test, $p<0.05$) than $Nano_{PSCOOH}$ and this data inferred that the pK_a for the carboxyl-modified particles was actually a little higher than 4.

(A)

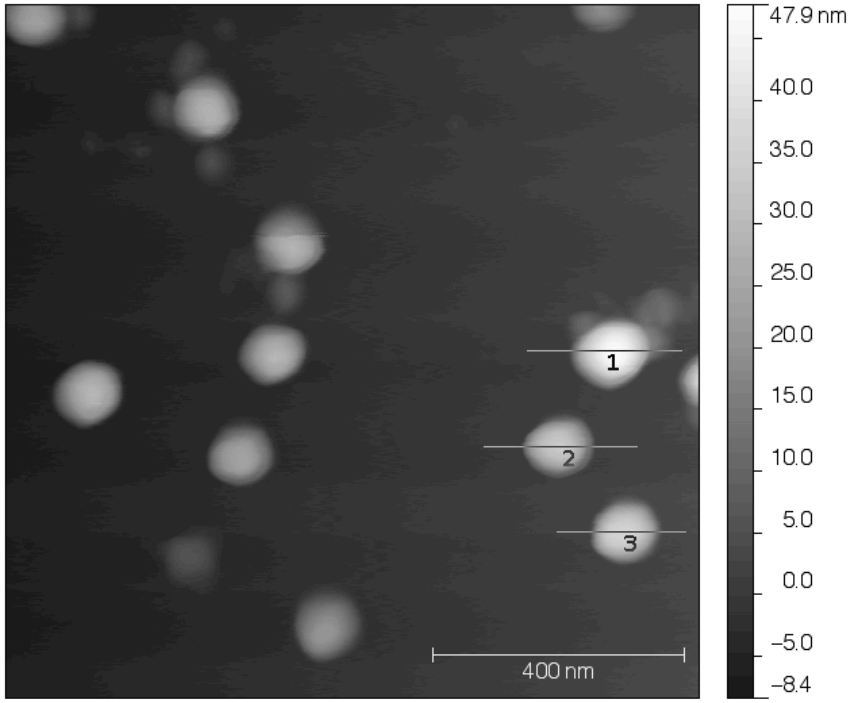

(B)

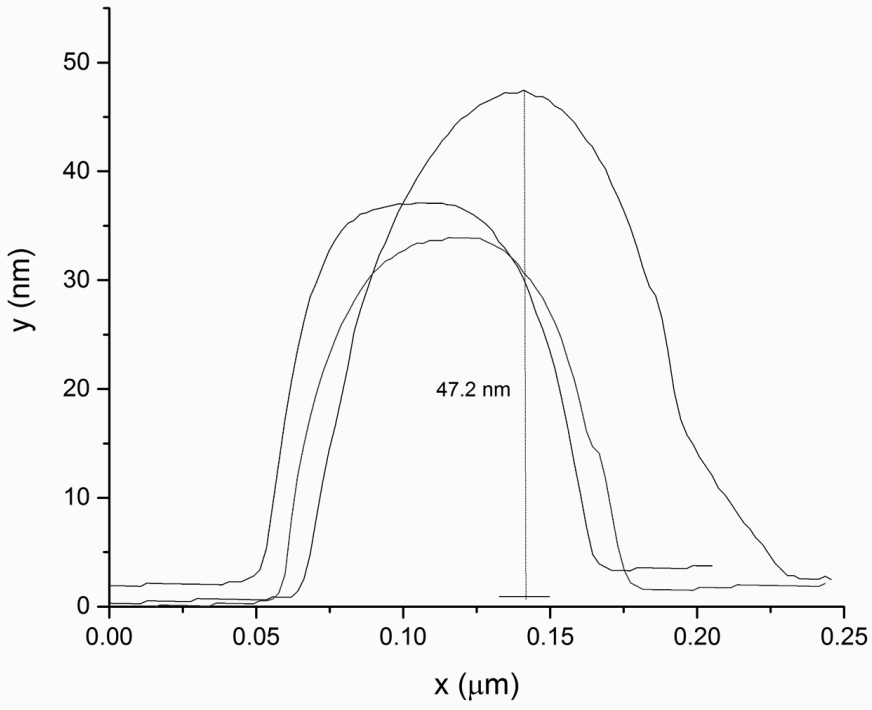

Figure 3.1. Tapping mode AFM topography image of carboxyl-modified polystyrene nanoparticles, $Nano_{PSCOOH}$, (A) and the cross-sectional profiles of 3 selected nanoparticles (B).

(A)

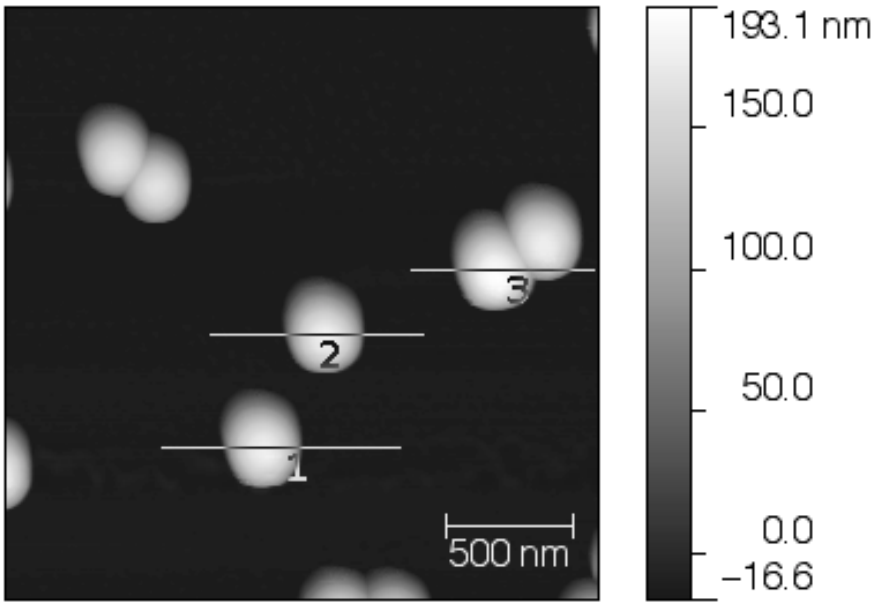

(B)

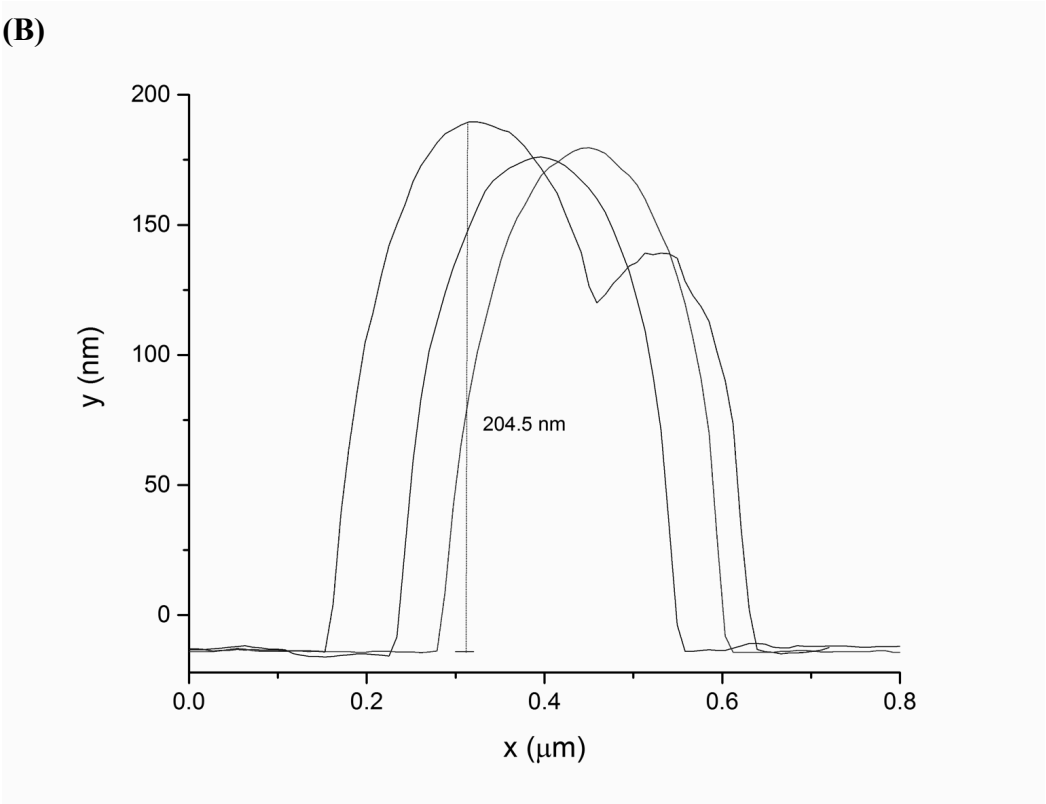

Figure 3.2. Tapping mode AFM topography image of silica nanoparticles $Nano_{SiO_2}$, (A) and the cross-sectional profiles of 3 selected nanoparticles (B).

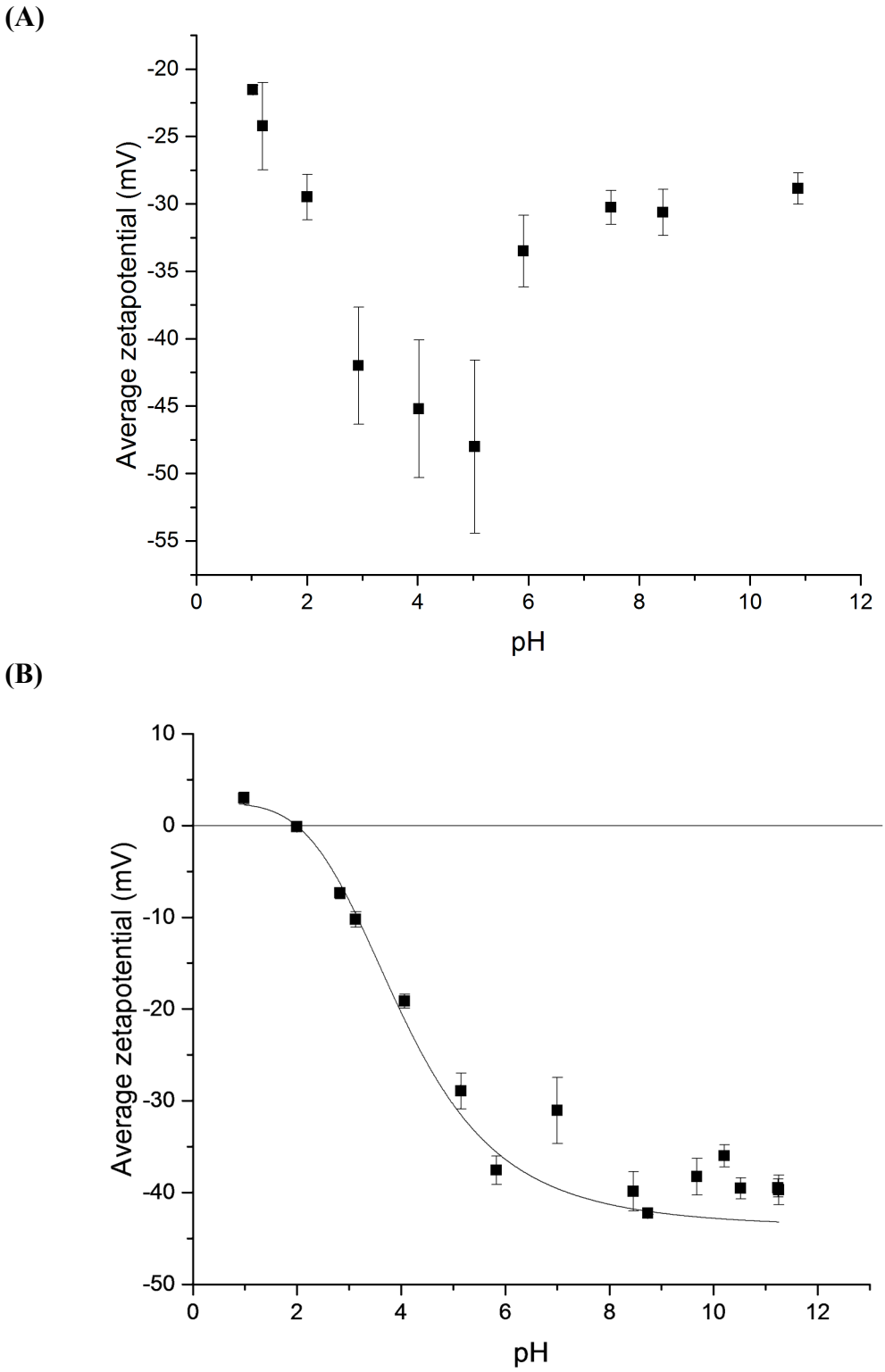

Figure 3.3. Surface charge distribution of carboxyl-modified polystyrene nanoparticles $Nano_{PSCOOH}$ (A), and silica nanoparticles $Nano_{SiO_2}$ (B).

3.4.2 Effect of nanomaterials on tetracaine transport

There was no significant difference between the fluxes through the skin when the tetracaine was added directly to the skin or if it was diluted on the surface of the skin to the same concentration (Table 3.4). This test was performed to validate the effects of mixing the formulations on the skin in subsequent experiments.

Donor solution	Flux ($ng/cm^2/h$)
1 mL of 10 μM tetracaine	2.0 ± 0.4
0.5 mL of 20 μM tetracaine + 0.5 mL of water	2.0 ± 0.6

Table. 3.4. Steady state flux of tetracaine through silicone membrane with a final concentration of 10 μM prepared by 2 different procedures.

Tetracaine transport was modified when the negative surfaces ($Nano_{PSCOOH}$ and $Nano_{SiO_2}$) were added to the tetracaine solution at both pH 4 and 8 (Table 3.5).

		Porcine epidermis		
	Concentration (mM)	Flux ($ng/cm^2/h$)	k_p (10^{-3} cm/h)	ER
pH 4	10 μM TET	36.2 ± 11.3	13.7 ± 4.3	-
	10 μM TET + $Nano_{PSCOOH}$	0	0	-*
	10 μM TET + $Nano_{SiO_2}$	122.5 ± 31.0	42.3 ± 11.7	3.6 ± 1.2*
pH 8	10 μM TET	79.1 ± 26.1	29.9 ± 9.9	-
	10 μM TET + $Nano_{PSCOOH}$	0	0	-*
	10 μM TET + $Nano_{SiO_2}$	148.1 ± 23.9	56.0 ± 8.9	2.0 ± 0.5*

Table 3.5. Steady state flux and permeability constants, k_p, and enhancement ratio of 10 μM of tetracaine in the presence of different additives in pH 4 and 8 across porcine epidermis. Data represent mean ± standard deviation of 3 independent tetracaine samples. * Significant differences were observed based on Dunnett's test.

At pH 4, the $Nano_{PSCOOH}$ significantly ($p<0.05$) hindered the percutaneous permeation of tetracaine through the porcine skin, reducing the drug flux from 36.2 ± 11.3 ng/cm^2/h to undetectable levels. When the same test systems were applied at pH 8, the addition of $Nano_{PSCOOH}$ to the tetracaine solutions showed similar adverse effect on tetracaine transport across the porcine epidermis (Table 3.5, Fig. 3.4 for permeation graphs).

At pH 4, the $Nano_{SiO_2}$ significantly enhanced ($p<0.05$) percutaneous tetracaine transport by 3.6-fold. At pH 8, the $Nano_{SiO_2}$ increased the transport rate across the porcine skin by 2.0-fold (Table 3.5, Fig. 3.4 for permeation graphs).

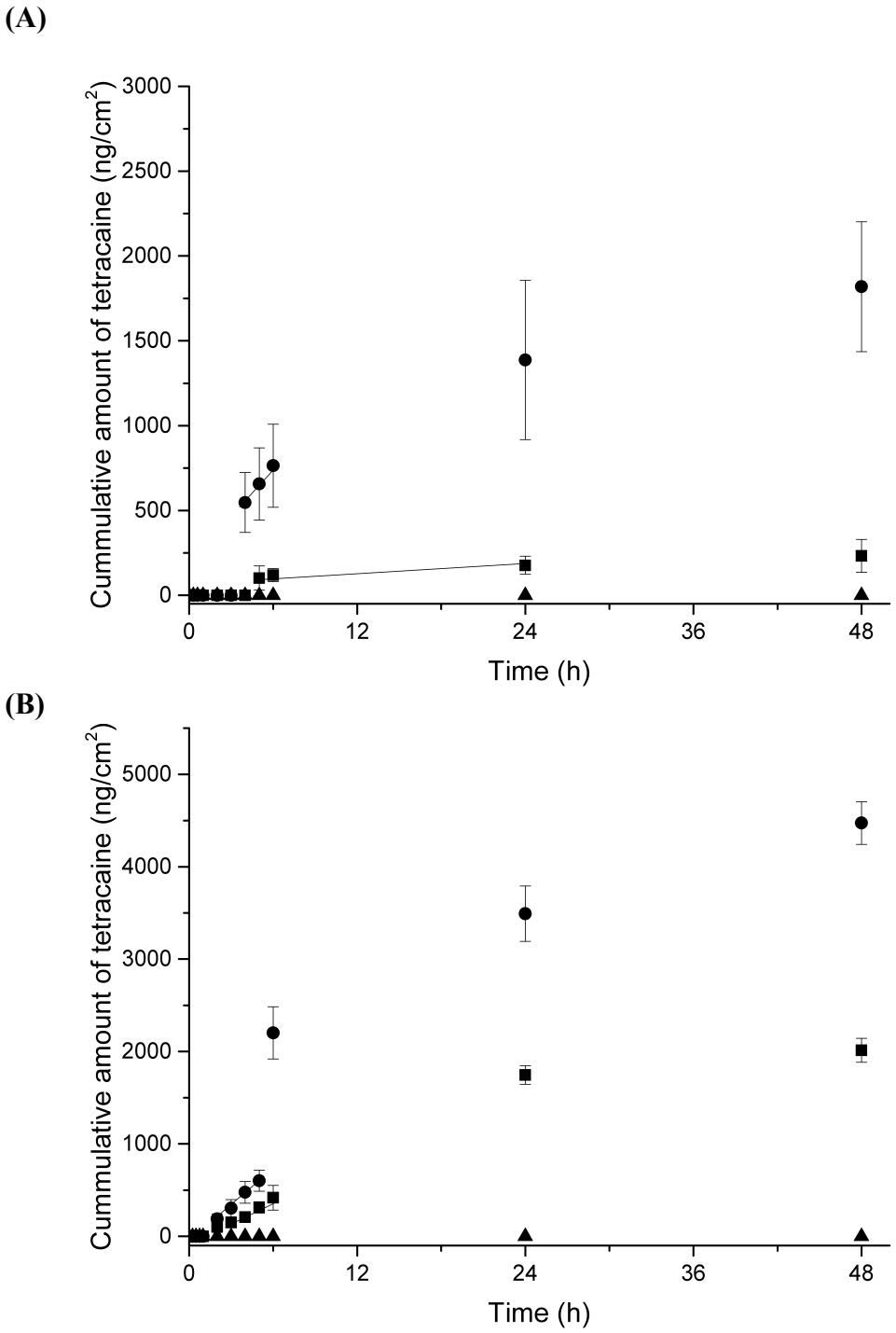

Figure 3.4. Permeation profiles of 10 μM of tetracaine (■) with the addition of carboxyl-modified polystyrene nanoparticles, $Nano_{PSCOOH}$ (▲) and unmodified silica nanoparticles, $Nano_{SiO_2}$(●) in pH 4 (A) and pH 8 (B) across porcine epidermis. Each point represents the mean ± standard deviation, n=5. The straight lines represent the steady-state portion of the permeation profiles.

The silicone membrane was used to attempt to understand the penetration enhancement observed through the porcine skin when the nanoparticles were mixed with the tetracaine (Table 3.6). These studies demonstrated that the simple addition of phosphate ions did not have a membrane penetration enhancement effect on tetracaine (1.7 ± 0.2 ng/cm^2/h, p>0.05)(Table 3.6).

Donor solution	Flux (ng/cm^2/h)	k_p (10^{-3} cm/h)	ER
10 μM TET	2.0 ± 0.4	0.8 ± 0.2	-
10 μM TET + phosphate ions	1.7 ± 0.2	0.6 ± 0.1	0.9 ± 0.2
10 μM TET + $Nano_{PSCOOH}$	0	0	- *
10 μM TET + $Nano_{PSCOOH}$ (equilibrated)	0	0	-*
10 μM TET + $Nano_{PSCOOH}$ vehicle	1.9 ± 0.6	0.7 ± 0.2	1.0 ± 0.3
10 μM TET + $Nano_{SiO_2}$	213.6 ± 40.4	80.8 ± 15.1	111.9 ± 38.5*
10 μM TET + $Nano_{SiO_2}$ (equilibrated)	273.3 ± 37.6	103.4 ± 14.2	140.6 ± 35.4*
10 μM TET + $Nano_{SiO_2}$ vehicle	48.6 ± 4.4	18.4 ± 1.7	24.7 ± 3.5*

Table 3.6. The effects of nanomaterial on the steady state flux, permeability coefficient (k_p) and enhancement ratio of 10 μM of tetracaine at pH 4 and 8 across silicone membrane. Data represent mean ± standard deviation of 3 independent tetracaine samples. * Significant differences were observed based on independent t-test or Mann-Whitney test.

The pre-equilibrated $Nano_{PSCOOH}$-tetracaine mixtures prior to application to the silicone membrane significantly reduced ($p<0.05$) tetracaine transport across the hydrophobic barrier to undetectable levels. Similar were obtained when the nanoparticles were co-administered directly in the donor compartment of the Franz diffusion cells prior to the start of the transport experiments and when they were pre-equilibrated for 30 days prior to addition to the membrane (Table 3.6, Fig. 3.5 for permeation profiles). The silicone membrane penetration studies also demonstrated that the vehicle isolated from the $Nano_{PSCOOH}$, which consists of 0.05% NaN_3 and 0.1% SDS according to manufacturer's data, did not play a role in enhancing tetracaine transport ($p>0.05$, Table 3.6, Fig. 3.5 for permeation profiles).

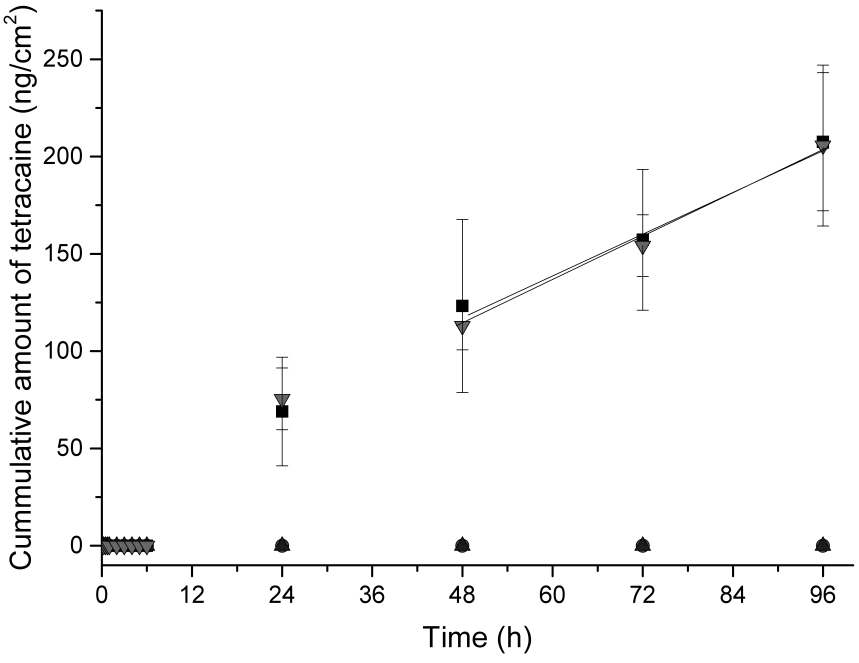

Figure 3.5. Permeation profiles of 10 μM of tetracaine (■) with the addition of carboxyl-modified polystyrene nanoparticles, $Nano_{PSCOOH}$ nanomaterials (▲), investigating the effects of 30-day equilibration (equilibrated, ●) and the vehicle of the $Nano_{PSCOOH}$ (▼). Each point represents the mean ± standard deviation, n=5. The straight lines represent the steady-state portion of the permeation profiles.

In the $Nano_{SiO_2}$-tetracaine mixtures, the incubated $Nano_{SiO_2}$-tetracaine mixture and the $Nano_{SiO_2}$mixture mixed on the surface of the membrane both significantly enhanced transport; there was only a very small, but statistically significant difference ($p<0.05$) between the two (Table 3.6, Fig. 3.6 for permeation profiles). Unlike the $Nano_{PSCOOH}$, the vehicle isolated from the $Nano_{SiO_2}$ suspension played a comparatively small, but significant role ($p<0.05$) in the penetration enhancement of tetracaine through a membrane – transport was significantly increased by approximately 25-fold (Table 3.6, Fig. 3.6 for permeation profiles). Based on the manufacturer's data, the $Nano_{SiO_2}$ consisted only of amorphous silica in water. Hence, the major constituent in the aqueous vehicle that suspended the nanoparticles was soluble silica.

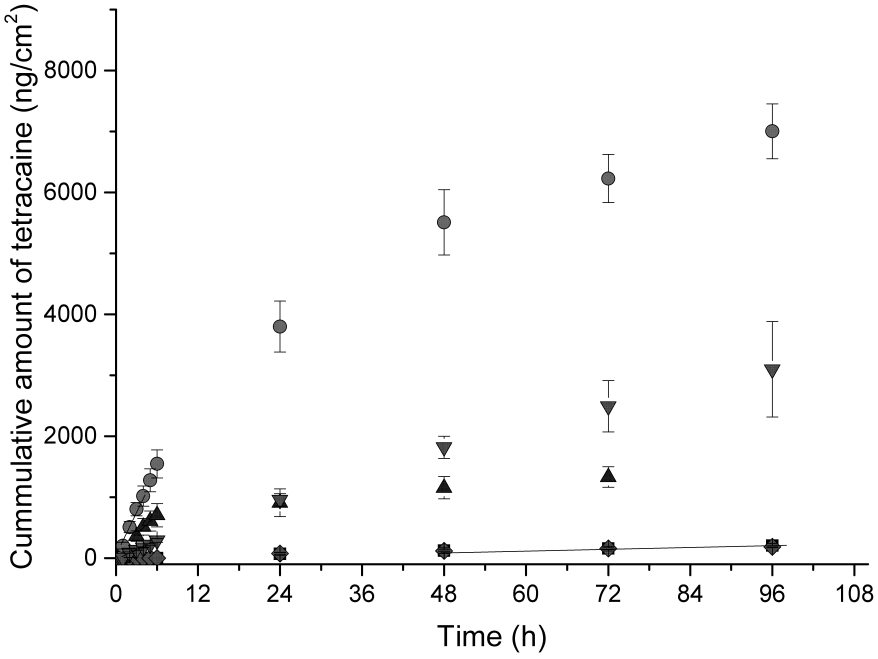

Figure 3.6. Permeation profiles of 10 μM of tetracaine (■) with the addition of phosphate ions (♦) and silica nanoparticles, $Nano_{SiO_2}$nanomaterials (▲), investigating the effects of 30-day equilibration (equilibrated, ●) and the vehicle of the $Nano_{SiO_2}$ (▼). Each point represents the mean ± standard deviation, n=5. The straight lines represent the steady-state portion of the permeation profiles.

3.5 Discussion

The ability of nanomaterials to enhance drug transport across hydrophobic membranes has been previously reported in the literature and this effect as replicated in the data reported in this study (Alves et al., 2007; Borgia et al., 2005; Chen et al., 2006). What was particular about the current work is that the transport was assessed upon the dynamic mixing of a solid nanoparticle and a drug, i.e., the drug was not loaded into the nanoparticles. Therefore, the enhanced transport was a direct consequence of the surface interactions of the solid substrate and the drug molecules in solution. The addition of equivalent drug to surface area ratios of $\mathrm{Nano_{PSCOOH}}$ and $\mathrm{Nano_{SiO_2}}$ to the Franz cell experiments resulted in very different tetracaine transport profiles.

In Chapter 2, the model drug tetracaine was shown to aggregate in aqueous solutions and that this process influenced percutaneous penetration. It was anticipated that nanoparticle surface interactions would modify the transport of a drug across a membrane by modifying this aggregation process. This idea was based on the prior reports that drug-drug interactions can be modified by the addition of substances that compete for association sites (Florence & Attwood, 2011). Theoretically, electrolytes, surfactants, polymers and solid interfaces can disrupt drug-drug interactions *via* competitive interaction. However, in this study, the addition of dihydrogen phosphate electrolytes had no effect on the transport rates of tetracaine (1:10000 tetracaine to phosphate ratio). This suggested that the tetracaine-tetracaine aggregation could not be

disrupted by the relatively weak ion-pair interactions that are formed between the phosphate and the drug.

Nanoparticles were used to introduce a solid interface into the mixture and this was shown to perturb tetracaine aggregation. However, this interaction did not induce a change in the size and zeta potential of the nanoparticles when subjected to 10 μM tetracaine concentration remained largely unchanged. This was contrary to the results obtained by Mocanu et al. (2012), who observed a decrease in zeta potential values and suggested the presence of electrostatic attractions between the nanoparticles and the tetracaine molecules. The difference in the results obtained in the current work was probably due to the different concentrations investigated. In this study, 10 μM of tetracaine was used, but in the previous work a concentration of more than 100 mM was used. A low concentration of tetracaine was used in the current study to increase the potential for nanoparticle surface interactions to have an influence on percutaneous penetration.

3.5.1 The introduction of $Nano_{PSCOOH}$

In pharmaceutical products applied to the skin, polymers can be used as thickening agents and drug carriers (Alvarez-Román et al., 2001; Lboutounne et al., 2002; Luengo et al., 2006). However, in this study, negatively charged polystyrene nanoparticles were used to provide a solid interface in the hope that drug-drug association would be broken to enhance drug transport across the skin.

When tetracaine was mixed with $\mathrm{Nano_{PSCOOH}}$, the particles prevented the drug's penetration through both the porcine and silicone barriers. Tetracaine was unable to penetrate through the membranes when the $\mathrm{Nano_{PSCOOH}}$ were mixed with the drug directly on the surface of the skin and when they were pre-equilibrated with the drug. Thus, it appeared that the pre-equlibration of the drug and the nanoparticles had little effect on this nanoparticle drug mixture. The vehicle of $\mathrm{Nano_{PSCOOH}}$, which constituted of SDS, did not significantly influenced tetracaine transport. As such, any modification to the tetracaine transport was assigned to interactions with the surface of $\mathrm{Nano_{PSCOOH}}$.

3.5.2 The introduction of $\mathrm{Nano_{SiO_2}}$

Silica nanoparticles are one of the four most used nanomaterial in terms of commercial production, together with titanium oxide, zinc oxide and silver nanoparticles. They are widely applied in the fields of pharmaceutical and cosmetic products (Lövestam et al., 2010). In terms of topical formulations, silica nanoparticles are often used as a viscosity modifier or suspending agent in gels, microemulsions and semi-solid preparations (Napierska et al., 2010). They are also used as an emulsion stabilizer to form Pickering emulsions due to their surface activity (Frelichowska, Bolzinger, Pelletier et al., 2009; Frelichowska, Bolzinger, Valour et al., 2009) and have been shown to modulate drug diffusion from the topical emulsions. For example, Frelichowska et al. (2009) demonstrated that Pickering emulsions (silica particle-stabilised w/o emulsions) exhibited 3-fold higher caffeine flux than conventional emulsions (surfactant-stabilised w/o emulsions.

However, using the nanoparticles as a physical surface to modify the aggregation state of a drug to enhance transmembrane transport does not seem to have been previously been reported. The $Nano_{SiO_2}$-tetracaine system that was incubated together for 30 days and the $Nano_{SiO_2}$-tetracaine system that was mixed on the surface of the skin both gave impressive enhancement effects when measuring transport across the silicone membrane. The tetracaine transport results from the vehicle of the nanoparticle suggested that soluble silica available in the aqueous phase of the $Nano_{SiO_2}$ suspension played a role in enhancing tetracaine transport even though these effects were comparably small compared to when the particles were also present in the system. The higher permeability when $Nano_{SiO_2}$ were added to the drug seems to suggest that the $Nano_{SiO_2}$-tetracaine interactions modified the tetracaine through barriers. The fact that this enhancement was greater in the silicone membrane rather than the skin is most probably due to known tetracaine binding to the keratin in the skin which could diminish the enhancement.

The difference in enhancement ratios when $Nano_{SiO_2}$ were added to tetracaine at different pHs supported the hypothesis that tetracaine permeation can be enhanced by the modification of drug aggregation. At pH 4, the tetracaine aggregates do not permeate through the membrane (Chapter 2) and the addition of $Nano_{SiO_2}$ may break up the non-permeating aggregates in a manner that could facilitate the temporal increase in drug monomers that could permeate across the skin. At pH 8, both the non-aggregated and aggregated tetracaine drove the drug transport (Chapter 2) and the break down of tetracaine aggregates when $Nano_{SiO_2}$ were added resulted in an increase in drug permeation, but not one that is as high as at pH 4.

3.6 Conclusion

The co-administration of $Nano_{SiO_2}$ with tetracaine in a simple aqueous formulation enhanced percutaneous drug penetration when applied topically. This finding suggests that some topical preparations could be improved simply by the addition of nanoparticles, i.e., there may be no need, in certain circumstances, to encapsulate the drug within the nanoparticle to gain a beneficial effect. However, the data suggested the type of nanoparticles was important as $Nano_{PSCOOH}$ hindered the tetracaine percutaneous penetration. This difference in tetracaine transport profiles suggest that the drug-nanomaterial interactions drove the differences in the transport profile and to understand this further, these interactions were carefully investigated in Chapter 4.

CHAPTER FOUR

A Mechanistic Investigation of how Tetracaine Adsorption onto Nanoparticulate Surfaces Influences Transmembrane Transport

4.1 Introduction

Nanomaterials may be used as drug carriers and penetrate into the *stratum corneum* as intact vesicles before releasing their contents in the skin. However, this mechanism is limited to elastic vesicles such as ethosomes and transfersomes, which have generated some evidence that they can enter the deeper layers of the *stratum corneum* (Honeywell-Nguyen et al., 2004). Rigid nanomaterials with a size of greater than 20 nm, the focus of this study, generally do not penetrate the skin to a great extent (Baroli et al., 2007; Ryman-Rasmussen et al., 2006; Wu, Price et al., 2009). Therefore, these types of nanoparticles must release their loaded drug at or near the skin surface so that it can subsequently penetrate into the tissue. When this occurs, enhancement of drug transport into the skin have been suggested to be a consequence of generating a drug reservoir on the skin surface (Alvarez-Roman et al., 2004a; Lademann et al., 2007), modifying the skin barrier (Peira et al., 2014; Schlupp et al., 2011), providing occlusion (Dingler et al., 1999; Pardeike et al., 2009), changing the physicochemical properties of the drug to increase the diffusivity in the skin (Luengo et al., 2006), changing the partition coefficient of the drug to increase its release from the formulation (Rouzes et al., 2003) or increasing the thermodynamic activity of the drug in the vehicle and the skin (Alvarez-Roman, Naik, Kalia et al., 2004c; Fangueiro et al., 2012).

One alternative suggestion of how nanomaterials could enhance topical drug delivery is through the surface interactions of the particulate with the drug. This is especially important if the therapeutic agent applied to the skin has a tendency to aggregate. For

surface-active drugs, the drug-nanoparticle surface interactions are probably more important than the other potential penetration enhancing effects aforementioned because drug-nanoparticle surface interactions may alter the drug-drug interaction equilibrium, similar to surfactants (Darwent, McCubbin et al., 1982; Rossetti, Lopes et al., 2011; Shao, Li et al., 1993; Spikes & Bommer, 1986) and polymers (Pygall, Griffiths et al., 2011). As shown in Chapter 2, the manner in which amphiphilic molecules, such as tetracaine, presents itself in the solution can influence the drug percutaneous penetration. The perturbation of drug-drug interactions by drug-nanoparticle surface interactions has the potential to change the self-diffusion coefficient of the drug in the application vehicle and thus, the rate of entry into the skin barrier. Nanomaterials were shown in Chapter 3 to enhance drug percutaneous penetration by 3.6-fold at pH 4 and 2.0-fold at pH 8. Although it was hypothesised that the enhancement in percutaneous penetration was brought about by nanoparticle surface interactions with the drug, just like previous studies, no direct spectroscopic evidence was generated to support this notion (Schlupp, Blaschke et al., 2011).

The aim of this chapter was to examine if the interactions that occurred between the nanoparticulate surface and the drug used in Chapter 3 conferred the capability to enhance percutaneous penetration. As the main aim of the PhD was to develop a nanomaterial formulation that enhanced drug transport, it was anticipated that understanding the mechanism of achieving an enhancement would enable us to further optimize this system in subsequent chapters of the thesis. To detect the presence of nanomaterials-drug aggregate interactions in the aqueous solutions, physical adsorption

and fluorescence spectroscopic studies were conducted. In order to acquire detailed knowledge of the magnitude of these tetracaine-nanoparticle interactions, AFM was utilized. Methyl and an ionized tertiary amide functionalized tips were generated in the work in order to mimic the two ends of the charged tetracaine molecule. Adhesion forces between the tetracaine molecule *via* these two functional representatives of tetracaine and the different nanomaterials were then measured.

4.2 Materials

Material	Specifications	Company
Tetracaine	Free base, ≥ 98%	Sigma Aldrich, UK
$Nano_{PSCOOH}$	Carboxyl-modified polystyrene nanoparticles with a diameter of 20 μm (PC07N)	2B Scientific, UK
$Nano_{SiO_2}$	Silica nanoparticles with a diameter of 20 μm (Psi-20.0)	Kisker Biotech GmbH and Co., Germany
Hydrochloric acid (HCl)	Fuming 37%	Sigma Aldrich, UK
De-ionised water	Electrical conductivity 0.5-1 μS	Produced in house
Centrifugal filters	Amicon Ultra 0.5 mL, Nominal molecular weight limit of 100 kDa	Millipore Limited, UK
Sodium acetate	Anhydrous, ≥ 99.9%	Sigma Adrich, UK
Acetic acid	ACS reagent, ≥ 99.7%	Sigma Aldrich, UK
Acetonitrile, methanol and water	High performance liquid chromatography (HPLC) grade	Fisher Scientific, UK
Methanol	HPLC grade	Fisher Scientific, UK
Poly-L-lysine solution	0.1% w/v	Sigma Aldrich, UK
1-octadecanethiol	98%	Sigma Aldrich, UK
(11-Mercaptoundecyl)-N,N-N-trimethylammonium bromide	-	Sigma Aldrich, UK
Ethanol	200 Proof, ACS Reagent	Sigma Aldrich, UK
Mica surfaces	-	Agar Scientific, Elektron Technology UK Limited
Cantilevers	Gold-coated Si_3N_4 V-shaped contact mode cantilevers with integrated pyramidal tips (Model: NPG10)	Bruker, France

Table 4.1. Materials used in Chapter 4.

4.3 Methods

4.3.1 Test sample preparation

Refer to Section 3.3.1.

4.3.2 Physical adsorption

Nanoparticles were added to tetracaine solutions at time point 0 h and at several subsequent time points (0.25, 0.50. 0.75, 1, 3, 5, 24 and 48 h). 500 µL of the tetracaine-nanoparticle mixtures were removed and centrifuged through a centrifugal filter with nominal molecular weight limit of 100 kDa at 1500 g for 10 min (Biofuge pico, Heraeus Instruments, Germany). A 300 µL aliquot of the centrifuged liquid phase was transferred into vials. The analyte was dissolved in a 1:2 ratio v/v with acetonitrile and unbound tetracaine concentrations were determined using the HPLC assay. Tetracaine-nanoparticle binding was calculated using equation 4.1:

$$C_B(\%) = \frac{C_t}{C_0} X\ 100\ \% \qquad \text{(Equation 4.1)}$$

where C_B is the concentration of the bound tetracaine, C_t is the unbound tetracaine analysed at the time point and C_0 is the initial tetracaine.

4.3.3 Fluorescence spectroscopy

Refer to Section 2.3.3.

Any background signal generated by the nanoparticles was subtracted from the measurements to focus the results on the tetracaine fluorescence.

4.3.4 Atomic force microscopy (AFM)

Refer to Section 3.3.2 for the AFM imaging procedure.

The force adhesion measurements between the functionalized tips and functionalized substrates were obtained using a Nanoscope V Dimension Icon atomic force microscope (Bruker, US). To mimic the conditions in the Franz cell experiments, the substrates were analysed using a fluid cell housed in a petri dish. The fluid cell was washed with detergent water and rinsed with ultrapure water before drying with a steam of nitrogen gas prior to the start of every experiment. The same individual AFM tip was used in all experiments in order to cancel out possible variations caused by different tip properties such as tip size, etc.

The functionalized materials employed in the force adhesion AFM measurements were produced using a gold-thiol coating procedure. 1-octadecanethiol and (11-Mercaptoundecyl)-N,N-N-trimethylammonium bromide were selected as the thiols

because they produced functional groups on the surface of the materials which best mimicked the two terminuses of the tetracaine molecule. The material functionalisation was achieved by incubating the gold-coated AFM materials (i.e., AFM substrates and AFM cantilevers) in freshly prepared 3 mM solution of the chosen thiol, which was dissolved in ethanol overnight in a sealed petri dish. After incubation, the substrates and AFM probes were washed thoroughly with ethanol. The substrates were dried with nitrogen while the AFM probes were allowed to dry in air.

Particles were deposited on the surface of mica substrates as described in Section 3.3.2. Microparticles of 20 μm in diameter from the same manufacturer and particle series were used in place of the nanoparticles to provide a wider contact surface for the AFM tip.

Prior to making the force-adhesion measurements, the spring constant of the cantilevers was determined. The photodetector sensitivity was first calibrated by determining the slope of the repulsive branch of a force curve on a hard surface (photodetector signal versus z-scanner displacement plot on mica). Then, thermal tuning was performed using the corresponding Nanoscope programme function to determine the actual spring constants of the cantilevers. Gold-coated Si_3N_4 V-shaped contact mode cantilevers with integrated pyramidal tips (Model: NPG10) were used to obtain the force measurements. The nominal spring constant specified in the cantilever datasheets was 0.35 N/m and the measured spring constants were (0.39 ± 0.01) N/m. Three independent measurements of 210 force curves were obtained from 10 randomly distributed areas on the sample

surfaces to ensure representative sampling. Average adhesion force values were determined by fitting a Gaussian profile to the histogram of the forces using OriginPro software.

Sessile drop contact angles were captured by a high resolution camera (Photron Ultima APX Monochrome, UK) and analysed using Image J with a Dropsnake plug-in to confirm the formation of surface modified gold substrate. In addition, force interactions between the tip and CH_3 substrates were measured before each sample substrate to confirm that the tip was not significantly modified during the sequential measurement of the different samples.

4.3.5 Statistical analysis

Refer to Section 2.3.8.

4.4 Results

4.4.1 Physical adsorption studies

The added 10 μM aliquot of tetracaine was completely adsorbed to $Nano_{PSCOOH}$ within 15 min of mixing the drug with the particle according to the physical adsorption studies (Fig 4.1). The adsorption of the same concentration of drug onto the $Nano_{SiO_2}$ was less rapid compared to the $Nano_{PSCOOH}$, but it was still rapid and extensive. The drug concentration bound to the $Nano_{SiO_2}$ gradually increased from the first time point at 15 min (87.2 ± 4.1%) to the last time point at 48 hours (97.9 ± 0.7%). The maximum recovery of the drug that could be obtained from the system was 28.2 ± 4.2% and therefore, it was thought prudent to confirm these trends using fluorescence spectroscopy and AFM microscopy.

4.4.2 Fluorescence studies

The nanoparticles gave a small signal in the 340-420 nm region of the spectrum but as the particles were not fluorescent, this was probably due to the turbidity of the samples caused by the nanoparticles (Fig. 4.1). This small signal was subtracted from the measurements to focus the results on the tetracaine fluorescence.

The fluorescence spectrum of $Nano_{PSCOOH}$ mixed with 10 μM of tetracaine displayed a blue shift of 21 nm, the maximum peak wavelength moved from 372 nm to 351 nm, and a 20-fold increase in fluorescence emission ($p<0.05$)(Fig. 4.2). There were no significant changes in the fluorescence spectra observed when $Nano_{SiO_2}$ were added to the 10 μM tetracaine solution ($p>0.05$) despite the adsorption process that was shown to occur previously.

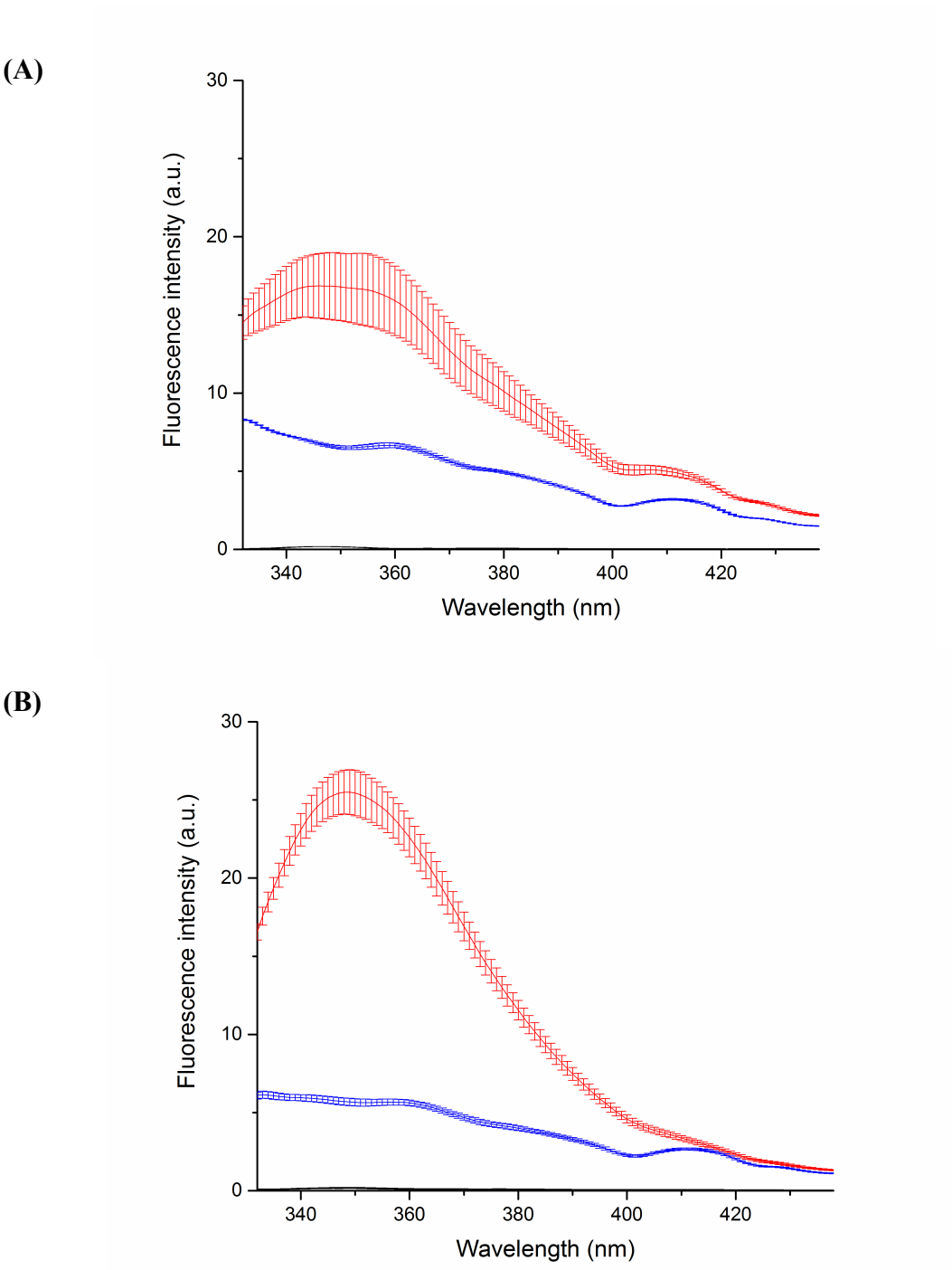

Figure 4.1. Fluorescence spectrum of pH 4 (A) and 8 (B) water (black) before and after the addition of carboxyl-modified polystyrene nanoparticles, $Nano_{PSCOOH}$ (red) and unmodified silica nanoparticles, $Nano_{SiO_2}$(blue).

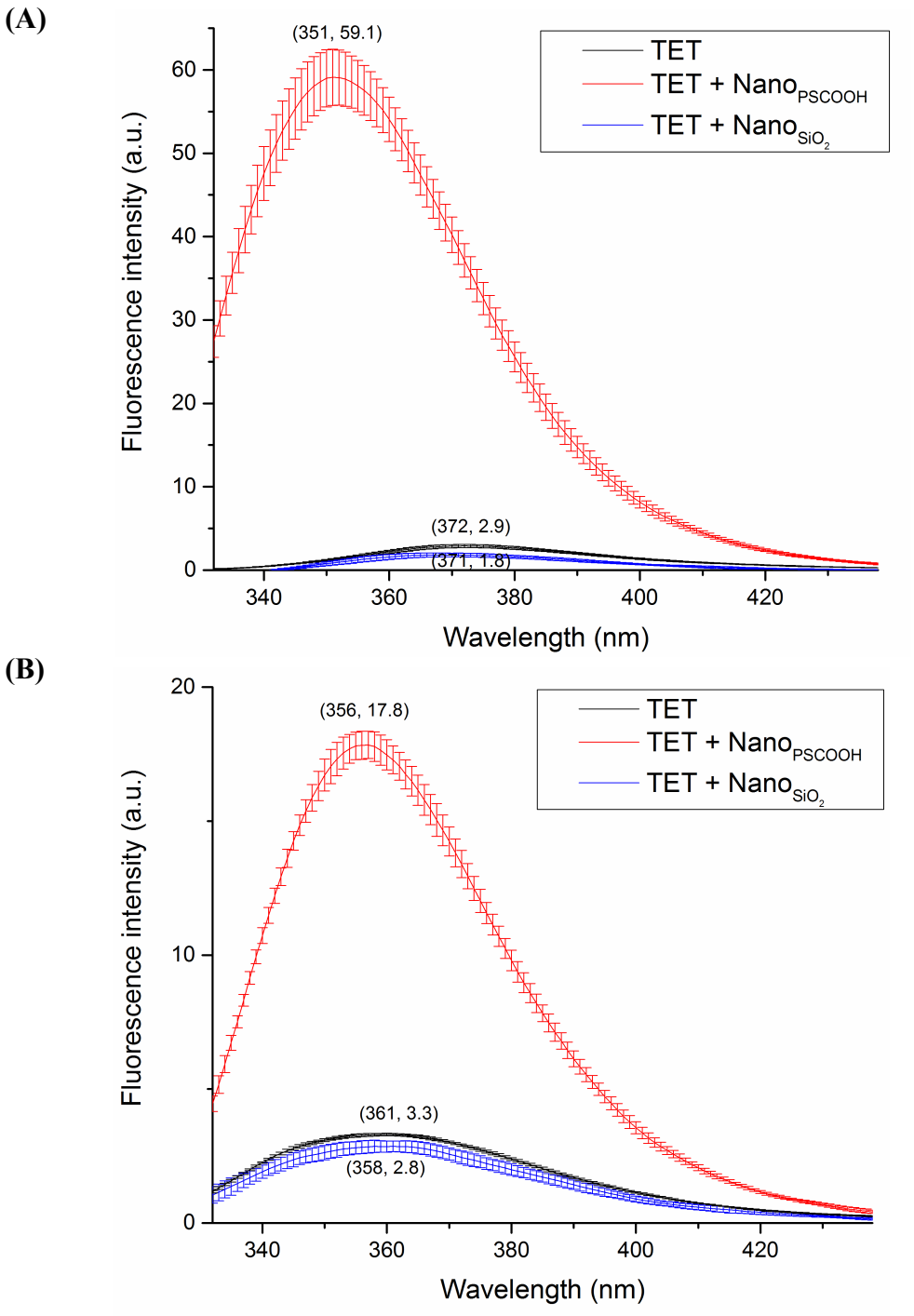

Figure 4.2. Fluorescence spectrum of 10 μM of tetracaine (TET) before and after the addition of carboxyl-modified polystyrene nanoparticles, ($Nano_{PSCOOH}$) and unmodified silica nanoparticles ($Nano_{SiO_2}$) in pH 4 (A) and pH 8 (B). Peak wavelength and intensity showed in parenthesis.

4.4.3 AFM adhesion force measurements method development

The commercially available gold cantilevers were selected over in-house gold-coated probe tips because they provided the least surface roughness (0.18 ± 0.02 nm) and highest signal voltage output (2V in air)(Table 4.2, Fig. 4.3 for tip image). Force measurements could not be determined with the in-house gold-coated cantilevers because the signal voltage outputs were too low to function.

Coatings on cantilever	Root mean square roughness (nm)
Uncoated	2.55 ± 0.84
Thermally evaporated gold	0.31 ± 0.03
Thermally evaporated gold (tip side)	3.15 ± 0.46
Sputtered gold	0.45 ± 0.05
Sputtered gold (tip side)	0.32 ± 0.04
Commercially available gold	0.18 ± 0.02

Table 4.2. Root mean square roughness values of various gold coated cantilevers.

(A)

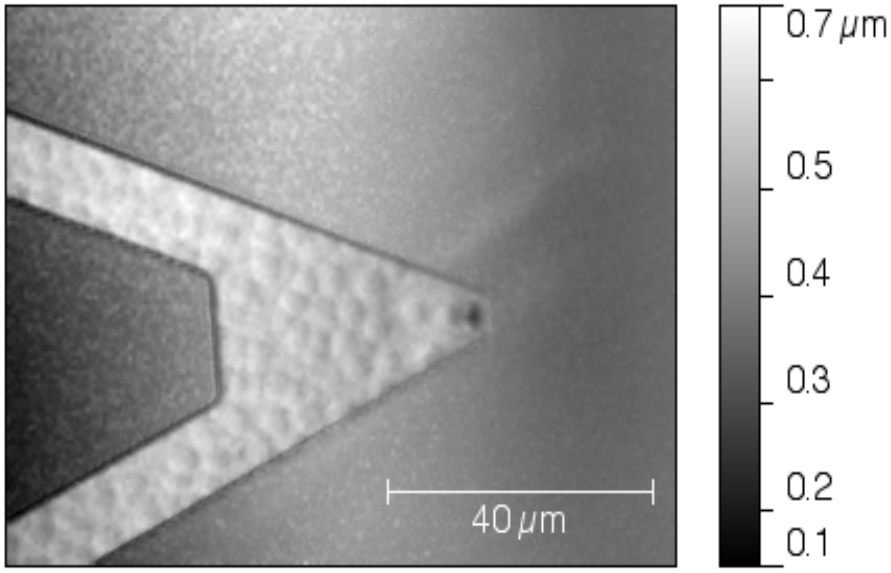

(B)

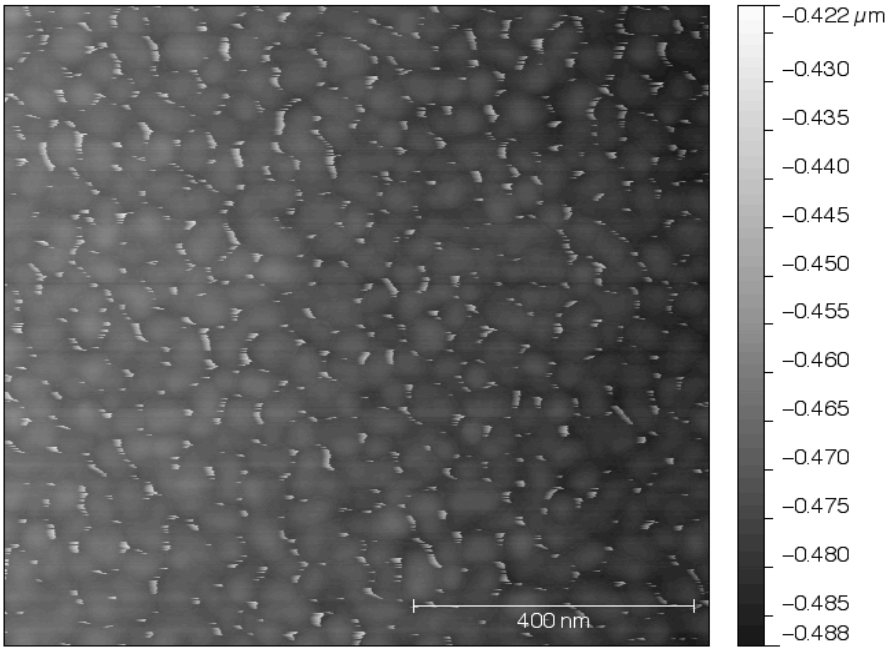

Figure 4.3. Optical images tip side of (A)(C) and Z-piezo (B)(C) images of cantilevers gold coated by thermal evaporation (A)(B) and commerically available gold cantilevers (C)(D).

(C)

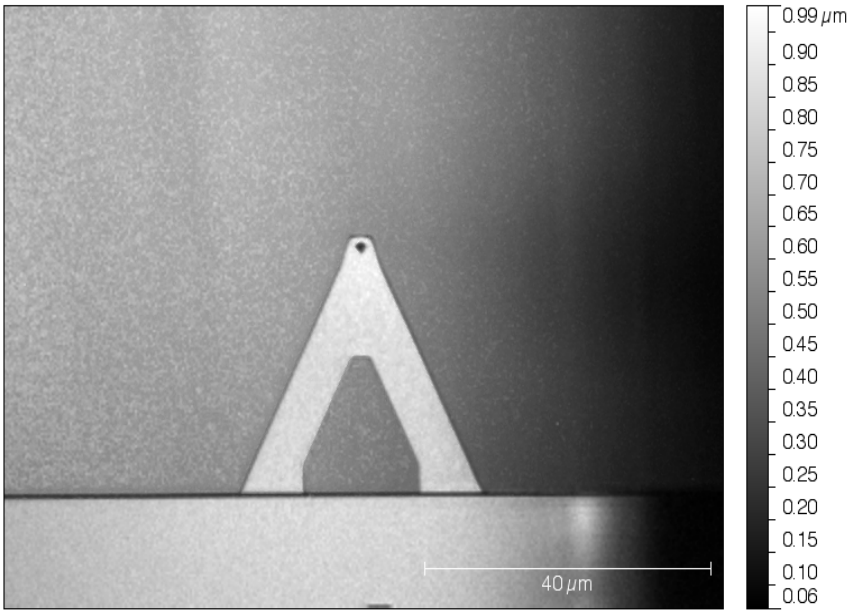

(D)

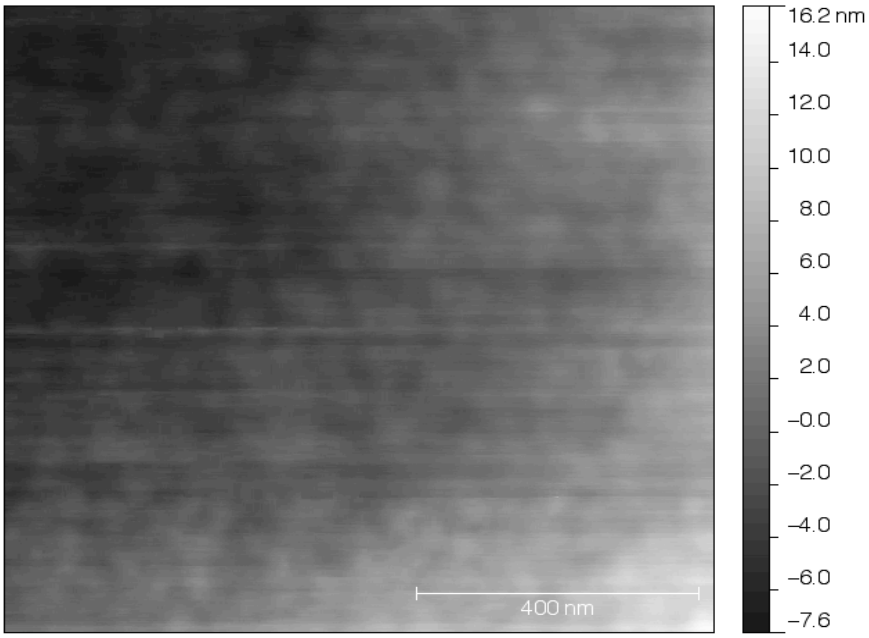

Figure 4.3. Optical images tip side of (A)(C) and Z-piezo (B)(C) images of cantilevers gold coated by thermal evaporation (A)(B) and commerically available gold cantilevers (C)(D).

The AFM tips were modified with methyl and amine groups using the known solution deposition method as evident from the contact angle measurements (Table 4.3, Fig. 4.4). The clean hydrophilic gold surface had a zero contact angle and when placed into the alkane-thiol solution, the CH_3-functionalised group produced a hydrophobic surface (>90°). The established solution deposition technique was used for the amine-functionalized gold surface and a hydrophilic amine surface (<90°) was formed. The polystyrene surface had a moderately hydrophobic surface (>90°)(Table 4.3, Fig 4.4).

Substrate material	Contact angle (°)
Gold	$0 \pm 0^*$
CH_3 functionalized gold surface	$180 \pm 0^*$
Amine functionalized gold surface	0 ± 0
Polystyrene	127.4 ± 6.1

Table 4.3. Contact angle of flat substrates. * Surfaces are very hydrophobic.

(A)

(B)

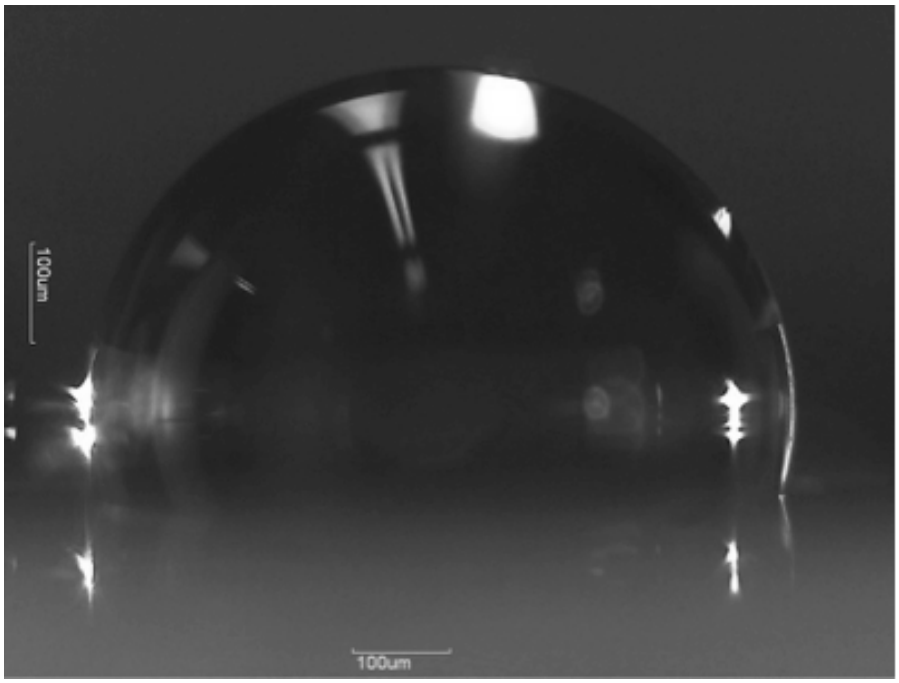

Figure 4.4. Contact angle of amine-functionalised surface (left) and polystyrene surface (right). The amine surface is hydrophilic and spreading takes place. The polystyrene surface is hydrophobic, having a contact angle of 127.4 ± 6.1°.

The CH_3-CH_3 force adhesion measurements taken before each sample measurement were not significantly different ($p>0.05$), thus suggesting that the tip used was not contaminated by the measurements or damaged during the moving between samples (Table 4.4).

Tip interaction with CH_3 substrate prior to the following tip-substrate interactions	$F_{tip\text{-}CH3}$ (nN)
CH_3-Amine	9.19 ± 5.46
CH_3-$Nano_{PSCOOH}$	9.97 ± 4.81
CH_3-$Nano_{SiO_2}$	9.31 ± 4.57
CH_3-PS	10.61 ± 3.86
Amine-$Nano_{PSCOOH}$	8.73 ± 5.36
Amine-$Nano_{SiO_2}$	7.29 ± 5.04
Amine-PS	9.00 ± 4.70

Table 4.4. Average adhesion force measurements ($F_{tip\text{-}CH3}$) between CH_3-functionalised tip and CH_3-functionalised substrate prior to sample measurements taken from 10 contact areas x 21 force curves in pH 8 water. Triplicates were performed. * Significant differences were observed compared to CH_3-CH_3 adhesion force measurements.

4.4.4 AFM adhesion force measurements

In the AFM measurements, methyl and ionised tertiary amine tips were used as a functional representative of the two ends of a charged tetracaine molecule in AFM. Using the methyl tip, the strength of adhesion force with the substrates were as follows:

$Nano_{SiO_2}$ < CH_3 = Amine = PS < $Nano_{PSCOOH}$ (Table 4.5, Fig. 4.5 and 4.6 for histograms). The methyl tip showed a preference in terms of adhesion force with the $Nano_{PSCOOH}$ surface in both pH 4 and pH 8 ($p<0.05$). The $Nano_{SiO_2}$ surface showed a lower force of adhesion with the methyl tip compared to all the other interactions assessed in both pHs ($p<0.05$).

	Tip-substrate	F_{ad} (nN)
pH 8	CH_3-CH_3	9.19 ± 5.46
	CH_3-Amine	8.27 ± 4.41
	CH_3-$Nano_{PSCOOH}$ *	67.61 ± 45.69
	CH_3-$Nano_{SiO_2}$ *	1.52 ± 0.78
	CH_3-PS	10.10 ± 2.86
pH 4	CH_3-$Nano_{PSCOOH}$ *	59.90 ± 56.24
	CH_3-$Nano_{SiO_2}$ *	1.47 ± 1.05

Table 4.5. Adhesion force measurements (F_{ad}) recorded between CH_3-functionalised tips and various substrates. The measurements were taken from 10 contact areas X 21 force curves in pH 8 and 4 water. Triplicates were performed. * Significant differences were observed compared to CH_3-CH_3 adhesion force measurements.

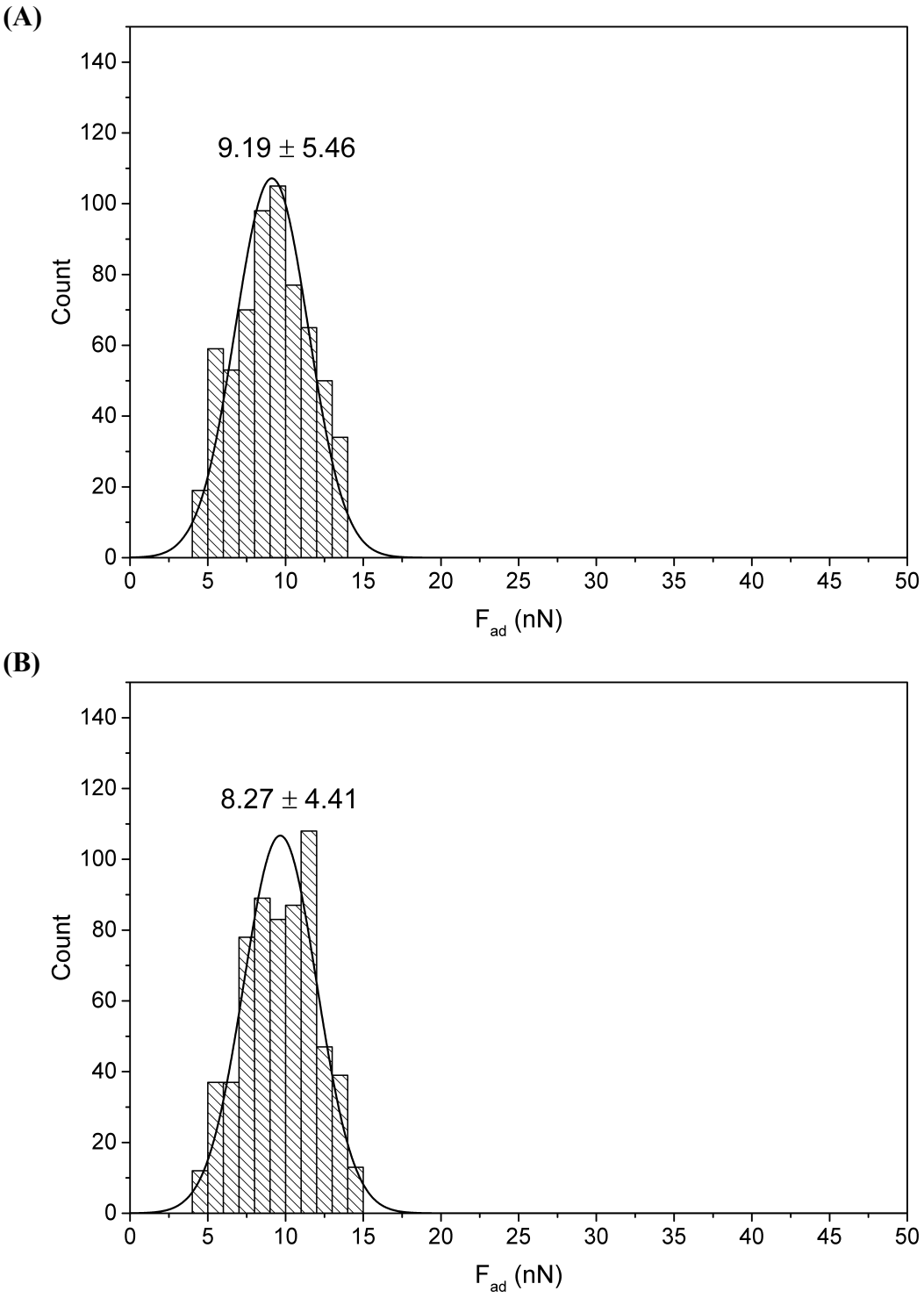

Figure 4.5. Histograms depicting adhesion force measurements (F_{ad}) between CH_3-functionalised tip and various substrates: (A) CH_3-functionalised substrate, (B) Amine-functionalised substrate, (C) $Nano_{PSCOOH}$, (D) $Nano_{SiO_2}$ and (E) polystyrene substrate. Measurements were taken from 10 contact areas x 21 force curves in pH 8 water. Triplicates were performed.

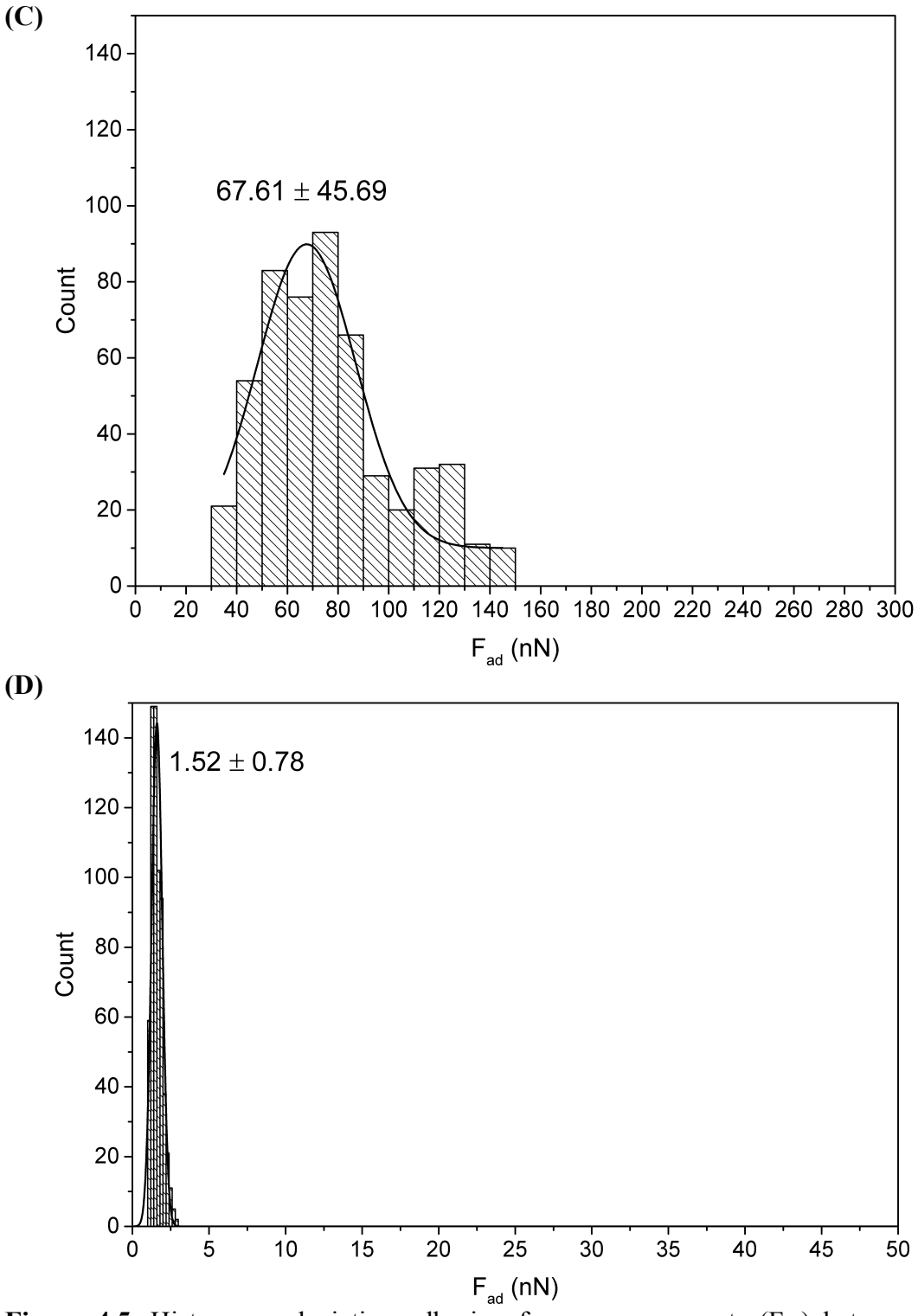

Figure 4.5. Histograms depicting adhesion force measurements (F_{ad}) between CH_3-functionalised tip and various substrates: (A) CH_3-functionalised substrate, (B) Amine-functionalised substrate, (C) $Nano_{PSCOOH}$, (D) $Nano_{SiO_2}$ and (E) polystyrene substrate. Measurements were taken from 10 contact areas x 21 force curves in pH 8 water. Triplicates were performed.

(E)

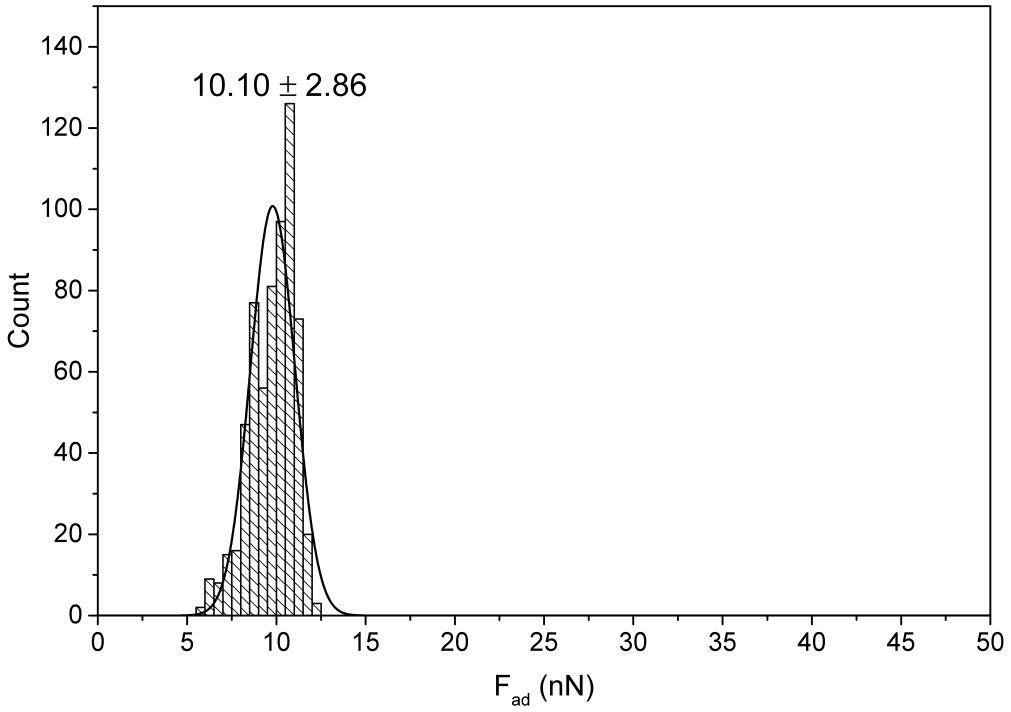

Figure 4.5. Histograms depicting adhesion force measurements (F_{ad}) between CH_3-functionalised tip and various substrates: (A) CH_3-functionalised substrate, (B) Amine-functionalised substrate, (C) $Nano_{PSCOOH}$, (D) $Nano_{SiO_2}$ and (E) polystyrene substrate. Measurements were taken from 10 contact areas x 21 force curves in pH 8 water. Triplicates were performed.

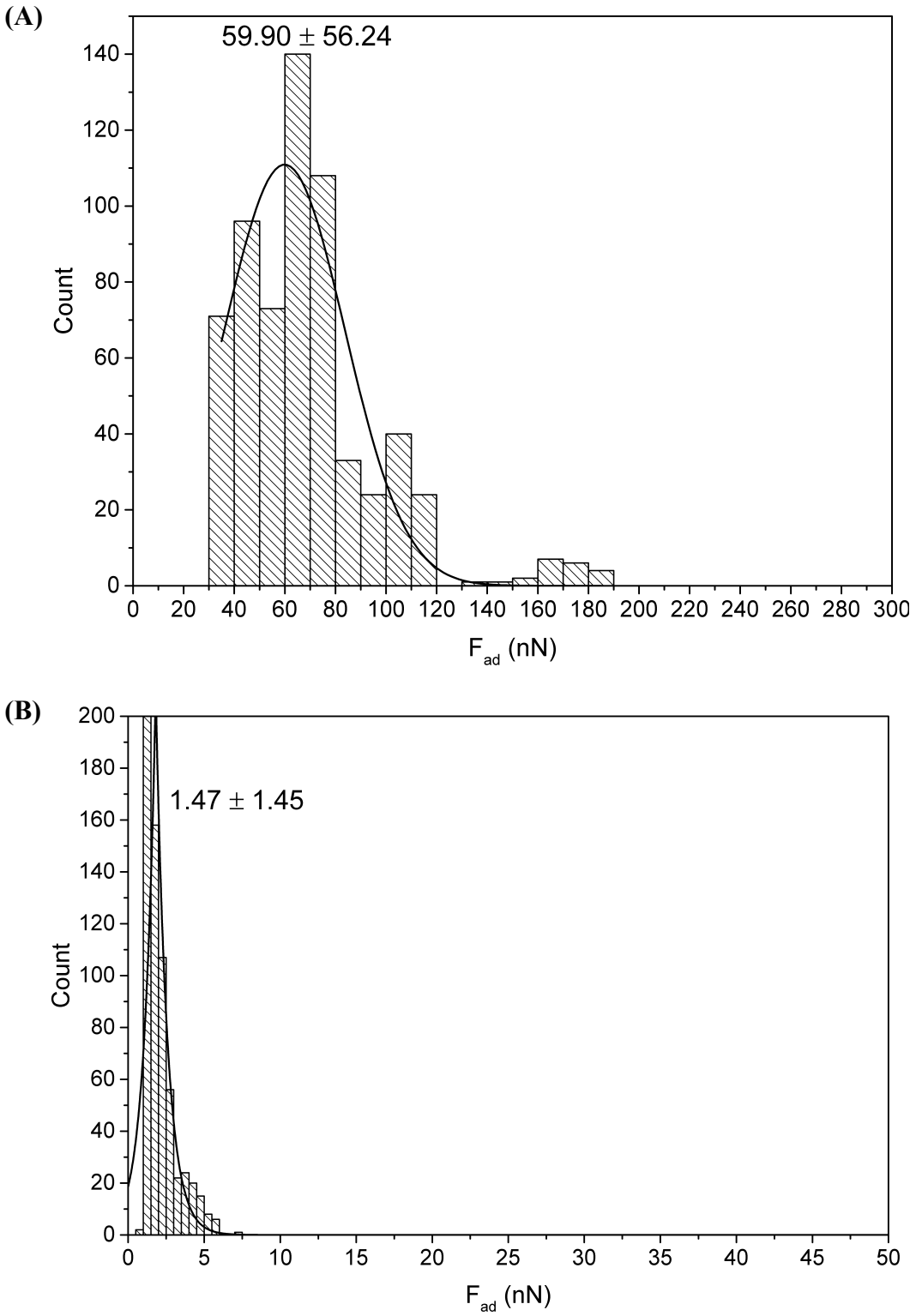

Figure 4.6. Histograms depicting adhesion force measurements (F_{ad}) between CH_3-functionalised tip and various substrates: (A) $Nano_{PSCOOH}$, (B) $Nano_{SiO_2}$. Measurements were taken from 10 contact areas x 21 force curves in pH 4 water. Triplicates were performed.

The strength of adhesion force between the amine tip and the substrates had the same trend as those with the methyl tip (Table 4.6, Fig. 4.7 and 4.8). However, the adhesion force between the amine tip and $Nano_{PSCOOH}$ were significantly stronger in pH 8 than in pH 4 ($p<0.05$).

	Tip-substrate	F_{ad} (nN)
pH 8	Amine – Amine	8.73 ± 5.36
	Amine – $Nano_{PSCOOH}$ *	156.26 ± 11.33
	Amine – $Nano_{SiO_2}$ *	1.77 ± 1.18
	Amine - PS	9.53 ± 4.65
pH 4	Amine - $Nano_{PSCOOH}$ *	86.72 ± 11.28
	Amine – $Nano_{SiO_2}$ *	1.74 ± 1.06

Table 4.6. Adhesion force measurements of between amine tips and different surfaces taken from 10 contact areas x 21 force curves in pH 8 and 4 water. Triplicates were performed. * Significant differences were observed compared to Amine-Amine adhesion force measurements.

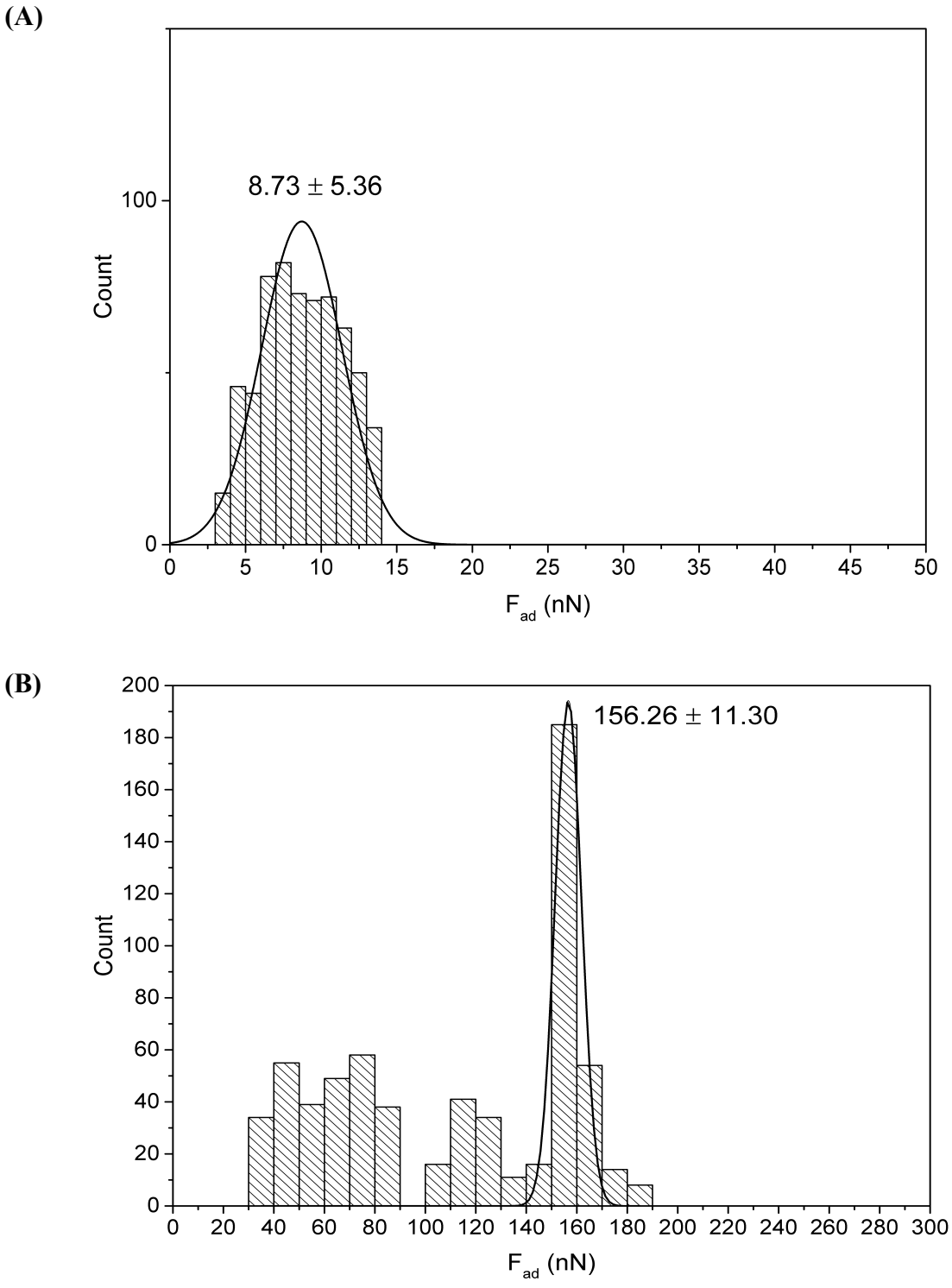

Figure 4.7. Histograms depicting adhesion force measurements (F_{ad}) between Amine-functionalised tip and various substrates: (A) Amine-functionalised substrate, (B) $Nano_{PSCOOH}$, (C) $Nano_{SiO_2}$ and (D) polystyrene substrate. Measurements were taken from 10 contact areas x 21 force curves in pH 8 water. Triplicates were performed.

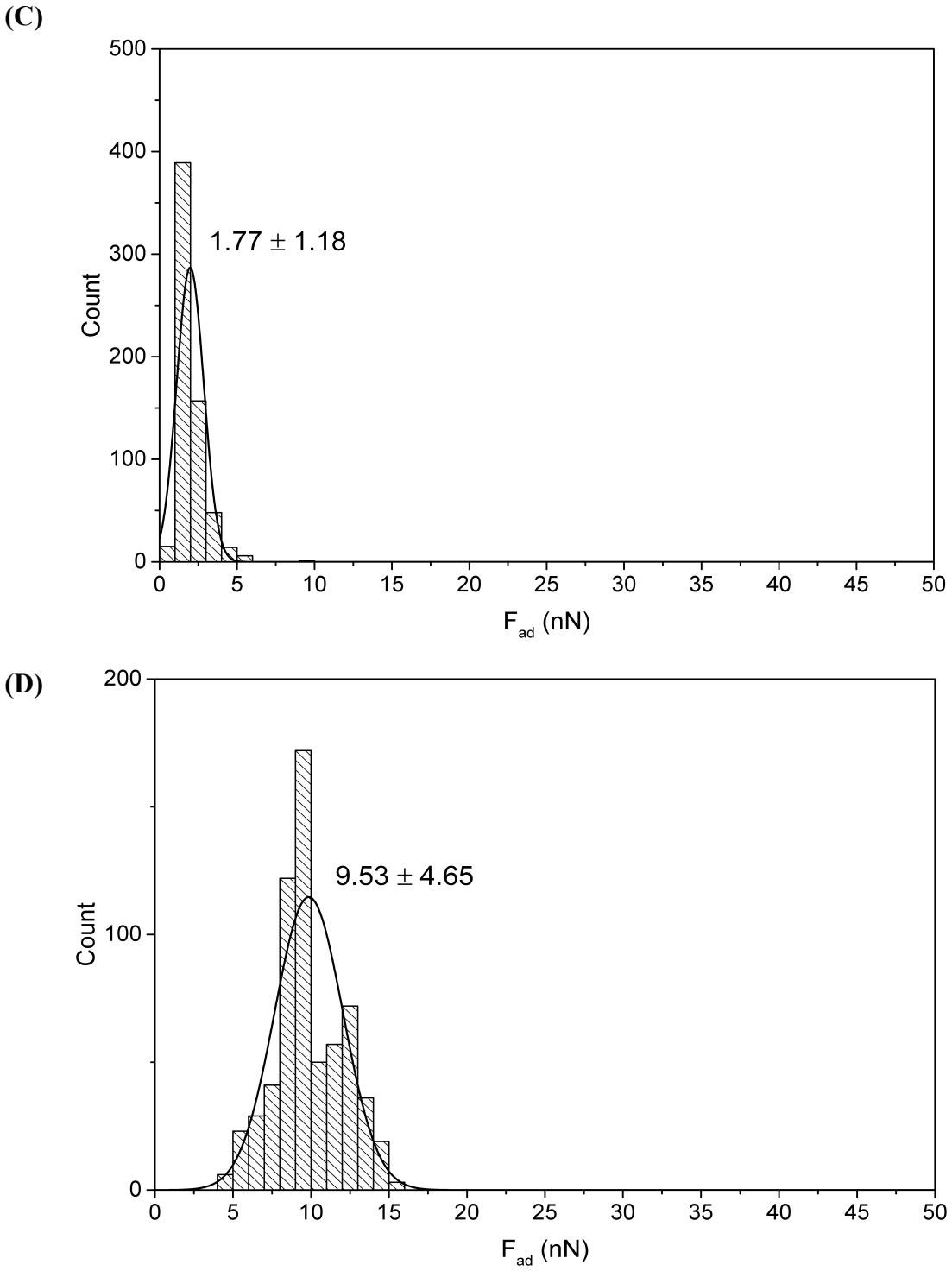

Figure 4.7. Histograms depicting adhesion force measurements (F_{ad}) between Amine-functionalised tip and various substrates: (A) Amine-functionalised substrate, (B) $Nano_{PSCOOH}$, (C) $Nano_{SiO_2}$ and (D) polystyrene substrate. Measurements were taken from 10 contact areas x 21 force curves in pH 8 water. Triplicates were performed.

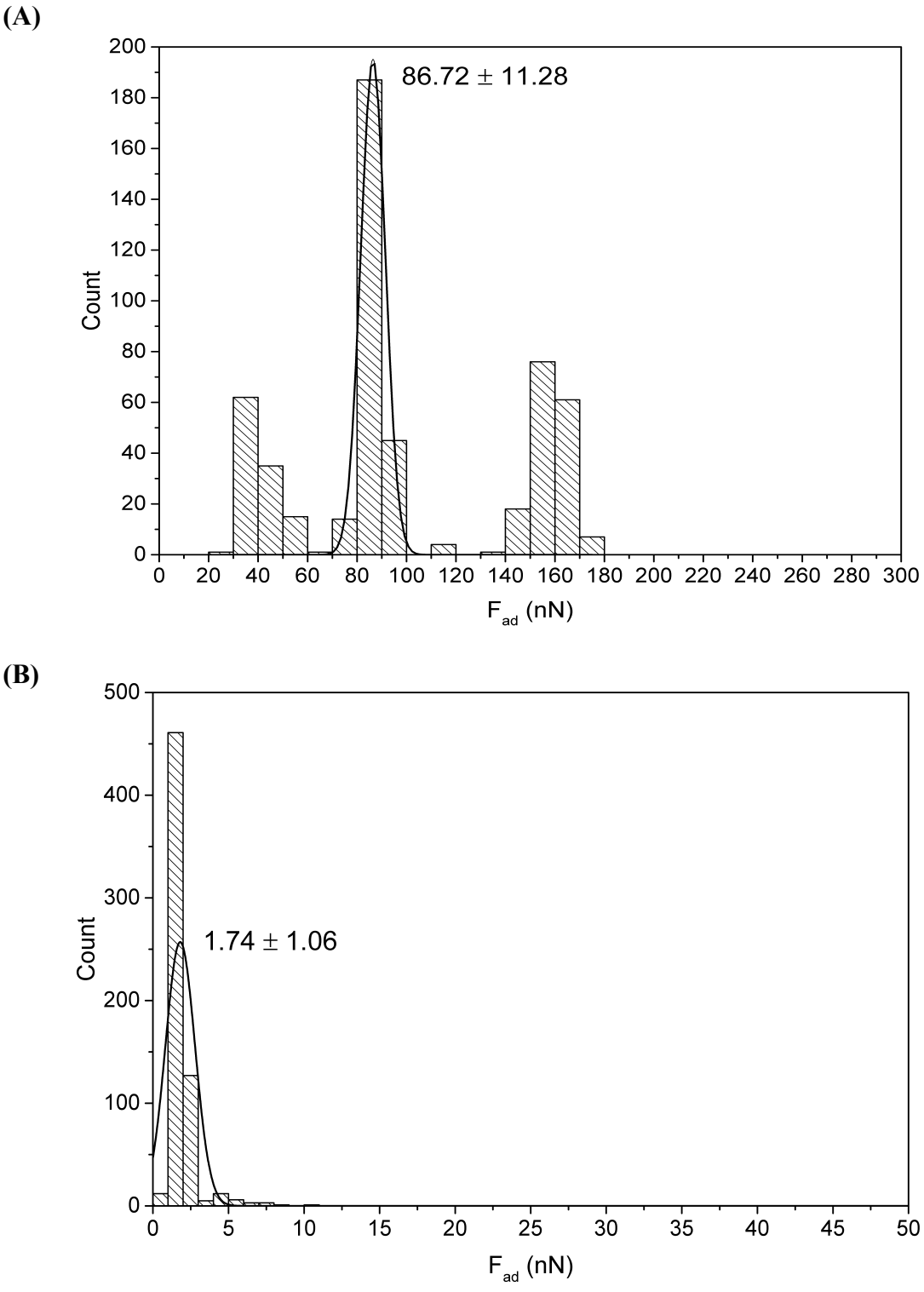

Figure 4.8. Histograms depicting adhesion force measurements (F_{ad}) between Amine-functionalised tip and various substrates: (A) $Nano_{PSCOOH}$, (B) $Nano_{SiO_2}$. Measurements were taken from 10 contact areas x 21 force curves in pH 4 water. Triplicates were performed.

4.5 Discussion

4.5.1 $Nano_{PSCOOH}$-tetracaine interactions

The physical adsorption studies suggested that tetracaine had a strong affinity with both the nanoparticles surfaces. However, the low recovery of tetracaine, which was probably a consequence of tetracaine aggregates remaining bound to the surface of the filter, meant that these results needed further confirmation. As a consequence, the data from physical absorption studies were supported by the generation of the fluorescence spectroscopy and AFM data. Previous work by Mertz et al. (1990) showed that when tetracaine aggregates were subjected to molecules known to form hydrogen bonds, a fluorescence blue shift was observed. The $Nano_{PSCOOH}$ completely adsorbed the tetracaine and generated a blue shift and it seemed reasonable to assume that, like the previous work, the addition of the nanoparticles caused aggregate break up of the hydrogen bonding involved in tetracaine self-association and resulted in surface adsorption to the particles (Guerin, Dumas et al., 1980; Mertz, Marques et al., 1990). The increase in fluorescence intensity further substantiates that tetracaine aggregates broke as tetracaine aggregates has been shown to generate fluorescence signal quenching (Chapter 2). When taken together, the blue shift and the increase in fluorescence intensity provided strong evidence that the tetracaine aggregates were being disrupted by the surface adsorption onto the nanoparticles. This supported the observations from the physical adsorption study.

According to the AFM data, the methyl and amine functional groups had strong electrostatic attractions to the strong negatively charged carboxyl and sulphate groups on the surfaces of $Nano_{PSCOOH}$. The sensitivity of the amine interactions to the pH of the suspension vehicle provided evidence that this functionality did interact with the particle surface through electrostatic interactions. In addition, because the forces of interactions with the amine were stronger than for the methyl group, it appeared that although it was possible for the tetracaine to interact with the particle surfaces *via* with the methyl or amine functionalities, it was the latter which was more likely to be the primary means by which the drug adsorbed at the particle surface. Perhaps the methyl group did interact with the non-charged regions of the polystyrene surface, which was known to be relatively hydrophobic, to some degree. However, this type of interaction would be limited compared to the electrostatic interactions of the amine because of the low number of sites for hydrophobic interaction on the carboxyl-modified particles. The presence of two competing sites of interaction could be the reason why the force-displacement measurements with the methyl functionality derived in this work were highly variable compared to similar measurements with the amide functionality.

Despite evidence of aggregation being disrupted, the transport of tetracaine did not increase following the addition of $Nano_{PSCOOH}$ to tetracaine (Chapter 3). A possible explanation for this phenomenon is that the strong affinity between tetracaine and $Nano_{PSCOOH}$ resulted in tetracaine residing on the nanoparticle surface. $Nano_{PSCOOH}$ are unable to penetrate even the most superficial *stratum corneum* (Alvarez-Roman et al., 2004a) and hence, this strong drug adsorption onto the particle surface could retard the

transport process by reducing the availability of free drug molecules to pass through the barrier. In previous studies by Wu et al. (2010), there was also little evidence of $Nano_{PSCOOH}$ retention on the skin surface and the model drug PMI was not released into the *stratum corneum*. A similar explanation was used when nile red fluorophores were shown to associate with the nanoparticles and were released only to a certain extent (Wu, Price et al., 2009).

4.5.2 $Nano_{SiO_2}$-tetracaine interactions

The $Nano_{SiO_2}$ interactions with tetracaine were weaker than the drugs interactions with $Nano_{PSCOOH}$. This was demonstrated by the physical adsorption measurements, the absence of a shift in the fluorescence spectra of the tetracaine solution in the presence of the nanoparticles and the relatively low adhesion force measurements recorded in the AFM studies. The interaction strength of the probes with the substrates was influenced by the vehicle pH in the case of the amide functionality and therefore, the origin of the weaker attraction between and the drug and the silica particles compared to the carboxyl-functionalised material was considered to be the relative strength of the electrostatic interactions that occurred between the drug and the particle surface.

There are mixed reviews on the extent of skin penetration of $Nano_{SiO_2}$ (Iannuccelli et al., 2014; Nafisi et al., 2015; Rancan, Gao et al., 2012; Staronova et al., 2012) but there is a general consensus that $Nano_{SiO_2}$ of more than 75 nm do not penetrate through the

epidermis (Rancan, Gao et al., 2012). Hence, the any drug penetration enhancement was most probably driven by the drug-nanoparticle interface occurring on the surface of the skin. Although tetracaine was not strongly bound to the $\mathrm{Nano}_{\mathrm{SiO_2}}$, the nanoparticles resulted in a 3.6-fold and 2.0-fold enhancement in tetracaine transport at pH 4 and pH 8 respectively. From this data, it does not seem unreasonable to assume that the interactions between tetracaine and the $\mathrm{Nano}_{\mathrm{SiO_2}}$ drove the enhanced permeation through the porcine epidermis and silicone membrane. It is possible that the weak $\mathrm{Nano}_{\mathrm{SiO_2}}$-tetracaine interactions broke up the tetracaine aggregates and increased drug permeation across the skin. However, none of the analytical techniques employed in this work could directly investigate this highly dynamic phenomenon.

By linking the analytical data with the transport studies, it was apparent that a balance of interaction strength between the nanomaterial surface and tetracaine was required to enhance membrane transport. If the interactions were too strong, this could retard permeation ($\mathrm{Nano}_{\mathrm{PSCOOH}}$), whereas a more moderate interaction could enhance transmembrane transport ($\mathrm{Nano}_{\mathrm{SiO_2}}$). This conclusion supports the work by Ueda et al. (2012), where excipient interaction-induced modification of drug aggregation was believed to be the reasons behind the improved permeation across a biological barrier. Similarly, in this project, nanoparticles were used to provide a solid interface that can modify drug aggregation.

4.6 Conclusion

The data generated in this chapter supported the hypothesis generated in Chapter 3 and that the addition of nanoparticles to a topical pharmaceutical preparation can modify drug delivery into the skin through physical interactions with the particulate surface. The search of the right balance of interaction strength between the nanomaterial surface and tetracaine is important as one that is too strong can retard permeation ($\mathrm{Nano}_{\mathrm{PSCOOH}}$), but one that has a moderate interaction to modify the state of tetracaine in a manner that can enhance transmembrane transport ($\mathrm{Nano}_{\mathrm{SiO_2}}$). It was anticipated that this better understanding of the mechanisms of nanomaterial enhancement of tetracaine transport into the skin would permit the design of effective topical formulations in Chapter 5.

CHAPTER FIVE

Topical Tetracaine Formulations Containing Nanomaterials to Increase Percutaneous Skin Permeation

5.1 Introduction

Tetracaine is commercially available as Ametop, a 4% gel that has an onset of action of 30 to 45 minutes (Joint Formulary Committee, online). This application time is too slow for optimal clinical action and this has driven formulators to design of a number of formulation strategies to try and improve the clinical use of this agent (Fang et al., 2008; Fisher et al., 1998; Hu et al., 2000). However, these strategies perturb the skin barrier and may result in long-term damage to the skin. One reason for the long onset of action may be that tetracaine is an amphiphilic drug that aggregates in aqueous vehicles (Attwood, 1995; Schreier, Malheiros et al., 2000). The relevance of drug molecular aggregation on membrane permeation has been highlighted in Chapter 2, wherein the drug aggregates of tetracaine exhibit different physicochemical properties in solution compared to the non-aggregated form of the molecule and at the high tetracaine drug concentrations typically found in topical preparations, this physical aggregation can modify penetration into the skin after topical application. Although it has been shown in Chapter 2 that formulating tetracaine at lower concentrations reduces the aggregation and improves drug transport, using a low drug concentration *in vivo* would reduce its clinical effect and is therefore not a viable strategy to improve anaesthesia. It is however, based on data from Chapter 3 and 4, reasonable to believe that a strategy that could break up tetracaine aggregation using nanoparticles could improve the onset of anaesthesia by improving drug penetration into the tissue.

In Chapter 3, the introduction of silica nanoparticles enhanced drug permeation by 3.6-fold at pH 4 and 2.0-fold at pH 8. However, rather than acting as a drug carrier, the solid nanomaterials, broke up drug aggregates without the particles themselves penetrating into the skin. This is an attractive drug delivery approach to improve the action of tetracaine because the added nanomaterials are unlikely to enter the body and hence raise additional toxicity concerns (Baroli, Ennas et al., 2007; Ryman-Rasmussen et al., 2006; Wu, Price et al., 2009). The data presented in Chapter 4 demonstrated that nanomaterials surface interactions were critical to the skin penetration enhancement process. However, to this point in the work, a topical formulation has not been designed with the purpose of enhancing percutaneous penetration simply by the addition of nanomaterials.

It is important if attempting to include nanomaterials in a topical semi-solid product to consider the nanoparticle-vehicle interactions (Benaouda, Brown, Ganguly et al., 2012). The vehicle can influence drug percutaneous penetration by controlling the drugs thermodynamic activity (Watkinson et al., 2009), modifying the membrane structure (Cross, Pugh, et al., 2001; Dal Pozzo & Pastori, 1996) and influencing the diffusion coefficient of the drug through the vehicle viscosity (Radebaugh & Simonelli, 1983; Welin-Berger et al., 2001). Although a solvent matrix must interact with a drug to solubilise it, a strong interaction in a complex solvent can have a detrimental effect on skin permeation through changes in drug diffusion (Benaouda, Brown, Martin et al., 2012). This is especially true if trying to increase the penetration of a drug from a

vehicle using nanoparticles because strong drug-vehicle interactions may influence the nanoparticle-drug interactions.

The aim of this chapter was to assess if adding nanomaterials to semi-solid topical preparations could enhance drug delivery. The experiments were conducted at pH 8 because Ametop, the commercially marketed gel, was formulated at pH 8 and the aggregation properties of tetracaine had been studied in previous chapters using this pH. Hydroxypropyl methycellulose (HPMC) was chosen as the excipient to produce a semi-solid formulation due to its inert nature and ability to form a gel with a large pore size (Mohamed et al., 2015). A spray formulation was used to apply the semi-solid as this allowed the mixing of the nanoparticles and the drug only upon drug application, which avoided any physical instability issues that could reduce the homogeneity of dosing. The sprays were optimised in terms of spray characterisation and viscosity to ensure accurate dosing. Tetracaine permeation from the different formulations was then assessed using porcine epidermis as a skin model. Comparisons with the commercially available Ametop were conducted to assess the potential for the developed formulation to provide superior drug deposition into the skin. Two drug application protocols were used to dose the drug to the skin: infinite dose studies were performed to understand the effects of vehicle composition on tetracaine delivery; finite dose studies were carried out to assess the clinical relevance of any differences observed in the formulations. Silica nanoparticles ($\mathrm{Nano_{SiO_2}}$) were used because in Chapter 3, they were shown to elicit the highest tetracaine enhancement effect when performed in aqueous solutions. Similar to the application protocol in Chapter 3, $\mathrm{Nano_{SiO_2}}$ were co-administered to the skin and no drug was encapsulated into the particles or adsorbed onto their surfaces

prior to administration. The semi-solid dosage form's macroviscosity were measured using traditional 'cone and plate' rheometry to have a better understanding of the interactions taking place in the system, i.e., between the drug, nanoparticle and formulation.

5.2 Materials

Material	Specifications	Company
Tetracaine	Free base, ≥ 98%	Sigma Aldrich, UK
HPMC powder	Grade 65SH viscosity 400 cP and 50 cP with the brand name Metolose	Shin-Etsu Chemical Ltd, Japan
$Nano_{SiO_2}$	Silica nanoparticles with a diameter of 200 nm (Psi-0.2)	Kisker Biotech GmbH and Co., Germany
Ametop gel	4.0% w/w tetracaine base	AAH Pharmaceuticals, UK
Hydrochloric acid (HCl)	Fuming, 37%	Sigma Aldrich, UK
Phosphate buffered saline	Tablets, pH 7.4, 0.172 M	Oxoid Ltd, UK
De-ionised water	Electrical conductivity 0.5-1 μS	Produced in house
Sodium acetate	Anhydrous, ≥ 99%	Sigma Aldrich, UK
Acetic acid	ACS reagent, ≥ 99.7%	Sigma Aldrich, UK
Acetonitrile	High performance liquid chromatography (HPLC) grade	Fisher Scientific, UK
Methanol	HPLC grade	Fisher Scientific, UK
Water	HPLC grade	Fisher Scientific, UK

Table 5.1. Materials used in Chapter 5.

5.3 Methods

5.3.1 Spray formulation preparation

The HPMC solutions were prepared by stirring HPMC powder slowly into pH 8 water at 70°C and allowing the system to hydrate for 24 h at 5°C. The formulations were then transferred into 50 mL plastic spray bottles (Boots, UK). Three HPMC formulations were produced with polymer concentrations of 1% and 2% of Grade 65 (viscosity 400 cP, 65SH400) and 3% of Grade 65 (viscosity 50 cP, 65SH50) because concentrations above these levels were unable to spray through the nozzle of the dosing system used to apply them to the skin in the permeation studies.

5.3.2 Spray characterisation

The spray formulation was placed at a distance of 5 cm vertically above a piece of filter paper and two shots of the formulation were actuated onto the paper to analyse the deposition characteristics of the semi-solid surface deposition. The film that was left on the filter paper after the formulation was sprayed onto it was outlined and the shortest diameter and the longest diameter of the outline were measured. The measurements were used to calculate the area covered by the product based on a perfect circle

(Equations 5.1 and 5.2) and the aspect ratio (AR, Equation 5.3). Triplicate measurements were performed for each formulation.

$$D_{mean} = \frac{D_{min} + D_{max}}{2} \quad \text{(Equation 5.1)}$$

$$Area = \pi \left(\frac{D_{mean}}{2}\right)^2 \quad \text{(Equation 5.2)}$$

$$AR = \frac{D_{min}}{D_{max}} \quad \text{(Equation 5.3)}$$

Ten actuations from the spray were applied to a tared weighing boat on an analytical balance and individually measured. The amount of formulation recovered in the nozzle (n_{nozzle}) was measured by the subtraction of the initial mass of the nozzle ($n_{initial}$) from the final mass of the nozzle (n_{final}) at the end of 10 actuations (Equation 5.4).

$$n_{nozzle} = n_{final} - n_{initial} \quad \text{(Equation 5.4)}$$

5.3.3 Viscosity of formulation

The rheological measurements were performed using CSL a cone and plate rheometer (Carri-med, USA) with plate diameter of 4.0 cm and cone angle of 1.5° at a 100 mm fixed gap. The test was performed over a 1-10 Hz frequency range at constant stress amplitude of 0.798 Pa. All the measurements were carried out at 20°C. Twenty data points were recorded for each rheogram and triplicates were performed for each formulation.

5.3.4 Tetracaine transport studies

Experiments to test the penetration of tetracaine through the porcine epidermis were performed as described previously in Section 2.3.6. The steady state flux (J) of tetracaine was determined and the enhancement ratios (ER) due to the various additives (water or $Nano_{SiO_2}$) were calculated using Equation 3.1.

In the studies in this chapter, two different formulation-dosing procedures were used. Infinite dosing studies applied 1 mL to the Franz cell and compared a saturated tetracaine solution of pH 8 to a HPMC formulation (developed in the study) and the commercial preparation Ametop. None of the systems contained nanoparticles, as the objective was to understand the drug-vehicle interactions.

The finite dosing tested the ability of the addition of nanoparticles on the formulations to deliver tetracaine into the skin. The nanoparticles were added at a concentration of 50 mg/mL to the tetracaine formulations immediately prior to application to the skin to avoid any potential problems induced by chemical or physical instability. The finite dosing transport study used 10 μL of Ametop or 3% HPMC formulation. The exact weight of the donor solution applied corresponded to 4.87 and 4.85 mg/cm^2 respectively. To these two 151 mM drug-loaded gels (drug loading was matched across the two formulations), an equal amount (10 μL) of with silica nanoparticles ($Nano_{SiO_2}$) or water (control) were added to the formulation at the 0 h time point after correcting the suspension medium pH to 8.

5.3.5 Tetracaine quantification

Refer to Section 2.3.7.

5.3.6 Statistical analysis

Refer to Section 2.3.8.

5.4 Results

5.4.1 Formulation optimisation and characterisation

A high spray volume, a low amount of residual formulation in the nozzle, a large spray deposit area and a moderately high viscosity were all thought to be desirable product characteristics for the spray systems. The 2% 65SH400 was thought not to be ideal because it had the lowest spray actuation mass (66.7 ± 43.7 mg), highest residual nozzle mass after spray actuation (66.0 ± 15.3 mg), lowest mean spray deposit diameter (2.4 ± 0.3 cm), lowest mean spray deposit area (4.5 ± 1.1 cm^2) and highest viscosity (Fig. 5.1).

The 1% 65SH400 and 3% 65SH50 formulations were not significantly different ($p>0.05$) in terms of the amount of spray actuated (157.7 ± 14.1 mg). However, 3% 65SH50 was chosen for further investigation rather than 1% 65SH400 because, although it covered a relatively small area (5.9 ± 0.5 cm^2), it showed appropriate viscosity to remain on the skin (Fig. 5.1) and 104-fold less residue was found on the nozzle ($p<0.05$). Furthermore, the 3% 65SH50 gel was the most efficient in terms of ejecting the dose of the three spray formulations.

	1% 65SH400	2% 65SH400	3% 65SH50
Mass of each spray actuation (mg)	157.7 ± 14.1	66.7 ± 43.7*	145.5 ± 27.5
Amount recovered in nozzle (mg)	31.4 ± 18.2*	66.0 ± 15.3*	0.3 ± 0.1
D_{mean} (cm)	3.5 ± 0.1*	2.4 ± 0.3	2.7 ± 0.1
Area (cm^2)	9.8 ± 0.6*	4.5 ± 1.1	5.9 ± 0.5
Aspect ratio	1.0 ± 0.0	0.9 ± 0.1	0.7 ± 0.1

Table 5.2. Characteristics of various HPMC formulations. Data represent mean ± standard deviation of 3 independent tetracaine samples. * Significant differences were observed based on one-way ANOVA test.

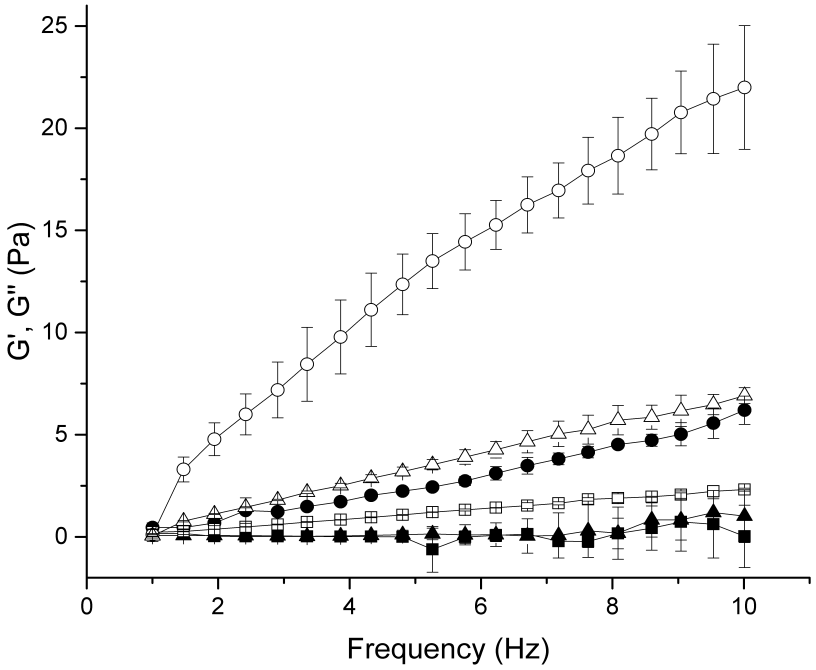

Figure 5.1. Storage modulus (G', solid) and loss modulus (G'', open) measured as a function of frequency (Hz) for various 1% 65SH400 (■), 2% 65SH400 (●) and 3% 65SH50 (▲) HPMC formulations. Data points represent mean ± standard deviation, n=3.

5.4.2 Infinite transport studies

Infinite doses of tetracaine were used to understand the effect of vehicle composition on tetracaine transport (Table 5.3, Fig. 5.2 for permeation profiles). According to manufacturer's data, the commercially available Ametop gel consisted of 151 mM of tetracaine with sodium hydroxide, sodium methyl-o-hydroxybenzoate, sodium propyl-p-hydroxybenzoate, monoboasic potassium phosphate, xanthan gum, sodium chloride and purified water. The HPMC formulation consisted of an equivalent concentraation of tetracaine with 3% HPMC. No nanoparticles were added to these systems. There was no significant difference ($p>0.05$) in steady-state tetracaine transport rate ((110.23 ± 40.93 $\mu g/cm^2/h$) and lag time (9.15 ± 2.05 min) when infinite doses of tetracaine were delivered by Ametop and the HPMC formulation compared to a simple saturated tetracaine solution, i.e. with no formulation additives.

	Flux ($\mu g/cm^2/h$)	k_p (10^{-3} cm/h)	m_{45min} (μg)	t_{lag} (min)
Tetracaine in HCl solution	110.23 ± 40.93	66.20 ± 24.58	64.5 ± 21.11	9.15 ± 2.05
Tetracaine in Ametop formulation	105.36 ± 21.97	63.27 ± 13.19	59.80 ± 9.31	10.10 ± 1.50
Tetracaine in HPMC formulation	107.28 ± 28.31	64.43 ± 17.00	67.19 ± 18.21	8.79 ± 2.43

Table 5.3. Steady state flux and permeability constants, k_p, accumulative mass at 45 minutes, m_{45min}, and lag time, t_{lag}, of infinite dosages of Ametop and tetracaine HPMC in the presence of different additives in pH 8 across porcine epidermis membrane. Data represent mean ± standard deviation of 3 independent tetracaine samples. * Significant differences were observed based on one-way ANOVA.

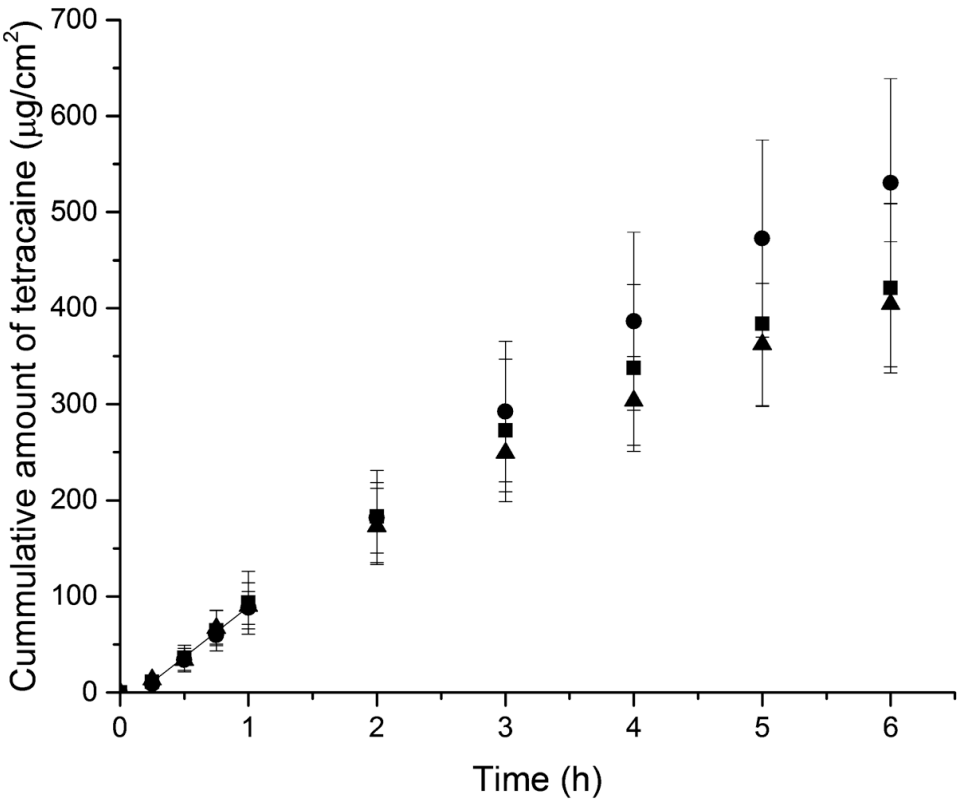

Figure 5.2. Permeation profiles of infinite dosages of tetracaine in HCl solution (■), Ametop formulation (●) and HPMC formulation (▲) in pH 8 across porcine epidermis. Each point represents the mean ± standard deviation, n=5. The straight lines represent the steady-state portion of the permeation profiles.

5.4.3 Finite transport studies

Finite studies were performed to study the transport of tetracaine from the semi-solid formulations using a dosing regime that matched clinical conditions (Table 5.4, Fig. 5.3 and 5.4 for permeation profiles of HPMC and Ametop formulations respectively). Based on manufacturer's data, the $Nano_{SiO_2}$, which were added to the formulations, only consisted of amorphous silica and water. Thus, water acted as a control to mimic the drug dilution effects that were experienced upon addition of the nanoparticles to the formulation.

	Flux ($\mu g/cm^2/h$)	ER	m_{45min} (μg)	t_{lag} (min)
Ametop	1.16 ± 0.14	-	0.25 ± 0.06	31.60 ± 3.00
Ametop + water	5.62 ± 2.25	4.71 ± 1.40*	2.53 ± 1.77*	20.20 ± 1.34*
Ametop + $Nano_{SiO_2}$	14.19 ± 2.27	12.86 ± 3.16*	8.12 ± 1.21*	10.69 ± 1.98*
HPMC	46.99 ± 7.96	-	31.13 ± 4.04	7.09 ± 1.80
HPMC + water	30.51 ± 12.16	0.69 ± 0.35	21.99 ± 10.48	3.97 ± 1.07*
HPMC + $Nano_{SiO_2}$	109.95 ± 28.63	2.48 ± 1.08*	76.83 ± 18.92 *	2.02 ± 0.79*

Table 5.4. Steady state flux, flux enhancement ratio, ER, accumulative mass at 45 min, m_{45min}, and lag time, t_{lag}, of finite dosages of Ametop and tetracaine HPMC in the presence of different additives in pH 8 across porcine epidermis membrane. Data represent mean ± standard deviation of 3 independent tetracaine samples. * Significant differences were observed based on one-way ANOVA.

Calculation of the lag time showed that the HPMC spray, with the added $Nano_{SiO_2}$, had the shortest permeation lag time (t_{lag})(2.02 ± 0.79 min). In addition, the tetracaine permeation rate (109.95 ± 28.63 $\mu g/cm^2/h$) and the amount of tetracaine permeating at the 45 min time point (m_{45min})(76.83 ± 18.92 μg) were the highest when tetracaine was formulated as the HPMC spray containing the $Nano_{SiO_2}$. The addition of water to the HPMC semi-solid formulation did not induce a significant change in tetracaine steady state flux (30.51 ± 12.16 $\mu g/cm^2/h$) and m_{45min} (21.99 ± 10.48 μg), but it did induce a 1.7 times reduction in t_{lag} from 7.09 ± 1.80 min to 3.97 ± 1.07 min. (Table 5.4, Fig. 5.3 for permeation profiles). Compared with the water control, the $Nano_{SiO_2}$ significantly enhanced ($p<0.05$) percutaneous tetracaine transport 3.6-fold when added to the HPMC

formulation (Table 5.4). In addition, the $Nano_{SiO_2}$ significantly increased m_{45min} by approximately 3 times and reduced t_{lag} by about 2-fold (Table 5.4).

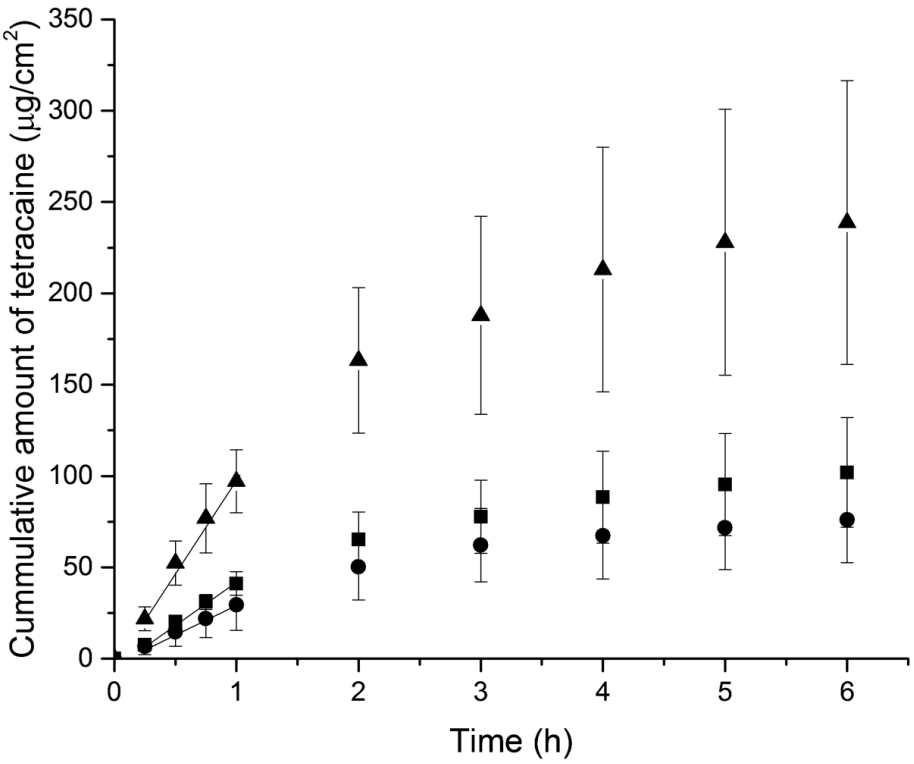

Figure 5.3. Permeation profiles of Ametop (■) with the addition of water (●) and unmodified silica nanoparticles, $Nano_{SiO_2}$ (▲), in pH 8 across porcine epidermis. Each point represents the mean ± standard deviation, n=5. The straight lines represent the steady-state portion of the permeation profiles.

In contrast to the HPMC formulation, the addition of water to the Ametop formulations significantly enhanced tetracaine permeation rates by 5-fold, increased accumulative mass by 10-fold and reduced t_{lag} by 1.5 times (Table 5.4, Fig. 5.4 for permeation profiles). Compared to the water control, the $Nano_{SiO_2}$ addition to the Ametop formulation increased the skin permeation by 2.7. However, of the two formulations

tested, the HPMC formulation was superior. It significantly enhanced the tetracaine flux (46.99 ± 7.96 μg/cm^2/h) by 40-fold, increased accumulative mass (31.13 ± 4.04 μg) by 124-fold and reduced t_{lag} (7.09 ± 1.80 min) by 8-fold, as compared to the Ametop formulation.

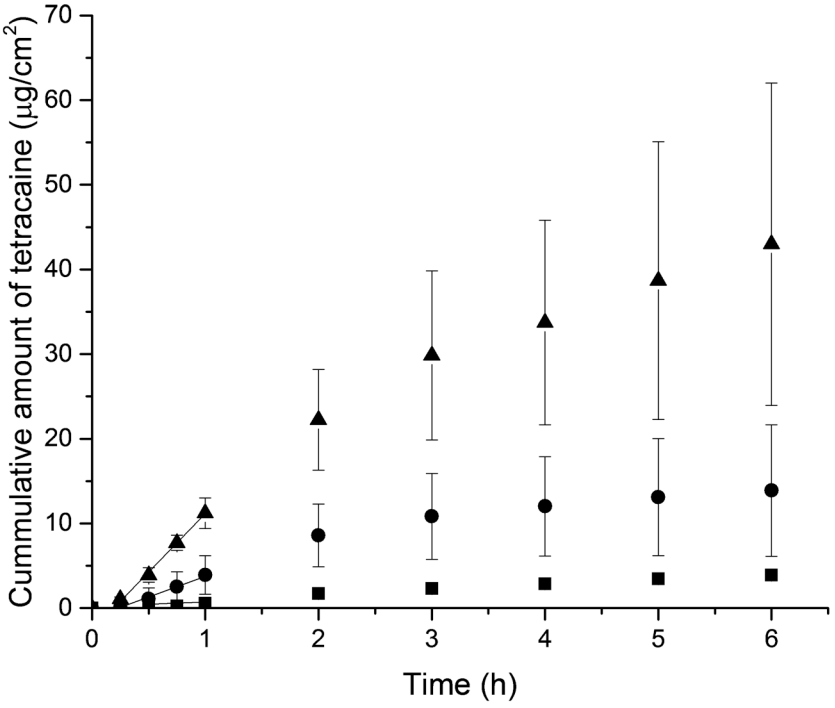

Figure 5.4. Permeation profiles of tetracaine in HPMC formulation (■) with the addition of water (●) and unmodified silica nanoparticles, $Nano_{SiO_2}$(▲), in pH 8 across porcine epidermis. Each point represents the mean ± standard deviation, n=5. The straight lines represent the steady-state portion of the permeation profiles.

5.4.4 Rheology of formulations

The rheological characteristics of the semi-solid formulations were examined to try and further understand the observed differences in the tetracaine permeation profiles (Fig. 5.5). All the Ametop formulations were significantly ($p<0.05$) more viscous (higher storage and loss modulus) than the HPMC formulations. The addition of water in both formulations significantly decreased ($p<0.05$) the viscoelasticity of the formulations. However, there were no significant changes ($p>0.05$) in rheological behaviour when the addition of water and $Nano_{SiO_2}$ were compared.

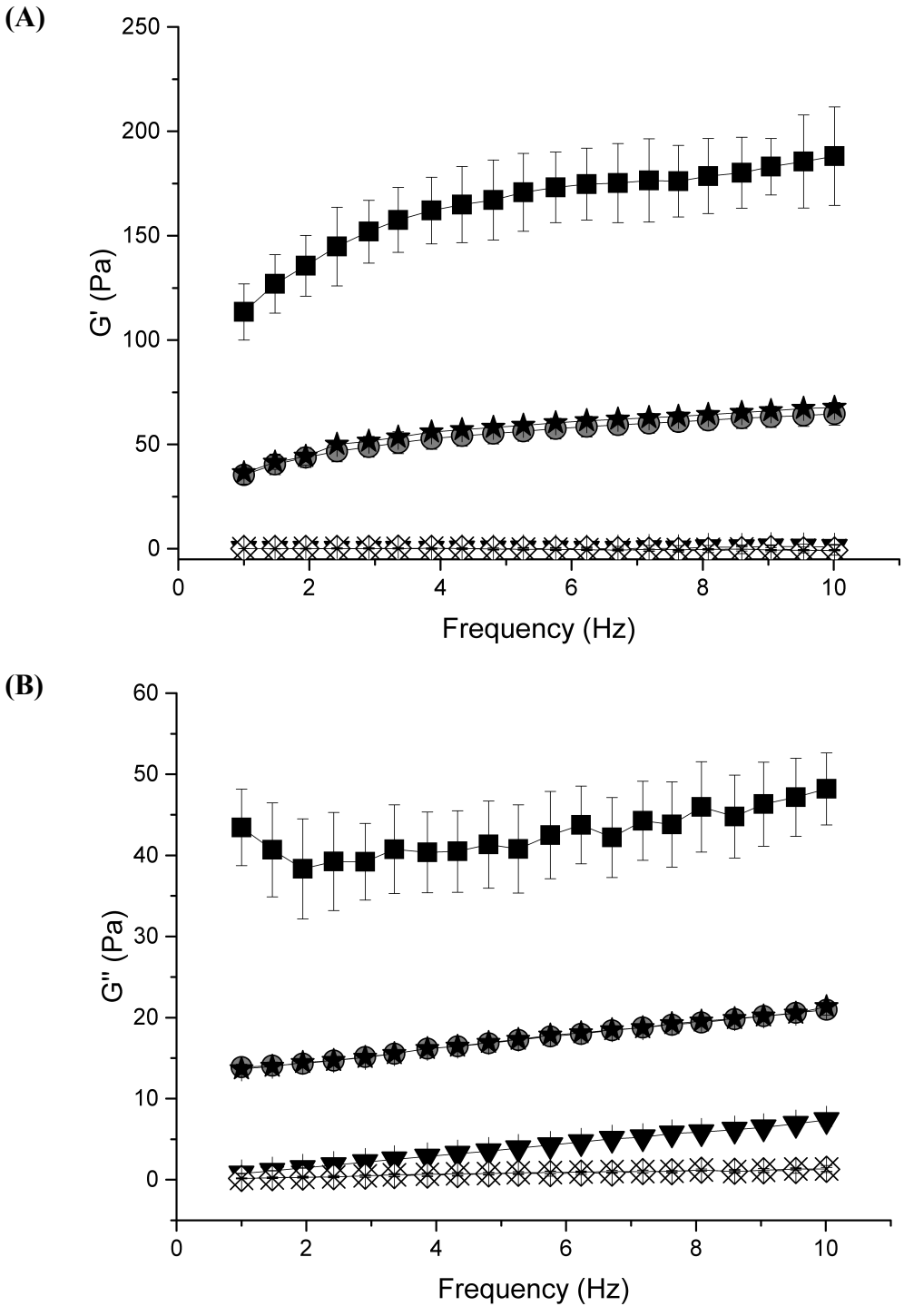

Figure 5.5. Storage modulus (G', (A)) and loss modulus (G'', (B)) measured as a function of frequency (Hz) for Ametop (■), Ametop with the addition of water (n), Ametop with the addition of silica nanoparticles, $Nano_{SiO_2}$ (★), HPMC formulations (▼), HPMC formulation with the addition of water (◇), formulation with the addition of $Nano_{SiO_2}$ (×). Data points represent mean ± standard deviation, n=3.

5.5 Discussion

Efficient release of a drug from a topically applied formulation is essential for topical preparations administered to the skin because of the highly resistant barrier that the cutaneous membrane provides. One reason why topical corticosteroid preparations elicit side effects, such as skin thinning, is that large doses are required on the surface of the skin due to the inefficient release of drug. For example, an investigation by Shah et al. (1989), only 5-10% of the applied hydrocortisone was released from commercial creams. To circumvent this problem, more effective topical administration vehicles are required, but the type of formulation vehicle must be matched to the issues presented by the drug. For example, Reid et al. (2013) showed that EtOH/PEG HFA spray could generate a 6-fold enhancement of BMV delivery through the skin as compared to commercial cream. However, Fiala et al. (2015) demonstrated that a similar approach when trying to improve the skin penetration of lidocaine compared to the commercial product was not successful. Therefore, a topical vehicle must be constructed with the issues of the drug in mind.

In the previous chapters, tetracaine was shown to interact with silica nanoparticles to break up its aggregates and improve permeation into the skin. However, this data was generated in simple solutions, which facilitated analytical characterisation of the system, but these systems could not be used clinically. Topical formulations need to exhibit a degree of viscosity and therefore, viscosity modifiers, such as xanthan gum and HPMC, are often incorporated into the topical system. Improved viscosity can

increase product acceptance by the patient, because it is easy to use, it adheres to the treated area, spreads well and have a good consistency. Viscosity is also an important consideration in the manufacturing process of the product. However, viscosity modifiers may hinder drug diffusion from the formulation into the skin. For example, the addition of a 7% gelling agent to thicken a Transcutol:isopropyl myristate binary mixture resulted in a four-fold decrease in clebopride diffusion (Rhee et al., 2007). The decrease was attributed to the increased viscosity of the gel formulation.

To investigate the possible effects of the added viscosity modifiers in this study, infinite dose studies were used. The infinite dose studies provided a mechanistic insight to investigate the effect of vehicle composition on drug delivery, as no nanomaterials were added to these systems. The data demonstrated that neither the xanthan gum or HPMC had a large effect on tetracaine permeation behaviour, i.e. the excipients were considered to be relatively inert. The influence of HPMC on drug permeability is dependent on its viscosity and this is critical in governing the drug-HPMC interactions. When higher concentrations of HPMC are used in a topical formulation, the polymer is known to show a bigger effect on the drug, even reducing drug permeability. For example, in supersaturated conditions, HPMC acts as an anti-nucleating agent, interacting with the drug to prevent nucleation (Iervolino et al., 2000; Megrab et al., 1995; Raghavan et al., 2000). However, when lower concentrations of HPMC have been used in the literature, similar observations have been made that were similar to the data generated in the current work (Charoo et al., 2008; Kim et al., 2001).

To investigate the clinical utility of the tetracaine HPMC spray formulation, finite dosing studies were conducted. There is often a significant difference between infinite finite dose studies. For example, in a study by Cross et al. (2001), thickening agents were shown to retard drug penetration through the skin in infinite dose studies but the opposite effect was observed in finite dose studies. The authors attributed the different results to the increased hydration due to less water evaporation and enhanced drug diffusivity through the *stratum corneum* when using finite doses. The difference in drug permeation behaviour between the HPMC gel and the commercial preparation in this study may be related to the manner in which the two high molecular weight molecules in the formulations alter the viscosity of the preparations. Xanthan gum is considered to be a non-gelling agent, whereas HPMC forms a gel (Mughal et al., 2011). When there is an infinite amount of drug applied to the skin, there is a little increase in the formulation viscosity but in the finite studies, there is a significant change in formulation viscosity due to the small amount of preparation applied to the skin. It may be that the HPMC system can resist the changes in viscosity upon application to the skin in finite conditions such that it does not alter the drug diffusion through the preparation, compared to the Ametop preparation. In the HPMC preparation, there is the possibility that changes in the macroviscosity of the polymer may not translate into the diffusional characteristics of molecules passing through the gel as the polymer produces a gel-like network. However, in the case of Xanthan gum, the changes in macroviscosity were proportional to the changes in viscosity experienced by the diffusing molecules.

In the present study, the nanomaterials were added on the skin just after application of the formulation and so, in order to generate comparative data in the control systems employed in the work, an equivalent amount of pH-adjusted water was used to match the volume modification effect of adding the nanoparticle suspensions to the semi-solid preparations. When the systems with and without nanomaterials were compared across both types of semi-solid vehicles used in this work, the nanomaterials enhanced drug permeation into the skin. Based on these results and the particle-drug interaction data from the previous chapter (Chapter 4), it was assumed that the drug permeation enhancement induced by the addition of the $\mathrm{Nano}_{\mathrm{SiO_2}}$ was caused by the breaking up of the tetracaine aggregates due to weak surface interactions between $\mathrm{Nano}_{\mathrm{SiO_2}}$ and the tetracaine molecules.

According to the rheological data, there was no difference between the viscoelasticity of the semi-solid formulations upon the addition of water and silica particles. This was unlike the results obtained by Moddaresi et al. (2010), where an increase in viscoelasticity was observed when lipid nanoparticles were added to hyaluronic acid vehicle. In the previous work, they attributed the change in rheological behaviour to the presence of strong interactions between the nanoparticles and the hyaluronic acid. In the current study, the rheology data implied that the formulation excipients and the nanoparticles did not generate a strong interaction. Thus, any change in the tetracaine permeation was largely due to the other interactions taking place in the system, i.e. tetracaine-nanoparticle and tetracaine-formulation interactions. This was supported by the fact that the enhanced permeation was observed both in the in-house manufactured

HPMC formulation and the commercially available Ametop preparation even though the two preparations exhibited very different rheological behaviour.

The addition of the liquid to the tetracaine formulations, regardless of whether or not the liquid contained nanoparticles, altered the drug permeation through the skin. Large error bars were encountered when liquid was added to the semi-solid systems, most probably due to the lack of mixing during application and/or due to the non-homogenous presence of nanoparticles within the drug in the gel. Nevertheless, a viscosity-dependent permeation behaviour was observed. This is not always the case with other preparations reported in the literature. It is possible for a semi-solid system to exhibit a viscosity-independent permeation behaviour (Gallagher & Heard, 2005; Suh & Jun, 1996). However, when a viscosity-dependant permeation behaviour is observed, it is more typically akin to the work by Pygall et al. (2011), who showed that meclofenamate aggregates formed hydrogen bonds with the HPMC, leading to an increase in the viscosity of the formulation and subsequently a decrease in drug release from HPMC structures. The data from the current study showed the opposite effect. This may have been because of the relatively strong drug-drug affinity of the tetracaine molecules (CAC – 7.38 μM as shown in Chapter 2) and the weak interactions between the drugs in the formulation vehicles (as shown by the infinite dosing studies).

5.6 Conclusion

An efficient tetracaine topical spray formulation with superior drug permeability and a more rapid onset of action compared to commercial Ametop was generated. This was obtained through the addition of nanoparticles to a semi-solid preparation that were sprayed onto the skin. Nanoparticles were thought to have disrupted the tetracaine aggregates, which retarded the drug permeation and hindered lag time. The HPMC spray formulation was thought to be superior to the commercial preparation due to the lower macroviscosity, which allowed the tetracaine to be more readily available to permeate through the skin. However, the addition of nanoparticles to the commercial formulation was also effective in improving the delivery of tetracaine, which suggests that this novel drug delivery strategy could even be applied to currently marketed products to enhance their performance.

CHAPTER SIX

General Discussion

Topical drug delivery to the skin presents an attractive alternative to other routes of administration by providing a non-invasive strategy that bypasses the first-pass metabolism, reduces the adverse side effects of systematic toxicity and improves patient compliance (Brown, Martin et al., 2006). However, efficient topical delivery can be problematic to achieve due to the relative impermeability of the *stratum corneum* (Scheuplein & Blank, 1971). Many enhancement strategies have been employed to overcome this problem (Hadgraft, 1999) and one such approach is the use of nanomaterials.

Nanomaterials in topical products can enhance the percutaneous penetration of therapeutic agents (Alves et al., 2007; Borgia et al., 2005; Chen et al., 2006). In particular, solid nanomaterials greater than 20 nm (the size most regularly employed in drug delivery studies) are an attractive formulation additive because they are too large to pass into the skin and hence, they probably will not illicit drug toxicity effects (Baroli, Ennas et al., 2007; Ryman-Rasmussen et al., 2006; Wu, Price et al., 2009). Despite the numerous reports documenting the ability of nanomaterials to enhance drug permeation across the skin, the mechanisms by which they do this remain less well defined. The literature has generated some general hypotheses of how nanomaterials aid topical skin delivery, including carrying the drug across the barrier (Alvarez-Roman et al., 2004a) and modifying the skin barrier (Wissing, Lippacher et al., 2001). Interestingly, there does not seem to be previous reports that have specifically aimed to enhance drug penetration into the skin using nanoparticle surfaces to modify the physical interactions of drugs applied topically to the skin. As such, the aim of the

thesis was to elucidate the interactions in drug-nanomaterial formulations and generate a dynamically triggered formulation that enhances drug permeation. It was hypothesised that the introduction of the nanoparticles at the point of administration would generate a dynamic system that could break up drug-drug aggregation in a manner that could enhance drug percutaneous penetration.

Tetracaine was selected as a model drug in this study because it is known to form aggregates and its commercially available preparation (Ametop 4% gel) has an onset of action of 30-45 minutes (Joint Formulary Committee, online). This long onset of action has previously been suggested to be a consequence of tetracaine's aggregation properties (Inacio, Barlow et al., In-press). Therefore, the deliberate perturbation of molecular aggregation would appear to be a sensible means to enhance topical drug delivery of this molecule.

In order to enhance the penetration of tetracaine into the skin, its skin permeation characteristics required further understanding (Fig. 6.1). Given the small size and dynamic nature of aggregates, direct analysis of the structures of monomers and aggregates was considered difficult when the molecules are at concentrations and in vehicles that are appropriate for pharmaceutical use. As the 'context' of the drug was of vital importance when direct analytical characterisation was impossible, indirect approach was employed to try to understand the aggregate structure and the functional consequences of aggregation in liquids that could be used for drug administration.

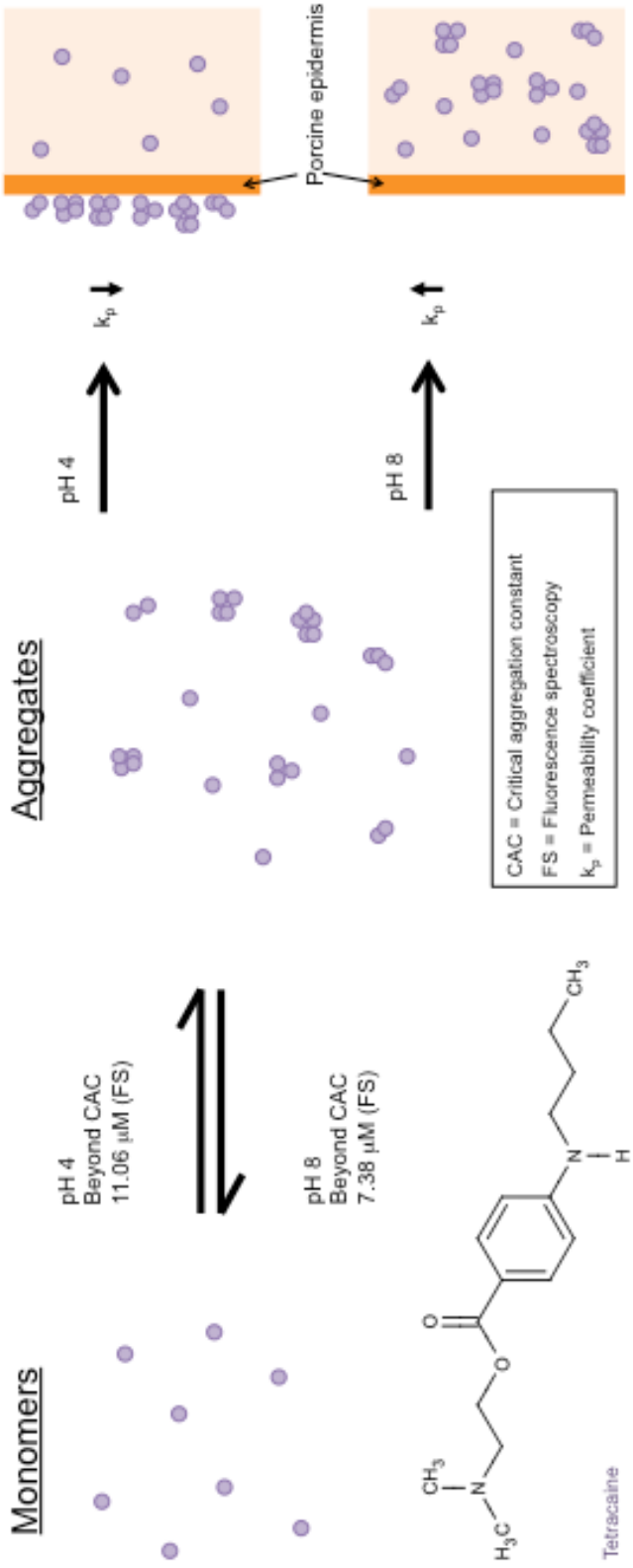

Figure 6.1. Drug aggregation can influence its passive transmembrane permeation.

Tetracaine was shown to form a series of different aggregates across the μM (fluorescence spectroscopy) to mM (light scattering analysis) concentration range and this was paramount to enable a better understanding of how the drug presented itself to the surface of a biological barrier after topical application. The aggregate formation process was demonstrated to be sensitive to the pH of the vehicle in which the drug was dissolved in due to the modification of tetracaine's ionisation. As the pH increased, the CAC decreased (pH 4, CAC – 11 μM; pH 8 CAC – 7 μM). A similar phenomenon was observed by Attwood and Natarajan in 5 different piperazine drugs (Attwood & Natarajan, 1981). It was suggested from the data that the types of aggregates formed varied in the different pH solutions due to the different ionisation environment of the molecules. In a water vehicle buffered at pH 8, unionised tetracaine molecules were thought to be trapped in a hydrophobic environment while in a pH 4 vehicle, charged aggregates were more likely to be formed. In both the pHs, hydrogen bonding was thought to govern the self association because previous work has shown that tetracaine molecules stack *via* $N-H\cdots N$ tertiary association with some $N-H\cdots C=O$ ester and $N-H\cdots N-H$ bonds (Guerin, Dumas et al., 1980).

The drug permeation data generated in Chapter 2 of the thesis demonstrated that the different presentation of tetracaine aggregates on the membrane had a significant impact upon the drug's percutaneous penetration. When porcine epidermis was used for the *in vitro* assessment of tetracaine transport through the skin at pH 4, concentration-dependent aggregation decreased the permeability of tetracaine. When silicone membrane was employed as the barrier, the trends in the porcine skin were mirrored and

this suggested that follicular route, which was only present in the porcine skin, was not playing a significant role in drug transport. This eliminated the possible hypothesis that the reduction of permeability of tetracaine could be caused by the saturation of the appendages by both the charged aggregates and non-aggregates. Therefore, it was suggested that only non-aggregated molecules drove the tetracaine transport and the formation of the more polar aggregates formed in pH 4 were reducing the proportion of membrane diffusing species passing through the skin *via* the intracellular or transcellular pathway, consequently decreasing the permeability of tetracaine.

At pH 8, the formation of uncharged aggregates due to the increase in tetracaine concentration increased the permeability of tetracaine across the skin. One possible hypothesis that could explain such a phenomenon is that drug aggregation increases the affinity of the drug to the skin. It was suggested that both non-aggregated and aggregated molecules drove the tetracaine transport at this pH and the more hydrophobic aggregates formed were actually contributing in some means to the membrane diffusing species. This relationship between drug aggregation and permeation suggested that controlling the aggregation of drugs could be a novel means to modulate transport through the skin (Fig. 6.1).

Drug aggregation can be perturbed by the addition of substances that compete for drug-drug association sites. Theoretically, these substances can include counter-ions (Attwood & Udeala, 1975), surfactants (Darwent, McCubbin et al., 1982; Rossetti, Lopes et al., 2011; Shao, Li et al., 1993; Spikes & Bommer, 1986) and polymers

(Pygall, Griffiths et al., 2011); all of which can disrupt drug-drug interactions *via* competitive interaction. However, in this PhD project, the addition of a high concentrations of negatively charged dihydrogen phosphate electrolytes (1:10000 tetracaine to phosphate ratio) had no effect to the fluorescence emission and transport rates of tetracaine, which suggested that tetracaine-tetracaine aggregation could not be disrupted by the relatively weak ion-pair interactions that were formed between the negatively charged phosphate and the positively charged drug in pH 4 environment. In contrast, the introduction of nanomaterials was able to modify drug aggregation (Fig. 6.2). Negatively charged carboxyl-modified polystyrene nanoparticles ($\mathrm{Nano_{PSCOOH}}$) and silica nanoparticles ($\mathrm{Nano_{SiO_2}}$) were used to represent two different nanoparticle surfaces with which the model drug tetracaine could interact, thereby generating very different tetracaine transport profiles. When tetracaine was mixed with $\mathrm{Nano_{PSCOOH}}$, the particles prevented the drug's penetration through both the porcine and silicone barriers. On the other hand, the $\mathrm{Nano_{SiO_2}}$ generated a 3.6-fold and a ca. 100-fold enhancement in tetracaine percutaneous penetration across porcine epidermis and silicone membrane respectively at pH 4. The higher permeation enhancement ratio at pH 4 (3.6-fold) compared to at pH 8 (2.0-fold) may be attributed to drug aggregation and their contribution to drug permeation. At pH 4, the addition of $\mathrm{Nano_{SiO_2}}$ may break up the non-permeating aggregates in a manner that could facilitate the temporal increase in drug monomers that could permeate across the skin while at pH 8, the modification of already permeating aggregates led to an increase, but not one as high as at pH 4.

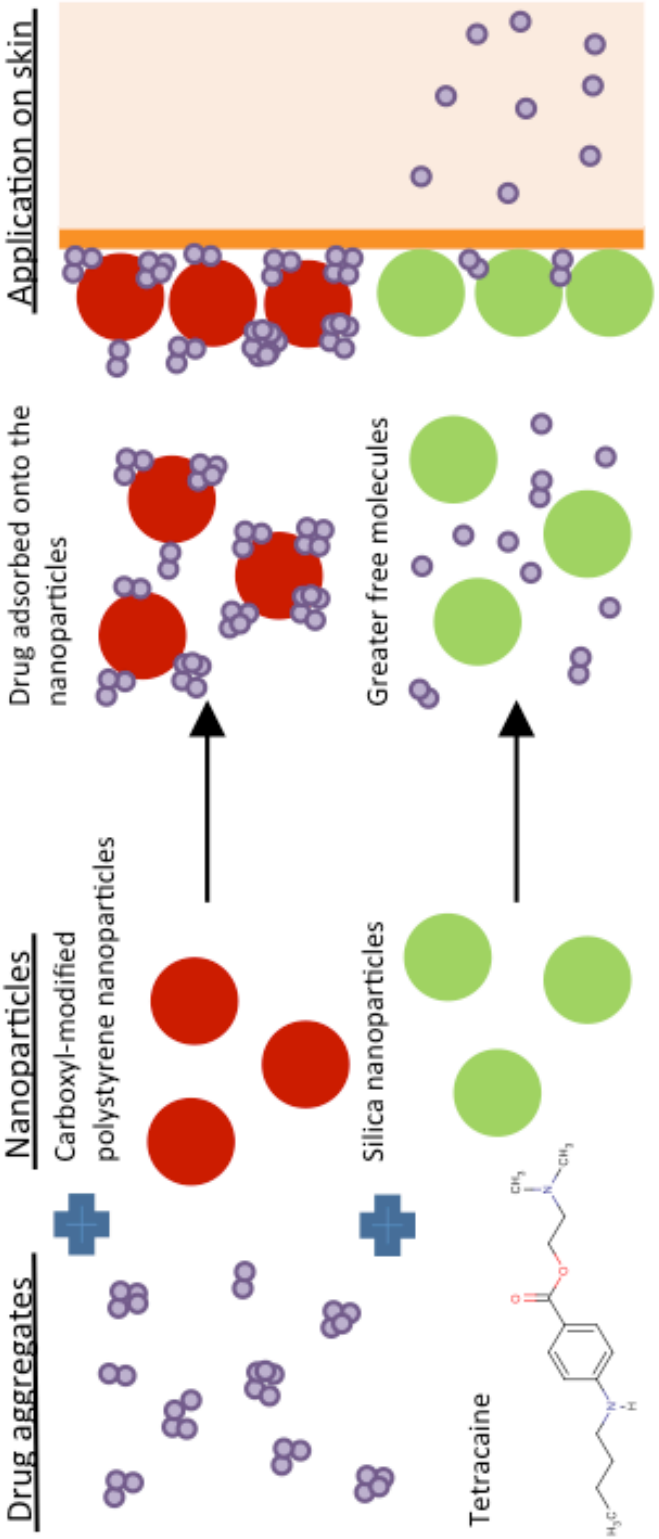

Figure 6.2. Nanomaterials can enhance drug percutaneous skin permeation by modification of drug aggregation.

Nanomaterial-induced drug enhancement across hydrophobic membranes has been reported in the literature (Alves et al., 2007; Borgia et al., 2005; Chen et al., 2006) and this effect was replicated in the data reported in this work. However, what was novel about the work in this study was that the transport was assessed upon the dynamic mixing of a solid nanoparticle and a drug on the membrane surface to which it was administered. This was unlike conventional usage of the nanoparticle as a drug carrier, where drug is encapsulated within the nanoparticle.

To understand more about the nanoparticle surface-drug interactions, the instant mixing of the drug with nanoparticles upon the barrier and the prior equilibration of the system, i.e. the incubation of drug and nanoparticles for a period of time (30 days), was compared. In both systems, the $\mathrm{Nano_{PSCOOH}}$ had a negative effect on the permeability of tetracaine, i.e. no tetracaine across the membrane was quantified. The equilibrated $\mathrm{Nano_{SiO_2}}$-tetracaine system that was incubated for 30 days and the dynamic $\mathrm{Nano_{SiO_2}}$ - tetracaine system that was mixed on the surface of the skin both gave impressive enhancement effects when measuring transport across the silicone membrane. The direct mixing of the drug and nanomaterials on the surface of the skin was the preferred application method as it minimised any potential interference from chemical or physical instability as a consequence of forming the mixture. Thus, this dynamic mixing was used throughout this study.

As the $\mathrm{Nano_{PSCOOH}}$ contained SDS, it was thought beneficial to test the effects of this additive. However, SDS did not appear to significantly alter tetracaine transport.

Conversely, the soluble silica available in the aqueous phase of the $Nano_{SiO_2}$ suspension played a role in enhancing tetracaine transport. This may have arisen due to ion-pairing, but the major benefit in terms of penetration enhancement still appeared to arise due to the presence of the nanoparticle surfaces according to the comparison of the different systems permeation rates. These results emphasised the importance of the solid interface provided by the nanoparticles (not the oppositely charged ions, equilibration time, carrier or vehicle) to perturb tetracaine aggregation demonstrated by the change in tetracaine permeation.

The reason why $Nano_{PSCOOH}$ and $Nano_{SiO_2}$ generated such very different tetracaine transport profiles was examined through a detailed investigation of the drug-nanoparticle surface interactions that occurred on the skin surface once the topical formulations had been applied to the skin. The particle drug interactions were monitored using physical adsorption studies, fluorescence spectroscopy and atomic force microscopy force adhesion measurements. Methyl and ionised tertiary amide tips were used as a functional representative of the two ends of a charged tetracaine molecule in AFM studies.

The $Nano_{PSCOOH}$ interactions with the drug were relatively strong. This was evident from the physical adsorption studies, the blue shift in the fluorescence measurements, and the high strong force adhesion measurements. The $Nano_{PSCOOH}$ has carboxyl and sulphate surface groups and therefore, the interaction with the tetracaine, which has at least one positive charge (it can have two positive charges depending on the solution

pH), was anticipated to be mainly *via* electrostatic forces. The amine functionality on the tetracaine was thought to be the primary means by which the drug adsorbed at the particle surface, as the force-adhesion measurements between tetracaine and the amine group were stronger than the drug interactions with the methyl group. These observations implied that tetracaine aggregates were disrupted by the drug surface adsorption onto the nanoparticles. However, these strong interactions resulted in tetracaine being retained on the nanoparticle surface and because the $\mathrm{Nano_{PSCOOH}}$ are unable to penetrate even the most superficial *stratum corneum* (Alvarez-Roman et al., 2004a), the strong drug adsorption onto the particle surface retarded the drug transport across the skin. A similar explanation was suggested in a previous study to explain why $\mathrm{Nano_{PSCOOH}}$ did not release their drug payload into the *stratum corneum* (Wu, Landfester et al., 2010).

Tetracaine had a weaker affinity with $\mathrm{Nano_{SiO_2}}$ than $\mathrm{Nano_{PSCOOH}}$ as demonstrated by the physical adsorption measurements, the absence of a shift in the fluorescence spectra of the tetracaine solution in the presence of the nanoparticles and the relatively low adhesion force measurements recorded in the AFM studies. This reduction was attributed to the lower surface charge of the $\mathrm{Nano_{SiO_2}}$ (ca. – 20 mV) compared to the $\mathrm{Nano_{PSCOOH}}$ (ca. -40 mV), which diminished to some degree the electrostatic interactions between positive amine of tetracaine and the negative particle surface. Despite the weak surface adsorption of tetracaine on to the particles, the $\mathrm{Nano_{SiO_2}}$ still resulted in a 3.6-fold and 2.0-fold increase in drug transport across the skin at pH 4 and 8 respectively. It is possible that the weak $\mathrm{Nano_{SiO_2}}$-tetracaine interactions broke up the

tetracaine aggregates and increased drug permeation but did not retain the drug for long periods on the particle surface. This conclusion supports the work by Ueda et al. (2012), where drug-excipient interactions-induced modification of drug aggregation modified drug permeation across a biological barrier.

By linking the analytical data with the transport studies, it was apparent that a balance of interaction strength between the nanomaterial surface and tetracaine was required to enhance membrane transport (Fig. 6.2). If the interactions were too strong, this could retard permeation ($\mathrm{Nano_{PSCOOH}}$), whereas a more moderate interaction could enhance transmembrane transport ($\mathrm{Nano_{SiO_2}}$).

The new understanding of the mechanism of nanomaterial-induced percutaneous enhancement enabled the design of a topical nanoparticle containing gel formulation that exhibited an improved permeation profile compared to the commercial formulation. The gel was administered to the skin as a spray, which was optimised in terms of spray characterisation and viscosity to ensure accurate dosing. The commercial comparator was Ametop. Both formulations were compared with and without the addition of $\mathrm{Nano_{SiO_2}}$. For comparative purposes, the tetracaine concentration in the HPMC formulations was matched to Ametop (4% w/w) and studies were conducted at pH 8. Two drug application protocols were used to dose the drug to the skin: infinite dose studies were performed to provide a mechanistic insight into the possible effects of vehicle composition on tetracaine delivery; finite dose studies were carried out to assess the clinical relevance of any differences observed in the formulations.

Finite dosing of the formulations to the porcine epidermis generated the fastest drug permeation, highest accumulative mass at 45 min and shortest lag time when the HPMC tetracaine spray was combined with silica nanoparticles ($Nano_{SiO_2}$). When compared to the commercial Ametop, the spray formulation enhanced tetracaine transport by 95-fold, improved accumulative mass by 307 times and reduced the lag time by 15.6-fold (Fig. 6.3). This enhancement was mainly attributed to the tetracaine-nanoparticle interactions. The $Nano_{SiO_2}$ enhanced percutaneous tetracaine transport by 3.6-fold and 2.7-fold in the HPMC formulation and Ametop formulation respectively when compared to the water control. In addition, in both formulations, the $Nano_{SiO_2}$ increased the accumulative mass at 45 min by approximately 3 times and reduced the lag time by about 2-fold when added to the HPMC formulation as compared to the water control. Based on these results and the drug-$Nano_{SiO_2}$ interaction data obtained previously, it was assumed that this enhancement induced by the $Nano_{SiO_2}$ was due to the breaking up of tetracaine aggregates facilitated by the weak surface interactions between the $Nano_{SiO_2}$ and the tetracaine molecules.

According to the infinite dose studies, the excipients (HPMC in the in-house spray or the xanthan gum present in the Ametop) did not significantly change the tetracaine permeation behaviour and were considered to be relatively inert. Similar observations were reported by Kim et al. (2001) and Charoo et al. (2008). The addition of liquid to both the tetracaine formulations altered the drug permeation through the skin but the

major effect arose from the addition of $\mathrm{Nano}_{\mathrm{SiO_2}}$. Furthermore, there was no difference between the viscoelasticity of the semi-solid formulations upon the addition of water and $\mathrm{Nano}_{\mathrm{SiO_2}}$, implying that formulation excipients and the $\mathrm{Nano}_{\mathrm{SiO_2}}$ did not generate a strong interaction. This was contrary to the investigation by Moddaresi et al. (2010), where strong interactions between lipid nanoparticles and hyaluronic acid in the form of an increase in viscoelasticity were reported. Thus, any change in the tetracaine permeation was largely due to the other interactions taking place in the system, i.e. tetracaine-nanoparticle and tetracaine-formulation interactions.

HPMC-based formulation exhibited superiority over Ametop in terms of drug permeation enhancement – it improved the tetracaine flux by 40-fold, increased accumulative mass by 124-fold and reduced lag time by 8-fold, as compared to the Ametop formulation. The two gel forming systems were very different, with Ametop using xanthan gum as a viscosity modifier, which primarily influenced both the micro and macroviscosity of the formulation, while HPMC only influenced the latter. However, as mentioned earlier, nanoparticle effects are independent of the formulation vehicle. Thus, even though the rheology data demonstrated that changing the viscosity of the formulation vehicle influenced the percutaneous penetration of tetracaine, this effect was not as important as the break up of drug aggregates through drug-nanoparticle interactions.

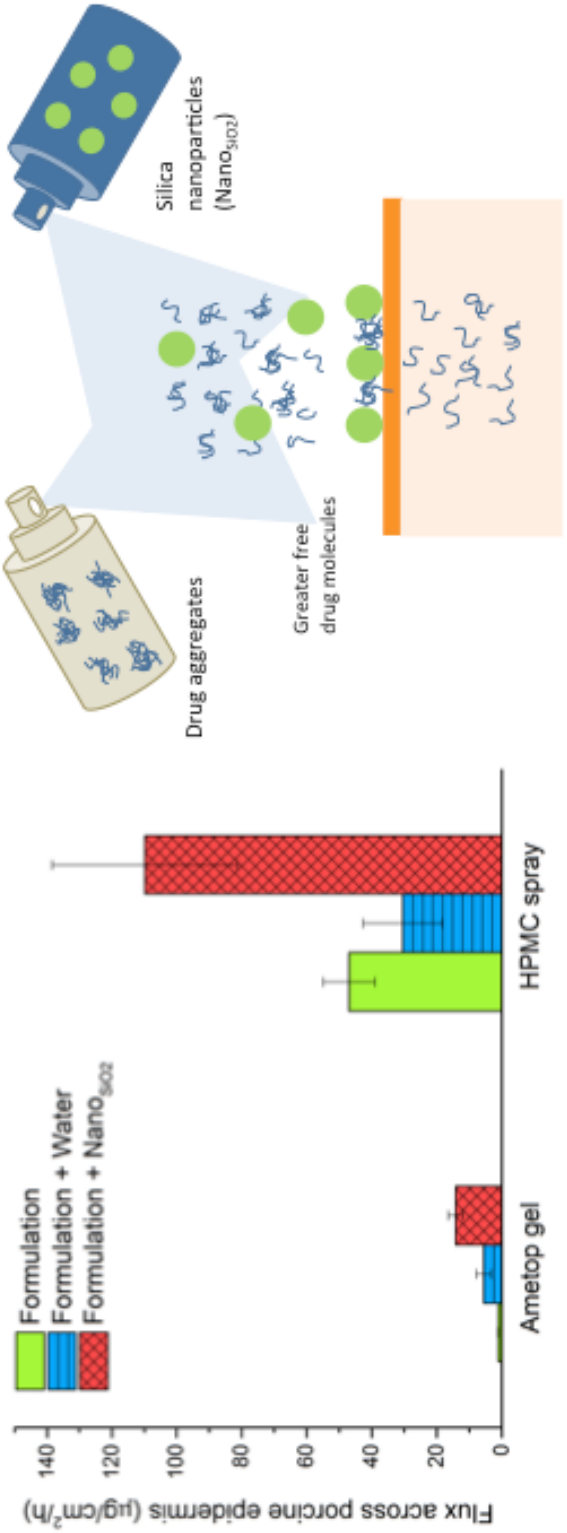

Figure 6.3. The dynamic HPMC spray formulation with co-administration of the nanomaterials provide higher drug percutaneous skin permeation enhancement as compared to the Ametop formulation.

From the thesis, it can be concluded that aggregation influences passive percutaneous skin permeation. Aggregation can occur in low concentrations and thus, it is not surprising that it will be prevalent in amphiphilic commercial products. Given that aggregation can hinder penetration into the skin after topical application, it may even be the cause of the slow onset of action and low penetrating amount of tetracaine observed in drugs. Studies using other amphiphilic drugs may provide more evidence to support this hypothesis. Currently, the investigation of molecular aggregation was conducted by indirect inference of the spectroscopic data. The development of a more direct and sensitive method could enable a more accurate conclusion to be made between drug aggregation and its percutaneous penetration.

Using the data in the thesis, it can also be concluded that nanomaterials could be added to a topical preparation after the loading of a drug into the system in order to enhance administration through the control of the drug aggregation process. This mechanism was demonstrated by the examination of drug-nanoparticle surface interactions. This examination was limited by the small surface area of the drug molecules and large surface area of the nanoparticles. As such, inferences about the interactions of tetracaine and the nanoparticles were made between the functional groups of both surfaces without taking consideration into the surface geometry or whole drug molecule properties. It would be preferable if a technique that probes these interactions more accurately were used.

Finally, it was concluded from the thesis that a HPMC using the nanoparticle technology to deliver tetracaine was found to be superior to a commercial product delivering the same drug. This demonstrates that this topical formulation can be used to produce clinical products. Further studies should be conducted to investigate the system using human skin *in vitro* experiments and using animals *in vivo* to explore the potential of generating a product that can be applied to humans. In addition, the minimum drug to nanoparticle ratios that could enhance the drug percutaneous penetration would help to reduce the material costs to manufacture this product. In order to facilitate patient compliance, the silica nanoparticles can also be introduced in a semi-solid formulation and the effects of such a vehicle can be further elucidated.

References

Abraham, M. H., Chadha, H. S. and Mitchell, R. C. (1995). The factors that influence skin penetration of solutes. *Journal of Pharmacy and Pharmacology* **47**(1): 8-16.

Albani, J. R. (2008). *Principles and applications of fluorescence spectroscopy*. Wiley-Blackwell.

Albery, W. and Hadgraft, J. (1979). Percutaneous absorption: *in vivo* experiments. *Journal of Pharmacy and Pharmacology* **31**(1): 140-147.

Alvarez-Román, R., Barre, G., Guy, R. and Fessi, H. (2001). Biodegradable polymer nanocapsules containing a sunscreen agent: preparation and photoprotection. *European Journal of Pharmaceutics and Biopharmaceutics* **52**(2): 191-195.

Alvarez-Roman, R., Naik, A., Kalia, Y., Guy, R. H. and Fessi, H. (2004a). Skin penetration and distribution of polymeric nanoparticles. *Journal of Controlled Release* **99**: 53-62.

Alvarez-Roman, R., Naik, A., Kalia, Y. N., Fessi, H. and Guy, R. H. (2004b). Visualization of skin penetration using confocal laser scanning microscopy. *European Journal of Pharmaceutics and Biopharmaceutics* **58**(2): 301-316.

Alvarez-Roman, R., Naik, A., Kalia, Y. N., Guy, R. H. and Fessi, H. (2004c). Enhancement of topical delivery from biodegradable nanoparticles. *Pharmaceutical Research* **21**: 1818-1825.

Alves, M. P., Scarrone, A. L., Santos, M., Pohlmann, A. R. and Guterres, S. S. (2007). Human skin penetration and distribution of nimesulide from hydrophilic gels containing nanocarriers. *International Journal of Pharmaceutics* **341**(1-2): 215-220.

Attwood, D. (1995). The mode of association of amphiphilic drugs in aqueous solution. *Advances in colloid and interface science* **55**: 271-303.

Attwood, D. and Fletcher, P. (1986). Self-association of local anaesthetic drugs in aqueous solution. *Journal of pharmacy and pharmacology* **38**(7): 494-498.

Attwood, D. and Natarajan, R. (1981). Effect of pH on the micellar properties of amphiphilic drugs in aqueous-solution. *Journal of Pharmacy and Pharmacology* **33**(3): 136-140.

Attwood, D. and Udeala, O. (1975). Aggregation of antihistamines in aqueous solution. Self-association of some pyridine derivatives. *The Journal of Physical Chemistry* **79**(9): 889-892.

Australian Government Therapeutic Goods Administration. (2009). A review of the scientific literature on the safety on nanopartoculate titanium dioxide or zinc oxide in sunscreens. Available at: https://www.tga.gov.au/sites/default/files/sunscreens-nanoparticles-2009.pdf (Accessed: 26 May 2016)

Barbero, A. M. and Frasch, H. F. (2006). Transcellular route of diffusion through stratum corneum: results from finite element models. *Journal of pharmaceutical sciences* **95**(10): 2186-2194.

Baroli, B. (2010a). Penetration of nanoparticles and nanomaterials in the skin: Fiction or reality? *Journal of pharmaceutical sciences* **99**(1): 21-50.

Baroli, B. (2010b). Skin absorption and potential toxicity of nanoparticulate nanomaterials. *Journal of biomedical nanotechnology*, **6**(5): 485-496.

Baroli, B., Ennas, M. G., Loffredo, F., Isola, M., Pinna, R. and Arturo Lopez-Quintela, M. (2007). Penetration of metallic nanoparticles in human full-thickness skin. *Journal of Investigative Dermatology* **127**: 1701-1712.

Barry, B. (1983). *Dermatological formulations: percutaneous absorption.* , New York: Marcel Dekker Inc.

Barry, B. (2001). Novel mechanisms and devices to enable successful transdermal drug delivery. *European Journal of Pharmaceutical Sciences* **14**(2): 101-114.

Barry, B. W. (1987). Mode of action of penetration enhancers in human skin. *Journal of Controlled Release* **6**(1): 85-97.

Benaouda, F., Brown, M., Ganguly, S., Jones, S. and Martin, G. (2012). Discriminating the molecular identity and function of discreet supramolecular structures in topical pharmaceutical formulations. *Molecular pharmaceutics*.

Benaouda, F., Brown, M., Martin, G. and Jones, S. (2012). Triggered *in situ* drug supersaturation and hydrophilic matrix self-assembly. *Pharmaceutical Research*: 1-9.

Berge, S. M., Bighley, L. D. and Monkhouse, D. C. (1977). Pharmaceutical salts. *Journal of Pharmaceutical Sciences* **66**(1): 1-19.

Blank, I. H., Scheuplein, R. J. and MacFarlane, D. J. (1967). Mechanism of percutaneous absorption. *Journal of Investigative Dermatology* **49**(6): 582-589.

Blume-Peytavi, U., Massoudy, L., Patzelt, A., Lademann, J., Dietz, E., Rasulev, U. and Bartels, N. G. (2010). Follicular and percutaneous penetration pathways of topically applied minoxidil foam. *European Journal of Pharmaceutics and Biopharmaceutics* **76**(3): 450-453.

Borgia, S. L., Regehly, M., Sivaramakrishnan, R., Mehnert, W., Korting, H. C., Danker, K., Roder, B., Kramer, K. D. and Schafer-Korting, M. (2005). Lipid nanoparticles for skin penetration enhancement-correlation to drug localization within the particle matrix as determined by fluorescence and parelectric spectroscopy. *Journal of Controlled Release* **110**(1): 151-163.

Borm, P.J., Robbins, D., Haubold, S., Kuhlbusch, T., Fissan, H., Donaldson, K., Schins, R., Stone, V., Kreyling, W., Lademann, J. and Krutmann, J. (2006). The potential risks of nanomaterials: a review carried out for ECETOC. *Particle and fibre toxicology*. **3**(1): 1.

Bos, J. D. and Meinardi, M. M. (2000). The 500 Dalton rule for the skin penetration of chemical compounds and drugs. *Experimental dermatology* **9**(3): 165-169.

Bouwstra, J. A., Honeywell-Nguyen, P. L., Gooris, G. S. and Ponec, M. (2003). Structure of the skin barrier and its modulation by vesicular formulations. *Progress in Lipid Research* **42**(1): 1-36.

British Standards Institution (2007). PAS 136:2007 Terminology for nanomaterials.

Brown, M. B., Martin, G. P., Jones, S. A. and Akomeah, F. K. (2006). Dermal and transdermal drug delivery systems: current and future prospects. *Drug delivery* **13**(3): 175-187.

Cappel, M. J. and Kreuter, J. (1991). Effect of nanoparticles on transdermal drug delivery. *Journal of Microencapsulation* **8**(3): 369-374.

Cevc, G. (1997). Drug delivery across the skin. *Expert opinion on investigational drugs* **6**(12): 1887-1937.

Cevc, G. and Blume, G. (1992). Lipid vesicles penetrate into intact skin owing to the transdermal osmotic gradients and hydration force. *Biochimica Et Biophysica Acta* **1104**(1): 226-232.

Charman, W. N., Lai, C. S. C., Finnin, B. C. and Reed, B. L. (1991). Self-association of nicotinamide in aqueous-solution - mass-transport, freezing-point depression, and partition-coefficient studies. *Pharmaceutical Research* **8**(9): 1144-1150.

Charoo, N. A., Shamsher, A. A. A., Kohli, K., Pillai, K. and Rahman, Z. (2008). Improvement in bioavailability of transdermally applied flurbiprofen using tulsi (Ocimum sanctum) and turpentine oil. *Colloids and Surfaces B-Biointerfaces* **65**(2): 300-307.

Chen, H. B., Chang, X. L., Du, D. R., Liu, W., Liu, J., Weng, T., Yang, Y. J., Xu, H. B. and Yang, X. L. (2006). Podophyllotoxin-loaded solid lipid nanoparticles for epidermal targeting. *Journal of Controlled Release* **110**(2): 296-306.

Christophers, E. (1971). Cellular architecture of the stratum corneum. *Journal of Investigative Dermatology* **56**(3): 165-169.

Christophers, E. and Kligman, A. M. (1964). Visualization of the cell layers of the stratum corneum. *Journal of Investigative Dermatology* **42**(6): 407-409.

Cross, S. E., Innes, B., Roberts, M. S., Tsuzuki, T., Robertson, T. A. and McCormick, P. (2007). Human skin penetration of sunscreen nanoparticles: In-vitro assessment of a novel micronized zinc oxide formulation. *Skin pharmacology and physiology* **20**(3): 148-154.

Cross, S. E., Jiang, R. Y., Benson, H. A. E. and Roberts, M. S. (2001). Can increasing the viscosity of formulations be used to reduce the human skin penetration of the sunscreen oxybenzone? *Journal of Investigative Dermatology* **117**(1): 147-150.

Cross, S. E., Pugh, W. J., Hadgraft, J. and Roberts, M. S. (2001). Probing the effect of vehicles on topical delivery: Understanding the basic relationship between solvent and solute penetration using silicone membranes. *Pharmaceutical Research* **18**(7): 999-1005.

Cross, S. E. and Roberts, M. S. (1993). Subcutaneous absorption kinetics and local tissue distribution of interferon and other solutes. *Journal of Pharmacy and Pharmacology* **45**(7): 606-609.

Dal Pozzo, A. and Pastori, N. (1996). Percutaneous absorption of parabens from cosmetic formulations. *International Journal of Cosmetic Science* **18**(2): 57-66.

Darwent, J. R., McCubbin, I. and Porter, G. (1982). Photoreduction of methyl viologen sensitized by sulphonated phthalocyanines in micellar solutions. *J. Chem. Soc., Faraday Trans. 2* **78**(6): 903-910.

Davies, D. G. and Bury, C. R. (1930). CCLXXXIX.—The partial specific volume of potassium n-octoate in aqueous solution. *Journal of the Chemical Society (Resumed)*: 2263-2267.

Dingler, A., Blum, R. P., Niehus, H., Muller, R. H. and Gohla, S. (1999). Solid lipid nanoparticles (SLN (TM)/Lipopearls (TM)) - a pharmaceutical and cosmetic carrier for the application of vitamin E in dermal products. *Journal of Microencapsulation* **16**(6): 751-767.

Donnelly, R. F. and Singh, T. R. R. (2015). *Novel Delivery Systems for Transdermal and Intradermal Drug Delivery*. John Wiley & Sons.

Dragicevic, N. and Maibach, H. I. (2015). *Percutaneous Penetration Enhancers Chemical Methods in Penetration Enhancement: Drug Manipulation Strategies and Vehicle Effects*. Springer.

Eckert, R. L. (1989). Structure, function, and differentiation of the keratinocyte. *Physiological Reviews* **69**(4): 1316-1346.

Edwards, D. A. and Langer, R. (1994). A linear-theory of transdermal transport phenomena. *Journal of Pharmaceutical Sciences* **83**(9): 1315-1334.

El Maghraby, G. M. M., Williams, A. C. and Barry, B. W. (1999). Skin delivery of oestradiol from deformable and traditional liposomes: Mechanistic studies. *Journal of Pharmacy and Pharmacology* **51**(10): 1123-1134.

El Maghraby, G. M. M., Williams, A. C. and Barry, B. W. (2006). Can drug-bearing liposomes penetrate intact skin? *Journal of Pharmacy and Pharmacology* **58**(4): 415-429.

Elias, P. M. (1981). Epidermal lipids, membranes, and keratinization. *International journal of dermatology* **20**(1): 1-19.

Elias, P. M. (1983). Epidermal lipids, barrier function, and desquamation. *Journal of Investigative Dermatology* **80**: S44-S49.

Ernandes, J., Chaimovich, H. and Schreier, S. (1977). Spin label study of detergents in the region of critical micelle concentration. *Chemistry and physics of lipids* **18**(3-4): 304-315.

Fang, C., Liu, Y., Ye, X., Rong, Z.-x., Feng, X.-m., Jiang, C.-b. and Chen, H.-z. (2008). Synergistically enhanced transdermal permeation and topical analgesia of tetracaine gel containing menthol and ethanol in experimental and clinical studies. *European Journal of Pharmaceutics and Biopharmaceutics* **68**(3): 735-740.

Fangueiro, J. F., Macedo, A. S., Jose, S., Garcia, M. L., Souto, S. B. and Souto, E. B. (2012). Thermodynamic behavior of lipid nanoparticles upon delivery of Vitamin E derivatives into the skin: *in vitro* studies. *Journal of Thermal Analysis and Calorimetry* **108**(1): 275-282.

Farhadieh, B., Hall, N. A. and Hammarlund, E. (1967). Aggregation of certain medicinal amines in aqueous solutions of their salts. *Journal of Pharmaceutical Sciences* **56**(1): 18-23.

Fiala, S., Roman, M., Inacio, R., Mashal, S., Brown, M. B. and Jones, S. A. (2015). New insights into eutectic cream skin penetration enhancement. *International journal of pharmaceutics*.

Fireman, S., Toledano, O., Neimann, K., Lobada, N. and Dayan, N. (2011). A look at emerging delivery systems for topical drug products. *Dermatologic therapy* **24**(5): 477-488.

Fisher, R., Hung, O., Mezei, M. and Stewart, R. (1998). Topical anaesthesia of intact skin: liposome-encapsulated tetracaine vs EMLA. *British Journal of Anaesthesia* **81**(6): 972-973.

Florence, A. T. and Attwood, D. (2011). *Physicochemical principles of pharmacy*. Pharmaceutical Pr.

Frelichowska, J., Bolzinger, M.-A., Pelletier, J., Valour, J.-P. and Chevalier, Y. (2009). Topical delivery of lipophilic drugs from o/w Pickering emulsions. *International journal of pharmaceutics* **371**(1): 56-63.

Frelichowska, J., Bolzinger, M.-A., Valour, J.-P., Mouaziz, H., Pelletier, J. and Chevalier, Y. (2009). Pickering w/o emulsions: drug release and topical delivery. *International Journal of Pharmaceutics* **368**(1): 7-15.

Gallagher, S. J. and Heard, C. M. (2005). Solvent content and macroviscosity effects on the *in vitro* transcutaneous delivery and skin distribution of ketoprofen from simple gel formulations. *Skin pharmacology and physiology* **18**(4): 186-194.

Gamer, A. O., Leibold, E. and van Ravenzwaay, B. (2006). The *in vitro* absorption of microfine zinc oxide and titanium dioxide through porcine skin. *Toxicology in Vitro* **20**(3): 301-307.

Godin, B. and Touitou, E. (2007). Transdermal skin delivery: Predictions for humans from *in vivo, ex vivo* and animal models. *Advanced drug delivery reviews* **59**(11): 1152-1161.

Gontier, E., Ynsa, M.-D., Biro, T., Hunyadi, J., Kiss, B., Gaspar, K., Pinheiro, T., Silva, J.-N., Filipe, P., Stachura, J., Dabros, W., Reinert, T., Butz, T., Moretto, P. and Surleve-Bazeille, J.-E. (2008). Is there penetration of titania nanoparticles in sunscreens through skin? A comparative electron and ion microscopy study. *Nanotoxicology* **2**(4): 218-231.

Guerin, M., Dumas, J.-M. and Sandorfy, C. (1980). Vibrational spectroscopic studies of molecular associations by local anesthetics. *Canadian Journal of Chemistry* **58**(19): 2080-2088.

Guterres, S. S., Alves, M. P. and Pohlmann, A. R. (2007). Polymeric nanoparticles, nanospheres and nanocapsules, for cutaneous applications. *Drug target insights* **2**: 147-157.

Hadgraft, J. (1999). Passive enhancement strategies in topical and transdermal drug delivery. *International Journal of Pharmaceutics* **184**(1): 1-6.

Hadgraft, J. and Guy, R. H. (1989). *Transdermal Drug Delivery: Developmental Issues and Research Initiatives*. Marcel Dekker Inc.

Hadgraft, J. and Lane, M. E. (2011). Skin: the ultimate interface. *Physical Chemistry Chemical Physics* **13**(12): 5215-5222.

Hadgraft, J. and Somers, G. (1956). Percutaneous absorption. *Journal of Pharmacy and Pharmacology* **8**(1): 625-634.

Harrison, S. M., Barry, B. W. and Dugard, P. H. (1984). Effects of freezing on human-skin permeability. *Journal of Pharmacy and Pharmacology* **36**: 261-262.

Helenius, A. and Simons, K. (1975). Solubilization of membranes by detergents. *Biochimica et Biophysica Acta (BBA)-Reviews on Biomembranes* **415**(1): 29-79.

Higuchi, T. (1960). Physical chemical analysis of percutaneous absorption process from creams and ointments. *J. Soc. Cosmet. Chem* **11**: 85-97.

Hofland, H. E. J., Bouwstra, J. A., Bodde, H. E., Spies, F. and Junginger, H. E. (1995). Interactions between liposomes and human stratum-corneum in-vitro - freeze-fracture electron-microscopic visualization and small-angle x-ray-scattering studies. *British Journal of Dermatology* **132**(6): 853-866.

Hofland, H. E. J., Vandergeest, R., Bodde, H. E., Junginger, H. E. and Bouwstra, J. A. (1994). Estradiol permeation from nonionic surfactant vesicles through human stratum-corneum in-vitro. *Pharmaceutical Research* **11**(5): 659-664.

Honeywell-Nguyen, P. L. and Bouwstra, J. A. (2003). The *in vitro* transport of pergolide from surfactant-based elastic vesicles through human skin: a suggested mechanism of action. *Journal of Controlled Release* **86**(1): 145-156.

Honeywell-Nguyen, P. L., de Graaff, A. M., Groenink, H. W. W. and Bouwstra, J. A. (2002). The *in vivo* and *in vitro* interactions of elastic and rigid Vesicles with human skin. *Biochimica Et Biophysica Acta-General Subjects* **1573**(2): 130-140.

Honeywell-Nguyen, P. L., Gooris, G. S. and Bouwstra, J. A. (2004). Quantitative assessment of the transport of elastic and rigid vesicle components and a model drug from these vesicle formulations into human skin *in vivo*. *Journal of Investigative Dermatology* **123**(5): 902-910.

Hu, Q., Liang, W., Bao, J. and Ping, Q. (2000). Enhanced transdermal delivery of tetracaine by electroporation. *International Journal of Pharmaceutics (Kidlington)* **202**(1-2): 121-124.

Iannuccelli, V., Bertelli, D., Romagnoli, M., Scalia, S., Maretti, E., Sacchetti, F. and Leo, E. (2014). *In vivo* penetration of bare and lipid-coated silica nanoparticles across the human stratum corneum. *Colloids and Surfaces B-Biointerfaces* **122**: 653-661.

Iervolino, M., Raghavan, S. L. and Hadgraft, J. (2000). Membrane penetration enhancement of ibuprofen using supersaturation. *International Journal of Pharmaceutics* **198**(2): 229-238.

Inacio, R., Barlow, D., Xiao, K., Keeble, J. and Jones, S. A. (In-press). Investigating how the attribute of self-associated drug complexes influence the passive transport of molecules through biological membranes. *European Journal of Pharmaceutics and Biopharmaceutics*.

James-Smith, M., Hellner, B., Annunziato, N. and Mitragotri, S. (2011). Effect of Surfactant Mixtures on Skin Structure and Barrier Properties. *Annals of Biomedical Engineering* **39**(4): 1215-1223.

Jenning, V., Schafer-Korting, M. and Gohla, S. (2000). Vitamin A-loaded solid lipid nanoparticles for topical use drug release properties. *Journal of Controlled Release* **66**(2-3): 115-126.

Jensen, L. B., Petersson, K. and Nielsen, H. M. (2011). *In vitro* penetration properties of solid lipid nanoparticles in intact and barrier-impaired skin. *European Journal of Pharmaceutics and Biopharmaceutics* **79**(1): 68-75.

Johnson, E. and Ludlum, D. (1969). Aggregation of local anesthetics in solution. *Biochemical pharmacology* **18**(10): 2675.

Joint Formulary Committee (online). *British National Formulary* London, BMJ Group and Pharmaceutical Press

Kalia, Y. N. and Guy, R. H. (2001). Modeling transdermal drug release. *Advanced drug delivery reviews* **48**(2-3): 159-172.

Kanitakis, J. (2002). Anatomy, histology and immunohistochemistry of normal human skin. *European Journal of Dermatology* **12**(4): 390-400.

Katz, M. and Poulsen, B. J. (1971). *Absorption of drugs through the skin*. In *Concepts in Biochemical Pharmacology*, Springer**:** 103-174.

Khan, A. M. and Shah, S. S. (2008). Determination of critical micelle concentration (CMC) of sodium dodecyl sulfate (SDS) and the effect of low concentration of pyrene on its CMC using ORIGIN software. *Journal of the Chemical Society of Pakistan* **30**(2): 186-191.

Kim, M. K., Zhao, H., Lee, C. H. and Kim, D. D. (2001). Formulation of a reservoir-type testosterone transdermal delivery system. *International Journal of Pharmaceutics* **219**(1-2): 51-59.

Kirjavainen, M., Urtti, A., Valjakka-Koskela, R., Kiesvaara, J. and Mönkkönen, J. (1999). Liposome–skin interactions and their effects on the skin permeation of drugs. *European journal of pharmaceutical sciences* **7**(4): 279-286.

Kitagawa, N., Oda, M. and Totoki, T. (2004). Possible mechanism of irreversible nerve injury caused by local anesthetics: detergent properties of local anesthetics and membrane disruption. *Anesthesiology* **100**(4): 962-967.

Kligman, A. M. and Christophel, E. (1963). Preparation of isolated sheets of human stratum corneum. *Archives of Dermatology* **88**: 702-&.

Knorr, F., Lademann, J., Patzelt, A., Sterry, W., Blume-Peytavi, U. and Vogt, A. (2009). Follicular transport route - Research progress and future perspectives. *European Journal of Pharmaceutics and Biopharmaceutics* **71**(2): 173-180.

Kuelkamp-Guerreiro, I. C., Berlitz, S. J., Contri, R. V., Alves, L. R., Henrique, E. G., Barreiros, V. R. M. and Guterres, S. S. (2013). Influence of nanoencapsulation on the sensory properties of cosmetic formulations containing lipoic acid. *International Journal of Cosmetic Science* **35**: 105-111.

Kumari, A., Yadav, S. K. and Yadav, S. C. (2010). Biodegradable polymeric nanoparticles based drug delivery systems. *Colloids and Surfaces B-Biointerfaces* **75**(1): 1-18.

L'oreal. (Online). "*The triumphs of formulation*." Available at: http://www.loreal.com/research-and-innovation/the-great-discoveries/the-triumphs-of-formulation (Accessed: 01 February 2016).

Lademann, J., Otberg, N., Jacobi, U., Hoffman, R. M. and Blume-Peytavi, U. (2005). Follicular penetration and targeting. *Journal of Investigative Dermatology Symposium Proceedings* **10**(3): 301-303.

Lademann, J., Otberg, N., Richter, H., Weigmann, H. J., Lindemann, U., Schaefer, H. and Sterry, W. (2001). Investigation of follicular penetration of topically applied substances. *Skin pharmacology and applied skin physiology* **14**: 17-22.

Lademann, J., Richter, H., Schaefer, U. F., Blume-Peytavi, U., Teichmann, A., Otberg, N. and Sterry, W. (2006). Hair follicles - A long-term reservoir for drug delivery. *Skin pharmacology and physiology* **19**(4): 232-236.

Lademann, J., Richter, H., Teichmann, A., Otberg, N., Blume-Peytavi, U., Luengo, J., Weiss, B., Schaefer, U. F., Lehr, C.-M., Wepf, R. and Sterry, W. (2007). Nanoparticles - An efficient carrier for drug delivery into the hair follicles. *European Journal of Pharmaceutics and Biopharmaceutics* **66**: 159-164.

Lademann, J., Weigmann, H. J., Rickmeyer, C., Barthelmes, H., Schaefer, H., Mueller, G. and Sterry, W. (1999). Penetration of titanium dioxide microparticles in a sunscreen formulation into the horny layer and the follicular orifice. *Skin pharmacology and applied skin physiology* **12**(5): 247-256.

Lakowicz, J. R. (2009). *Principles of fluorescence spectroscopy*. Springer.

Langbein, L., Grund, C., Kuhn, C., Praetzel, S., Kartenbeck, J., Brandner, J. M., Moll, I. and Franke, W. W. (2002). Tight junctions and compositionally related junctional structures in mammalian stratified epithelia and cell cultures derived therefrom. *European Journal of Cell Biology* **81**(8): 419-435.

Lauer, A. C., Ramachandran, C., Lieb, L. M., Niemiec, S. and Weiner, N. D. (1996). Targeted delivery to the pilosebaceous unit *via* liposomes. *Advanced drug delivery reviews* **18**(3): 311-324.

Lawaetz, A. J. and Stedmon, C. (2009). Fluorescence intensity calibration using the Raman scatter peak of water. *Applied spectroscopy* **63**(8): 936-940.

Lboutounne, H., Chaulet, J.-F., Ploton, C., Falson, F. and Pirot, F. (2002). Sustained ex vivo skin antiseptic activity of chlorhexidine in poly (ϵ-caprolactone) nanocapsule encapsulated form and as a digluconate. *Journal of Controlled Release* **82**(2): 319-334.

Lee, S. H., Jeong, S. K. and Ahn, S. K. (2006). An update of the defensive barrier function of skin. *Yonsei medical journal* **47**(3): 293-306.

Lövestam, G., Rauscher, H., Roebben, G., Klüttgen, B. S., Gibson, N., Putaud, J.-P. and Stamm, H. (2010). *Considerations on a definition of nanomaterial for regulatory purposes*.

Luengo, J., Weiss, B., Schneider, M., Ehlers, A., Stracke, F., Koenig, K., Kostka, K. H., Lehr, C. M. and Schaefer, U. F. (2006). Influence of nanoencapsulation on human skin transport of flufenamic acid. *Skin pharmacology and physiology* **19**: 190-197.

Matsuki, H., Hashimoto, S., Kaneshina, S. and Yamanaka, M. (1994). Surface adsorption and volume behavior of local anesthetics. *Langmuir* **10**(6): 1882-1887.

Matsuki, H., Ichikawa, R., Kaneshina, S., Kamaya, H. and Ueda, I. (1996). Differential scanning calorimetric study on the Krafft phenomenon of local anesthetics. *Journal of colloid and interface science* **181**(2): 362-369.

Mavon, A., Miquel, C., Lejeune, O., Payre, B. and Moretto, P. (2007). *In vitro* percutaneous absorption and *in vivo* stratum corneum distribution of an organic and a mineral sunscreen. *Skin pharmacology and physiology* **20**(1): 10-20.

McBain, J. (1913). Micellar formation of aqueous solution. *Trans. Faraday Soc* **9**: 99-112.

Megrab, N. A., Williams, A. C. and Barry, B. W. (1995). Estradiol permeation through human skin and silastic membrane - effects of propylene-glycol and supersaturation. *Journal of Controlled Release* **36**(3): 277-294.

Mehnert, W. and Mader, K. (2001). Solid Lipid Nanoparticles - Production, characterization and applications. *Advanced drug delivery reviews* **47**(2-3): 165-196.

Mei, Z. N., Chen, H. B., Weng, T., Yang, Y. J. and Yang, X. L. (2003). Solid lipid nanoparticle and microemulsion for topical delivery of triptolide. *European Journal of Pharmaceutics and Biopharmaceutics* **56**(2): 189-196.

Meidan, V. M. (2010). Methods for quantifying intrafollicular drug delivery: a critical appraisal. *Expert Opinion on Drug Delivery* **7**(9): 1095-1108.

Menon, G. and Ghadially, R. (1997). Morphology of lipid alterations in the epidermis: a review. *Microscopy research and technique* **37**(3): 180-192.

Mertz, C., Marques, A., Williamson, L. N. and Lin, C. (1990). Photophysical studies of local anesthetics, tetracaine and procaine: drug aggregations. *Photochemistry and photobiology* **51**(4): 427-437.

Mezei, M. and Gulasekharam, V. (1980). Liposomes - a selective drug delivery system for the topical route of administration .1. Lotion dosage form. *Life Sciences* **26**(18): 1473-1477.

Michaels, A. S., Chandrasekaran, S. K. and Shaw, J. E. (1975). Drug permeation through human skin - theory and invitro experimental measurement. *Aiche Journal* **21**(5): 985-996.

Mikkelson, T. J., Watanabe, S., Rytting, J. H. and Higuchi, T. (1980). Effect of self-association of phenol on its transport across polyethylene film. *Journal of Pharmaceutical Sciences* **69**(2): 133-137.

Miller, K., Goodwin, S., Westermann-Clark, G. and Shah, D. (1993). Importance of molecular aggregation in the development of a topical local anesthetic. *Langmuir* **9**(1): 105-109.

Mitragotri, S., Anissimov, Y. G., Bunge, A. L., Frasch, H. F., Guy, R. H., Hadgraft, J., Kasting, G. B., Lane, M. E. and Roberts, M. S. (2011). Mathematical models of skin permeability: an overview. *International journal of pharmaceutics* **418**(1): 115-129.

Mocanu, A., Pasca, R.-D., Tomoaia, G., Avranas, A., Horovitz, O. and Tomoaia-Cotisel, M. (2012). Selective effect of procaine, tetracaine and dibucaine on gold nanoparticles. *Journal of nanoscience and nanotechnology* **12**(12): 8935-8939.

Moddaresi, M., Brown, M. B., Zhao, Y., Tamburic, S. and Jones, S. A. (2010). The role of vehicle–nanoparticle interactions in topical drug delivery. *International journal of pharmaceutics* **400**(1): 176-182.

Mohamed, F. A. A., Roberts, M., Seton, L., Ford, J. L., Levina, M. and Rajabi-Siahboomi, A. R. (2015). The effect of HPMC particle size on the drug release rate and the percolation threshold in extended-release mini-tablets. *Drug Development and Industrial Pharmacy* **41**(1): 70-78.

Moore, P. N., Puvvada, S. and Blankschtein, D. (2003). Challenging the surfactant monomer skin penetration model: Penetration of sodium dodecyl sulfate micelles into the epidermis. *Journal of Cosmetic Science* **54**(1): 29-46.

Moore, P. N., Shiloach, A., Puvvada, S. and Blankschtein, D. (2003). Penetration of mixed micelles into the epidermis: Effect of mixing sodium dodecyl sulfate with dodecyl hexa(ethylene oxide). *Journal of Cosmetic Science* **54**(2): 143-159.

Moser, K., Kriwet, K., Naik, A., Kalia, Y. N. and Guy, R. H. (2001). Passive skin penetration enhancement and its quantification *in vitro*. *European Journal of Pharmaceutics and Biopharmaceutics* **52**(2): 103-112.

Mughal, M. A., Igbal Z and Neau, S. H. (2011). Guar gum, xanthan gum and HPMC can definite release mechanisms and sustain release of propranolol hydrochloride. *AAPS PharmSciTech* **12**(1): 77-87.

Mukerjee, P. and Karol, J. (1971). *Critical Micelle Concentrations of Aqueous Surfactant Systems*. National Bureau of Standards.

Muller, B. and Kreuter, J. (1999). Enhanced transport of nanoparticle associated drugs through natural and artificial membranes - a general phenomenon? *International Journal of Pharmaceutics* **178**(1): 23-32.

Muller, R. H., Radtke, M. and Wissing, S. A. (2002). Solid lipid nanoparticles (SLN) and nanostructured lipid carriers (NLC) in cosmetic and dermatological preparations. *Advanced drug delivery reviews* **54 Suppl 1**: S131-155.

Nafisi, S., Schafer-Korting, M. and Maibach, H. I. (2015). Perspectives on percutaneous penetration: Silica nanoparticles. *Nanotoxicology* **9**: 643-657.

Napierska, D., Thomassen, L. C., Lison, D., Martens, J. A. and Hoet, P. H. (2010). The nanosilica hazard: another variable entity. *Particle and fibre toxicology* **7**(1): 1.

National Science Foundation. (2014). "*Market report on emerging nanotechnology now available*." Available at: http://www.nsf.gov/news/news_summ.jsp?cntn_id=130586&org=NSF&from=news (Accessed: 01 February 2016).

Newman, M. D., Stotland, M., & Ellis, J. I. (2009). The safety of nanosized particles in titanium dioxide–and zinc oxide–based sunscreens. *Journal of the American Academy of Dermatology*, **61**(4): 685-692.

Nohynek, G. J., Lademann, J., Ribaud, C., & Roberts, M. S. (2007). Grey goo on the skin? Nanotechnology, cosmetic and sunscreen safety. *Critical reviews in toxicology*, **37**(3): 251-277.

Nohynek, G. J., Dufour, E. K., & Roberts, M. S. (2008). Nanotechnology, cosmetics and the skin: is there a health risk?. *Skin pharmacology and physiology*, **21**(3): 136-149.

Oberdörster, G., Maynard, A., Donaldson, K., Castranova, V., Fitzpatrick, J., Ausman, K., Carter, J., Karn, B., Kreyling, W., Lai, D. and Olin, S. (2005). Principles for characterizing the potential human health effects from exposure to nanomaterials: elements of a screening strategy. *Particle and Fibre toxicology*, **2**(1): 1.

Otberg, N., Patzelt, A., Rasulev, U., Hagemeister, T., Linscheid, M., Sinkgraven, R., Sterry, W. and Lademann, J. (2008). The role of hair follicles in the percutaneous absorption of caffeine. *British Journal of Clinical Pharmacology* **65**(4): 488-492.

Otberg, N., Richter, H., Knuttel, A., Schaefer, H., Sterry, W. and Lademann, J. (2004). Laser spectroscopic methods for the characterization of open and closed follicles. *Laser Physics Letters* **1**(1): 46-49.

Papakostas, D., Rancan, F., Sterry, W., Blume-Peytavi, U. and Vogt, A. (2011). Nanoparticles in dermatology. *Archives of dermatological research* **303**(8): 533-550.

Pardeike, J., Hommoss, A. and Mueller, R. H. (2009). Lipid nanoparticles (SLN, NLC) in cosmetic and pharmaceutical dermal products. *International Journal of Pharmaceutics* **366**: 170-184.

Patist, A., Jha, B. K., Oh, S. G. and Shah, D. O. (1999). Importance of micellar relaxation time on detergent properties. *Journal of Surfactants and Detergents* **2**(3): 317-324.

Pegoraro, C., MacNeil, S. and Battaglia, G. (2012). Transdermal drug delivery: from micro to nano. *Nanoscale* **4**(6): 1881-1894.

Peira, E., Turci, F., Corazzari, I., Chirio, D., Battaglia, L., Fubini, B. and Gallarate, M. (2014). The influence of surface charge and photo-reactivity on skin-permeation enhancer property of nano-TiO_2 in ex vivo pig skin model under indoor light. *International journal of pharmaceutics* **467**(1-2): 90-99.

Pflucker, F., Wendel, V., Hohenberg, H., Gartner, E., Will, T., Pfeiffer, S., Wepf, R. and Gers-Barlag, H. (2001). The human stratum corneum layer: An effective barrier against dermal uptake of different forms of topically applied micronised titanium dioxide. *Skin pharmacology and applied skin physiology* **14**: 92-97.

Potts, R. O. and Guy, R. H. (1992). Predicting skin permeability. *Pharmaceutical research* **9**(5): 663-669.

Potts, R. O. and Guy, R. H. (1995). A predictive algorithm for skin permeability: the effects of molecular size and hydrogen bond activity. *Pharmaceutical research* **12**(11): 1628-1633.

Prausnitz, M. R. and Langer, R. (2008). Transdermal drug delivery. *Nature biotechnology* **26**(11): 1261-1268.

Prow, T. W., Grice, J. E., Lin, L. L., Faye, R., Butler, M., Becker, W., Wurm, E. M., Yoong, C., Robertson, T. A. and Soyer, H. P. (2011). Nanoparticles and microparticles for skin drug delivery. *Advanced drug delivery reviews* **63**(6): 470-491.

Pugh, W. J., Roberts, M. S. and Hadgraft, J. (1996). Epidermal permeability - Penetrant structure relationships .3. The effect of hydrogen bonding interactions and molecular size on diffusion across the stratum corneum. *International Journal of Pharmaceutics* **138**(2): 149-165.

Puglia, C., Blasi, P., Rizza, L., Schoubben, A., Bonina, F., Rossi, C. and Ricci, M. (2008). Lipid nanoparticles for prolonged topical delivery: An *in vitro* and *in vivo* investigation. *International Journal of Pharmaceutics* **357**(1-2): 295-304.

Pygall, S. R., Griffiths, P. C., Wolf, B., Timmins, P. and Melia, C. D. (2011). Solution interactions of diclofenac sodium and meclofenamic acid sodium with hydroxypropyl methylcellulose (HPMC). *International Journal of Pharmaceutics* **405**(1): 55-62.

Radebaugh, G. W. and Simonelli, A. P. (1983). Phenomenological viscoelasticity of a heterogeneous pharmaceutical semisolid. *Journal of Pharmaceutical Sciences* **72**(4): 415-422.

Raghavan, S. L., Trividic, A., Davis, A. F. and Hadgraft, J. (2000). Effect of cellulose polymers on supersaturation and *in vitro* membrane transport of hydrocortisone acetate. *International Journal of Pharmaceutics* **193**(2): 231-237.

Rancan, F., Gao, Q., Graf, C., Troppens, S., Hadam, S., Hackbarth, S., Kembuan, C., Blume-Peytavi, U., Ruehl, E., Lademann, J. and Vogt, A. (2012). Skin penetration and cellular uptake of amorphous silica nanoparticles with variable size, surface functionalization, and colloidal stability. *Acs Nano* **6**(8): 6829-6842.

Rancan, F., Papakostas, D., Hadam, S., Hackbarth, S., Delair, T., Primard, C., Verrier, B., Sterry, W., Blume-Peytavi, U. and Vogt, A. (2009). Investigation of polylactic acid (PLA) nanoparticles as drug delivery systems for local dermatotherapy. *Pharmaceutical Research* **26**(8): 2027-2036.

Reid, M. L., Benaouda, F., Khengar, R., Jones, S. A. and Brown, M. B. (2013). Topical corticosteroid delivery into human skin using hydrofluoroalkane metered dose aerosol sprays. *International Journal of Pharmaceutics* **452**(1-2): 157-165.

Reuters, U. (2014). "*Research and Markets: Transdermal Drug Delivery Market & Clinical Pipeline Insight Report 2014 - Detailed Analysis of the $25 Billion Industry*." Available at: http://uk.reuters.com/article/research-and-markets-idUKnBw025656a+100+BSW20140502 (Accessed: 01 February 2016).

Rhee, Y.-S., Huh, J.-Y., Park, C.-W., Nam, T.-Y., Yoon, K.-R., Chi, S.-C. and Park, E.-S. (2007). Effects of vehicles and enhancers on transdermal delivery of clebopride. *Archives of Pharmacal Research* **30**(9): 1155-1161.

Roberts, M. S., Roberts, M. J., Robertson, T. A., Sanchez, W., Thoerling, C., Zou, Y., Zhao, X., Becker, W. and Zvyagin, A. V. (2008). *In vitro* and *in vivo* imaging of xenobiotic transport in human skin and in the rat liver. *Journal of Biophotonics* **1**(6): 478-493.

Rolland, A., Wagner, N., Chatelus, A., Shroot, B. and Schaefer, H. (1993). Site-specific drug-delivery to pilosebaceous structures using polymeric microspheres. *Pharmaceutical Research* **10**(12): 1738-1744.

Rossetti, F. C., Lopes, L. B., Carollo, A. R. H., Thomazini, J. A., Tedesco, A. C. and Bentley, M. V. L. B. (2011). A delivery system to avoid self-aggregation and to improve *in vitro* and *in vivo* skin delivery of a phthalocyanine derivative used in the photodynamic therapy. *Journal of Controlled Release* **155**(3): 400-408.

Rouzes, C., Leonard, M., Durand, A. and Dellacherie, E. (2003). Influence of polymeric surfactants on the properties of drug-loaded PLA nanospheres. *Colloids and Surfaces B-Biointerfaces* **32**: 125-135.

Ryman-Rasmussen, J. P., Riviere, J. E. and Monteiro-Riviere, N. A. (2006). Penetration of intact skin by quantum dots with diverse physicochemical properties. *Toxicological Sciences* **91**: 159-165.

SCCNP (2000). Opinion of the scientific comittee on cosmetic products and non-food products intended for consumer concerning titanium oxide. *Brussels: European Commission*.

Schaefer, H. and Lademann, J. (2001). The role of follicular penetration - A differential view. *Skin pharmacology and applied skin physiology* **14**: 23-27.

Schäfer-Korting, M., Mehnert, W. and Korting, H.-C. (2007). Lipid nanoparticles for improved topical application of drugs for skin diseases. *Advanced drug delivery reviews* **59**(6): 427-443.

Scheuple, R.J. (1967). Mechanism of percutaneous absorption .2. Transient diffusion and relative importance of various routes of skin penetration. *Journal of Investigative Dermatology* **48**(1): 79-&.

Scheuplein, R. J. (1965). Mechanism of percutaneous adsorption. *Journal of Investigative Dermatology* **45**(5): 334-346.

Scheuplein, R. J. and Blank, I. H. (1971). Permeability of the skin. *Physiological Reviews* **51**(4): 702-747.

Schlupp, P., Blaschke, T., Kramer, K. D., Holtje, H. D., Mehnert, W. and Schafer-Korting, M. (2011). Drug release and skin penetration from solid lipid nanoparticles and a base cream: a systematic approach from a comparison of three glucocorticoids. *Skin pharmacology and physiology* **24**(4): 199-209.

Schreier, S., Ernandes, J. R., Cuccovia, I. and Chaimovich, H. (1978). Spin label studies of structural and dynamical properties of detergent aggregates. *Journal of Magnetic Resonance (1969)* **30**(2): 283-298.

Schreier, S., Malheiros, S. V. and de Paula, E. (2000). Surface active drugs: self-association and interaction with membranes and surfactants. Physicochemical and biological aspects. *Biochimica et Biophysica Acta (BBA)-Biomembranes* **1508**(1): 210-234.

Schulz, J., Hohenberg, H., Pflucker, F., Gartner, E., Will, T., Pfeiffer, S., Wepf, R., Wendel, V., Gers-Barlag, H. and Wittern, K. P. (2002). Distribution of sunscreens on skin. *Advanced drug delivery reviews* **54**: S157-S163.

Shah, V. P., Elkins, J., Lam, S. Y. and Skelly, J. P. (1989). Determination of *in vitro* drug release from hydrocortisone creams. *International Journal of Pharmaceutics* **53**(1): 53-59.

Shaikh, V. R., Dagade, D. H., Hundiwale, D. G. and Patil, K. J. (2011). Volumetric studies of aqueous solutions of local anesthetical drug compounds [hydrochlorides of procaine (PC HCl), lidocaine (LC HCl) and tetracaine (TC HCl)] at 298.15 K. *Journal of Molecular Liquids* **164**(3): 239-242.

Shao, Z., Li, Y., Krishnamoorthy, R., Chermak, T. and Mitra, A. K. (1993). Differential effects of anionic, cationic, nonionic, and physiologic surfactants on the dissociation, α-chymotryptic degradation, and enteral absorption of insulin hexamers. *Pharmaceutical research* **10**(2): 243-251.

Shim, J., Kang, H. S., Park, W. S., Han, S. H., Kim, J. and Chang, I. S. (2004). Transdermal delivery of mixnoxidil with block copolymer nanoparticles. *Journal of Controlled Release* **97**(3): 477-484.

Shore, P. A., Brodie, B. B. and Hogben, C. A. M. (1957). The gastric secretion of drugs: a pH partition hypothesis. *Journal of Pharmacology and Experimental Therapeutics* **119**(3): 361-369.

Souto, E. B., Muller, R. H. and Gohla, S. (2005). A novel approach based on lipid nanoparticles (SLN (R)) for topical delivery of alpha-lipoic acid. *Journal of Microencapsulation* **22**: 581-592.

Spikes, J. D. and Bommer, J. C. (1986). Zinc tetrasulphophthalocyanine as a photodynamic sensitizer for biomolecules. *International Journal of Radiation Biology* **50**(1): 41-45.

Staronova, K., Nielsen, J. B., Roursgaard, M. and Knudsen, L. E. (2012). Transport of SiO2 Nanoparticles through Human Skin. *Basic & Clinical Pharmacology & Toxicology* **111**(2): 142-144.

Stewart, M. (1992). *Sebaceous gland lipids*. Seminars in dermatology.

Stracke, F., Weiss, B., Lehr, C.-M., Koenig, K., Schaefer, U. F. and Schneider, M. (2006). Multiphoton microscopy for the investigation of dermal penetration of nanoparticle-borne drugs. *Journal of Investigative Dermatology* **126**(10): 2224-2233.

Suh, H. and Jun, H. W. (1996). Physicochemical and release studies of naproxen in poloxamer gels. *International Journal of Pharmaceutics* **129**(1-2): 13-20.
Szabo, G. (1962). The number of eccrine sweat glands in human skin. *Adv Biol Skin* **3**: 1-5.

Tinkle, S.S., Antonini, J.M., Rich, B.A., Roberts, J.R., Salmen, R., DePree, K. and Adkins, E.J. (2003). Skin as a route of exposure and sensitization in chronic beryllium disease. *Environmental Health Perspectives*, **111**(9):1202.

Toll, R., Jacobi, U., Richter, H., Lademann, J., Schaefer, H. and Blume-Peytavi, U. (2004). Penetration profile of microspheres in follicular targeting of terminal hair follicles. *Journal of Investigative Dermatology* **123**(1): 168-176.

Trombino, S., Cassano, R., Muzzalupo, R., Pingitore, A., Cione, E. and Picci, N. (2009). Stearyl ferulate-based solid lipid nanoparticles for the encapsulation and stabilization of beta-carotene and alpha-tocopherol. *Colloids and Surfaces B-Biointerfaces* **72**: 181-187.

Ueda, K., Higashi, K., Limwikrant, W., Sekine, S., Horie, T., Yamamoto, K. and Moribe, K. (2012). Mechanistic differences in permeation behavior of supersaturated and solubilized solutions of carbamazepine revealed by nuclear magnetic resonance measurements. *Molecular pharmaceutics* **9**(11): 3023-3033.

Umemura, J. and Mantsch, H. H. (1981). The molecular association of tetracaine with ethylpalmitate: An Infrared Spectroscopic Study. *Bulletin of the Institute for Chemical Research, Kyoto University* **58**(5-6): 548-554.

Valenta, C. and Auner, B. G. (2004). The use of polymers for dermal and transdermal delivery. *European journal of pharmaceutics and biopharmaceutics* **58**(2): 279-289.

Vogt, A., Combadiere, B., Hadam, S., Stieler, K. M., Lademann, J., Schaefer, H., Autran, B., Sterry, W. and Blume-Peytavi, U. (2006). 40 nm, but not 750 or 1,500 nm, nanoparticles enter epidermal CD1a+ cells after transcutaneous application on human skin. *Journal of Investigative Dermatology* **126**(6): 1316-1322.

Wagner, A. and Vorauer-Uhl, K. (2011). Liposome technology for industrial purposes. *Journal of drug delivery* **2011**: 591325-591325.

Walters, K. A. (2002). *Dermatological and transdermal formulations*. Informa Healthcare.

Watkinson, R. M., Herkenne, C., Guy, R. H., Hadgraft, J., Oliveira, G. and Lane, M. E. (2009). Influence of ethanol on the solubility, ionization and permeation characteristics of ibuprofen in silicone and human skin. *Skin pharmacology and physiology* **22**(1): 15-21.

Welin-Berger, K., Neelissen, J. A. M. and Bergenstahl, B. (2001). The effect of theological behaviour of a topical anaesthetic formulation on the release and permeation rates of the active compound. *European Journal of Pharmaceutical Sciences* **13**(3): 309-318.

Wilkes, G., Brown, I. and Wildnauer, R. (1973). The biomechanical properties of skin. *CRC critical reviews in bioengineering* **1**(4): 453.

Williams, A. (2003). *Transdermal and topical drug delivery: From theory to clinical practice*. Pharmaceutical Press London.

Williams, A. C. and Barry, B. W. (2012). Penetration enhancers. *Advanced drug delivery reviews* **64**: 128-137.

Wissing, S. A., Lippacher, A. and Muller, R. H. (2001). Investigations on the occlusive properties of solid lipid nanoparticles (SLN). *Journal of Cosmetic Science* **52**(5): 313-324.

Wissing, S. A. and Muller, R. G. (2002). The influence of the crystallinity of lipid nanoparticles on their occlusive properties. *International Journal of Pharmaceutics* **242**(1-2): 377-379.

Wissing, S. A. and Muller, R. H. (2003). Cosmetic applications for solid lipid nanoparticles (SLN). *International Journal of Pharmaceutics* **254**(1): 65-68.

Wu, X., Landfester, K., Musyanovych, A. and Guy, R. H. (2010). Disposition of charged nanoparticles after their topical application to the skin. *Skin pharmacology and physiology* **23**(3): 117-123.

Wu, X., Price, G. J. and Guy, R. H. (2009). Disposition of nanoparticles and an associated lipophilic permeant following topical application to the skin. *Molecular pharmaceutics* **6**(5): 1441-1448.

Wyn-Jones, E. and Gormally, J. (1983). *Aggregation processes in solution*. Elsevier Science Ltd.

Zhang, J., Sun, M., Fan, A., Wang, Z. and Zhao, Y. (2012). The effect of solute-membrane interaction on solute permeation under supersaturated conditions. *International journal of pharmaceutics*.

Zhao, Y., Brown, M. B. and Jones, S. A. (2010). The effects of particle properties on nanoparticle drug retention and release in dynamic minoxidil foams. *International journal of pharmaceutics* **383**(1): 277-284.

Zhuravlev, L. T. (2000). The surface chemistry of amorphous silica. Zhuravlev model. *Colloids and Surfaces a-Physicochemical and Engineering Aspects* **173**(1-3): 1-38.

Zvyagin, A. V., Zhao, X., Gierden, A., Sanchez, W., Ross, J. A. and Roberts, M. S. (2008). Imaging of zinc oxide nanoparticle penetration in human skin *in vitro* and *in vivo*. *Journal of Biomedical Optics* **13**(6).